

RAPPORT D'ACTIVITÉ

Titre du projet :

Ciblage de l'inflammation du tissu adipeux, du foie et de l'intestin via l'Ostéopontine/CD44 dans les complications de l'obésité (diabète de type 2 et NAFLD)

Porteur du projet : P. Gual (Ph. D., DR2 INSERM).

INSERM U1065, C3M, Équipe 8 "Complications hépatiques de l'obésité", Nice

1. CONTEXTE ET OBJECTIFS

Les mécanismes physiopathologiques des complications de l'obésité (Diabète, NAFLD) sont complexes, et multi-organes. L'Ostéopontine (OPN) (chimiokine, cytokine Th1 et Th17, pro-fibrosant, agissant via CD44) régule les fonctions du tissu adipeux (TA), du foie et de l'intestin et constitue une cible pertinente. Nos objectifs sont de :

- Caractériser cette voie dans le foie et le TA des patients obèses (810 patients)
- Étudier le rôle de cette voie dans la fibrose du TA et les NAFLD chez la souris (souris OPN, CD44 et IL17R KO).
- Évaluer des approches thérapeutiques visant l'OPN (neutralisation, nutritionnelle) afin de prévenir ou corriger la fibrose du TA, le diabète et les NAFLD chez la souris.

De l'ensemble de ce projet, nous espérons mieux comprendre le rôle de l'OPN/CD44/IL17 dans les complications de l'obésité (l'insulino-résistance, la fibrose du TA, les complications hépatiques) dans le but de mieux prendre en charge ces complications et d'identifier de nouvelles cibles thérapeutiques.

1. Résultats obtenus

Un nouveau rôle de Ostéopontine dans la régulation l'inflammation du tissu adipeux et le développement des complications hépatiques associées à l'obésité. L'inflammation et l'insulino-résistance du tissu adipeux (TA) et du foie jouent un rôle important dans le développement du diabète de type 2 et des NAFLD. La mise en place de cette inflammation dans le TA et le foie est un mécanisme complexe et multifactoriel. Le recrutement et la régulation des cellules immunes jouent un rôle important.

Parmi les acteurs responsables de la mise en place de l'inflammation du tissu adipeux, l'équipe s'est intéressée à une molécule particulière : l'ostéopontine (OPN). Appartenant à la famille des SIBLING (Small Integrin-Binding Ligand N-linked Glycoprotein), cette molécule a d'abord été identifiée dans la matrice osseuse, puis en tant que cytokine produite par les lymphocytes T activés lors des réponses inflammatoires. Cytokine et chimiokine, elle est sécrétée par de nombreux types cellulaires (macrophages, lymphocytes, cellules dendritiques) et participe à la régulation de leur fonction biologique (migration, survie, activation, polarisation). Dans des modèles de souris rendues obèses par un régime riche en graisse, l'expression de l'OPN est fortement augmentée dans le tissu adipeux, cette expression étant corrélée à un recrutement de macrophages inflammatoires (1) (2) et de cellules dendritiques (3). L'inactivation de l'OPN entraîne une diminution du recrutement des macrophages et une meilleure sensibilité à l'insuline sans modifier la prise de poids ni la dépense énergétique. De plus, l'OPN est intimement liée aux complications hépatiques. L'inactivation de l'OPN est associée à une diminution de l'inflammation, de la stéatose et de la fibrose hépatique dans des modèles murins d'obésité (régime HFD), de NAFLD (régime MCD) et

de fibrose hépatique (CCl₄) (1; 4; 5). Cependant, le rôle de l'OPN sur le recrutement et/ou la polarisation des LT dans l'obésité n'a pas encore été étudié. Les objectifs ont été de caractériser l'implication de l'OPN dans l'inflammation du tissu adipeux et le foie associée à l'obésité, et particulièrement sur les LT :

Nous avons pu montrer que l'OPN induisait une inflammation dans le TA et le foie au cours de l'obésité par des mécanismes différents. Dans le TA, l'OPN favoriserait le recrutement des macrophages mais aussi des CD et des LT. De plus, l'OPN participe à la polarisation des LT en Th1 et à la diminution des Treg. Dans le foie, l'OPN ne semble pas jouer de rôle important dans le recrutement des LT. Cependant, l'OPN participe à la mise en place des réponses Th1 et Th17. Cette inflammation induite par l'OPN pourrait favoriser le développement de la fibrose hépatique. Bien que l'OPN soit exprimé au niveau des monocytes, OPN semble dispensable pour leur différenciation en cellules dendritiques et à la maturation de ces dernières.

Manuscrit en préparation.

CD44 est un marqueur, un acteur et une cible thérapeutique potentielle de la NASH. La prévalence des complications hépatiques de l'obésité (Non Alcoholic fatty liver disease : NAFLD), ne fait qu'augmenter (25%) et constitue un problème majeur de santé publique. L'inflammation hépatique sur un foie gras (Non Alcoholic steatohepatitis, NASH), la forme évolutive de la maladie, conduit à terme à une cirrhose et au carcinome hépatocellulaire. Il est donc urgent de comprendre les mécanismes précis de cette réponse inflammatoire afin de proposer des cibles thérapeutiques aux patients atteints par cette pathologie. Nous avons mis en évidence que la protéine CD44, exprimée majoritairement sur les cellules immunitaires et un des récepteurs de l'OPN, est un marqueur, un acteur et une cible thérapeutique de la NASH. Dans des modèles murins de stéatohépatite, le ciblage de CD44 (souris invalidée pour CD44 et déplétion des cellules CD44+ par un anticorps) prévient fortement et corrige en partie l'inflammation hépatique, l'infiltration des macrophages et la souffrance hépatique, respectivement. En plus de la régulation du recrutement des macrophages au niveau du foie, CD44 est nécessaire à l'activation des macrophages en réponse aux signaux de dangers provenant d'hépatocytes en souffrance (molécules associées à des dégâts cellulaires, DAMPs), motifs moléculaires associés aux pathogènes (PAMP, comme le LPS) et aux acides gras saturés (Palmitate). Nous avons aussi démontré la relevance humaine de cette expression hépatique de CD44. Chez les patients obèses, l'expression hépatique de CD44 est fortement augmentée avec la NASH et corrèle avec la souffrance hépatocytaire et la quantité de macrophages dans le foie (évaluée par l'expression du marqueur CD68). La correction de la NASH est associée à une forte diminution des cellules CD44-positives dans le foie. Finalement, la forme soluble de CD44 est augmentée avec la stéatose sévère et la NASH. Ces données humaines et expérimentales sur l'animal suggèrent que CD44 est un marqueur et un acteur clef de l'inflammation hépatique et son ciblage corrige partiellement la NASH.

*Patouraux S, Rousseau D, Bonnafous S, Lebeau-pin C, Luci C, Canivet CM, Schneck AS, Bertola A, Saint-Paul MC, Iannelli A, Gugenheim J, Anty R, Tran A, Bailly-Maitre B, **Gual P.** CD44 is a key player in non-alcoholic steatohepatitis. *J Hepatol.* 2017 Mar 16. pii: S0168-8278(17)30137-X. doi: 10.1016/j.jhep.2017.03.003. (IF: 10.59)*

La chirurgie bariatrique (by pass en Y) conduit à une rémission à long terme de l'apoptose hépatocytaire et des caractéristiques histologiques qui définissent la NASH. Les effets à long terme de la chirurgie bariatrique sur la NASH, et plus particulièrement sur la souffrance hépatique et l'apoptose hépatocytaire ne sont pas bien établis. Nous avons réalisé une étude longitudinale avec les biopsies de foie appareillées de neuf femmes avec une obésité morbide (la médiane du BMI : 42 [38.7; 45.1] kg/m²) et avec une NASH avec un suivi médian de 55 [44; 75] mois après une

chirurgie bariatrique (laparoscopic Roux-en-Y gastric bypass (LRYGB) surgery). La chirurgie LRYGB est associée à une perte de poids significative (la médiane de la perte de BMI -13.7 [-16.4;-9.5] kg/m²), la stéatose hépatique est améliorée dans chez tous les patients (55.5 % avec une correction totale) et résolution de l'inflammation hépatique et du ballooning hépatocyttaire dans 100 et 88.8 % des cas, respectivement. Les niveaux des ALAT baissent au niveau des valeurs normales et le niveau hépatique de la caspase 3 activée diminue fortement après un suivi médian de 55 mois. L'apoptose hépatocyttaire évaluée par le niveau circulant des fragments de la keratine 18 générés par les caspases est améliorée dès la première année après la chirurgie LRYGB et ces améliorations persistent pendant au moins 55 mois. La chirurgie LRYGB chez les patients obèses morbides avec une NASH est donc associée à des effets bénéfiques de longue durée sur la stéatohépatite et la mort hépatocyttaire. Cette cohorte nous a aussi permis de mettre en évidence que la correction de la NASH est associée à une forte diminution des cellules positives pour CD44 dans le foie, comme décrit ci-dessus.

*Schneck AS, Anty R, Patouraux S, Bonnafous S, Rousseau D, Lebeaupin C, Bailly-Maitre B, Sans A, Tran A, Gugenheim J, Iannelli A\$, **Gual P**\$ (co-last authors). Roux-en Y gastric bypass results in long-term remission of hepatocyte apoptosis and hepatic histological features of non-alcoholic steatohepatitis. *Front. Physiol.* 2016, 7:344. (IF: 4.031)*

Le stress du réticulum endoplasmique hépatocyttaire participe à la souffrance hépatique par une voie dépendante de l'activation de l'inflammasome et de la pyroptose. Dans cette recherche des mécanismes impliqués dans la mise en place de l'inflammation chronique au niveau du foie d'obèse, nous avons pu mettre en évidence que les stress du réticulum endoplasmique (RE) dans les hépatocytes régule l'activation de l'inflammasome NLRP3 et induit une mort hépatocyttaire par pyroptose. Inhibition du stress du RE a donc des effets bénéfiques sur le l'inflammation hépatique et la souffrance hépatique (pyroptose) et pourrait constituer une nouvelle cible thérapeutique des NAFLD.

*Lebeaupin C, Proics E, Desnoyers de Bieville CH, Rousseau D, Bonnafous S, Patouraux S, Adam G, Lavallard VJ, Rovere C, Le Thuc O, Saint-Paul MC, Anty R, Schneck AS, Iannelli A, Gugenheim J, Tran A, **Gual P**, Bailly-Maitre B. ER stress induces NLRP3 inflammasome activation and hepatocyte death. *Cell Death Dis.* 2015 Sep 10;6:e1879. doi: 10.1038/cddis.2015.248. (IF: 5.378)*

Études collaboratives

-Nous avons aussi participé à la mise en évidence du rôle des Cavin-1 et -2 dans la régulation des Caveolae adipocytaires. Brièvement, l'hypoxie inhibe l'expression des cavin-1 et 2, aboutissant à la disparition de caveolae. Ceci conduit à l'inhibition de la voie de signalisation de l'insuline et l'établissement de résistance à l'insuline.

*Regazzetti C, Dumas K, Lacas-Gervais S, Pastor F, Peraldi P, Bonnafous S, Dugail I, Le Lay S, Valet P, Le Marchand-Brustel Y, Tran A, **Gual P**, Tanti JF, Cormont M, Giorgetti-Peraldi S. Hypoxia inhibits Cavin-1 and Cavin-2 expression and down-regulates Caveolae in adipocytes, *Endocrinology*, 2015;156(3):789-801. (IF: 4.159)*

-Nous avons aussi mis en évidence que l'expression hépatique de Promyelocytic Leukemia Protein est augmentée avec l'obésité et la stéatose hépatique chez nos patients obèses.

Carracedo A, Rousseau D*, Douris N*(co-first authors), Fernández-Ruiz S, Martín-Martín N, Weiss D, Webster K, Adams AC, Vazquez-Chantada M, Martinez-Chantar ML, Anty R, Tran A,*

Maratos-Flier E, **Gual P**, Pandolfi PP. The promyelocytic leukemia protein is upregulated in metabolic tissues in conditions of obesity and liver steatosis. *Int J Biol Sci.* 2015; 11(6): 629-632. (IF: 3.982)

2. Publications en rapport avec cette subvention de recherche

1 - PUBLICATIONS ORIGINALES

1: Regazzetti C, Dumas K, Lacas-Gervais S, Pastor F, Peraldi P, Bonnafous S, Dugail I, Le Lay S, Valet P, Le Marchand-Brustel Y, Tran A, **Gual P**, Tanti JF, Cormont M, Giorgetti-Peraldi S. Hypoxia inhibits Cavin-1 and Cavin-2 expression and down-regulates Caveolae in adipocytes, *Endocrinology*, 2015;156(3):789-801. (IF: 4.159)

2: Carracedo A*, Rousseau D*, Douris N*(co-first authors), Fernández-Ruiz S, Martín-Martín N, Weiss D, Webster K, Adams AC, Vazquez-Chantada M, Martinez-Chantar ML, Anty R, Tran A, Maratos-Flier E, **Gual P**, Pandolfi PP. The promyelocytic leukemia protein is upregulated in metabolic tissues in conditions of obesity and liver steatosis. *Int J Biol Sci.* 2015; 11(6): 629-632. (IF: 3.982)

3: Lebeaupin C, Proics E, Desnoyers de Bievil CH, Rousseau D, Bonnafous S, Patouraux S, Adam G, Lavallard VJ, Rovere C, Le Thuc O, Saint-Paul MC, Anty R, Schneck AS, Iannelli A, Gugenheim J, Tran A, **Gual P**, Bailly-Maitre B. ER stress induces NLRP3 inflammasome activation and hepatocyte death. *Cell Death Dis.* 2015 Sep 10;6:e1879. doi: 10.1038/cddis.2015.248. (IF: 5.378)

4: Schneck AS, Anty R, Patouraux S, Bonnafous S, Rousseau D, Lebeaupin C, Bailly-Maitre B, Sans A, Tran A, Gugenheim J, Iannelli A^s, **Gual P**^s (co-last authors). Roux-en Y gastric bypass results in long-term remission of hepatocyte apoptosis and hepatic histological features of non-alcoholic steatohepatitis. *Front. Physiol.* 2016, 7:344. (IF: 4.031)

5: Patouraux S*, Rousseau D* (co-first authors), Bonnafous S, Lebeaupin C, Luci C, Canivet CM, Schneck AS, Bertola A, Saint-Paul MC, Iannelli A, Gugenheim J, Anty R, Tran A, Bailly-Maitre B, **Gual P**. CD44 is a key player in non-alcoholic steatohepatitis *J Hepatol.* 2017 *In Press*, Accepted Manuscript, Available online 16 March 2017 (IF: 10.59)

2- COMMUNICATIONS ORALES

1: Vallée D, Rousseau D, Patouraux S, Adam G, Bonnafous S, Reed JC, Tran A, **Gual P**, Bailly-Maitre B. Bax-Inhibitor-1 deficiency predisposes to the development of type 2 diabetes overwhelming NLRP3 inflammasome: consequences on chronic liver diseases. *2nd International Congress. Cell Death in Cancer.* La Baule. 14-17 May. 2014. (CO).

2: Lebeaupin C, Rousseau D, Vallée D, Bonnafous S, Patouraux S, Anty R, Schneck AS, Iannelli A, Gugenheim J, Tran A, **Gual P** and Bailly-Maitre B. "IRE1alpha active l'inflammasome NLRP3 dans la stéatopathie métabolique" ; " IRE1a activates NLRP3 inflammasome in NASH" *77 emes journées de l'Association Française d'Etude du Foie.*, 30 september-03 october 2015. Toulouse. (CO-02)

3: Patouraux S, Rousseau D, Bonnafous S, Schneck AS, Anty R, Iannelli A, Saint-Paul MC, Gugenheim J, Bailly-Maitre B, Tran A, **Gual P**. "CD44 est un acteur important dans la stéatohépatite

non alcoolique (NASH)". *77 emes journées de l'Association Française d'Etude du Foie*. 30 september-03 october 2015. Toulouse. (CO-36)

4: Lebeauvin C, Vallée D, Rousseau D, Patouraux S, Bonnafous S, Tran A, **Gual P** and Bailly-Maitre B. Bax-Inhibitor-1 deficiency predisposes to type 2 diabetes overwhelming NLRP3 inflammasome: consequences on chronic liver diseases". *23 rd ECDO conference "Death pathways and beyond"* October 7-10, 2015. Geneva. (Oral presentation)

5: Lebeauvin C, Proics E, Desnoyers de Bieville CH, Rousseau D , Bonnafous S, Patouraux S, Adam G, Rovere C, Tran A, **Gual P**, Bailly-Maitre B. "ER stress induces inflammasome activation and hepatocyte death". *Symposium C3M "Inflammation & Disease"* 2 November 2015. Nice. (Oral presentation)

3 COMMUNICATIONS AFFICHEES :

1: Rousseau D., Anty R., Bonnafous S., Patouraux S., Schneck A.-S., Iannelli A., Saint-Paul V, Gugenheim J., Bailly-Maitre B., Tran A., **Gual P**. CD44 is an important actor in Non Alcoholic Steatohepatitis. *50th Annual Meeting of the EASL*, Vienna, April 22-16, 2015. *J of Hepatology*, 2015, 62, Supplement 2, S45–S66, P0941

2: Patouraux S, Rousseau D, Bonnafous S, Lebeauvin C, Anty R, Schneck AS, Iannelli A, Gugenheim J, Saint-Paul MC, Bertola A, Bailly-Maitre B, Tran A, **Gual P**. "CD44 is an important actor in non alcoholic steatohepatitis . *Symposium C3M "Inflammation & Disease"* 2 November 2015. Nice. (CA-7)

3: Lebeauvin C, Proics E, Desnoyers de Bieville CH, Rousseau D , Bonnafous S, Patouraux S, Adam G, Rovere C, Tran A, **Gual P**, Bailly-Maitre B. "ER stress induces inflammasome activation and hepatocyte death". *2nd Labex Cell Signallife Meeting"* 9-19 November 2015 Nice (CA)

4: Patouraux S, Rousseau D, Bonnafous S, Lebeauvin C, Anty R, Schneck AS, Iannelli A, Gugenheim J, Saint-Paul MC, Bertola A, Bailly-Maitre B, Tran A, **Gual P**. "CD44 is an important actor in non alcoholic steatohepatitis . "ER stress induces inflammasome activation and hepatocyte death". *2nd Labex Cell Signallife Meeting"* 9-19 November 2015 Nice (CA)

5: Lebeauvin C., Proics E., de Bieville C.-H.D., Rousseau D., Bonnafous S., Patouraux S., Tran A., Gual P., Bailly-Maitre B. "TUDCA protects against endoplasmic reticulum stress induced inflammasome activation and hepatocyte death in non-alcoholic steatohepatitis". *Annual Meeting of the EASL International Liver Congress*, Barcelona, April 13-17, *J of Hepatology*, 2016. Volume 64, Issue 2, Supplement, SAT-037, S676

4 RÉFÉRENCES:

1. Nomiyama T, Perez-Tilve D, Ogawa D, Gizard F, Zhao Y, Heywood EB, Jones KL, Kawamori R, Cassis LA, Tschop MH, Bruemmer D: Osteopontin mediates obesity-induced adipose tissue macrophage infiltration and insulin resistance in mice. *J Clin Invest* 2007;117:2877-2888

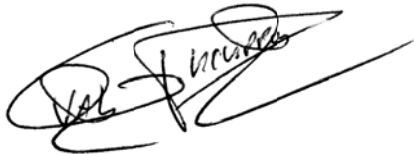
2. Bertola A, Deveaux V, Bonnafous S, Rousseau D, Anty R, Wakkach A, Dahman M, Tordjman J, Clement K, McQuaid SE, Frayn KN, Huet PM, Gugenheim J, Lotersztajn S, Le Marchand-Brustel Y, Tran A, Gual P: Elevated expression of osteopontin may be related to adipose tissue macrophage accumulation and liver steatosis in morbid obesity. *Diabetes* 2009;58:125-133

3. Bertola A, Ciucci T, Rousseau D, Bourlier V, Duffaut C, Bonnafous S, Blin-Wakkach C, Anty R, Iannelli A, Gugenheim J, Tran A, Bouloumie A, Gual P, Wakkach A: Identification of adipose tissue dendritic cells correlated with obesity-associated insulin-resistance and inducing th17 responses in mice and patients. Diabetes 2012;61:2238-2247

4. Sahai A, Malladi P, Melin-Aldana H, Green RM, Whittington PF: Upregulation of osteopontin expression is involved in the development of nonalcoholic steatohepatitis in a dietary murine model. Am J Physiol Gastrointest Liver Physiol 2004;287:G264-273

5. Lorena D, Darby IA, Gadeau AP, Leen LL, Rittling S, Porto LC, Rosenbaum J, Desmouliere A: Osteopontin expression in normal and fibrotic liver. altered liver healing in osteopontin-deficient mice. J Hepatol 2006;44:383-390

Rapport fait le 09 Juin 2017

A handwritten signature in black ink, appearing to read 'Philippe Gual', with a large, sweeping flourish extending to the right.

Philippe Gual, Research Director, INSERM
Co-Head of the Team 8 "hepatic complications of obesity"
INSERM U1065, C3M

ANNEXES

PDF des publications en rapport avec cette subvention de recherche

Hypoxia Inhibits Cavin-1 and Cavin-2 Expression and Down-Regulates Caveolae in Adipocytes

Claire Regazzetti,* Karine Dumas,* Sandra Lacas-Gervais, Faustine Pastor, Pascal Peraldi, Stéphanie Bonnafous, Isabelle Dugail, Soazig Le Lay, Philippe Valet, Yannick Le Marchand-Brustel, Albert Tran, Philippe Gual, Jean-François Tanti, Mireille Cormont, and Sophie Giorgetti-Peraldi

INSERM Unité 1065 (C.R., K.D., F.P., Y.L.M.-B., J.-F.T., M.C., S.G.-P.), C3M, Mediterranean Research Centre for Molecular Medicine, Team 7 (Cellular and Molecular Physiopathology of Obesity and Diabetes), Unité de Formation et de Recherche (UFR) Médecine (C.R., K.D., F.P., P.P., S.B., Y.L.M.-B., A.T., P.G., J.-F.T., M.C., S.G.-P.), and INSERM Unité 1065 (S.B., A.T., P.G.), C3M, Mediterranean Research Centre for Molecular Medicine, Team 8 (Hepatic Complications in Obesity), University of Nice, Sophia Antipolis F-06204 Nice, France; Centre Commun de Microscopie Appliquée (S.L.-G.), University of Nice, Sophia Antipolis, UFR Sciences, Parc Valrose, F-06108 Nice, France; Unité Mixte de Recherche Centre National de la Recherche Scientifique 7277 (P.P.), Unité Mixte de Recherche INSERM Unité 1091, UFR Médecine, F-06107 Nice, France; Centre Hospitalier Universitaire de Nice, Digestive Center (S.B., A.T.), Nice F-06202, Cedex 3, France; INSERM Unité Mixte de Recherche S872 (I.D.), Centre de Recherche des Cordeliers, Eq8, F-75006 Paris, France; INSERM Unité 1063 (S.L.L.), Stress Oxydant et Pathologies Métaboliques, Institut de Biologie en Santé, F-49933 Angers, France; and INSERM Unité Mixte de Recherche 1048 (P.V.), Institut des Maladies Métaboliques et Cardiovasculaires, Université Paul Sabatier, F-31432 Toulouse, France

During obesity, a hypoxic state develops within the adipose tissue, resulting in insulin resistance. To understand the underlying mechanism, we analyzed the involvement of caveolae because they play a crucial role in the activation of insulin receptors. In the present study, we demonstrate that in 3T3-L1 adipocytes, hypoxia induces the disappearance of caveolae and inhibits the expression of Cavin-1 and Cavin-2, two proteins necessary for the formation of caveolae. In mice, hypoxia induced by the ligation of the spermatic artery results in the decrease of cavin-1 and cavin-2 expression in the epididymal adipose tissue. Down-regulation of the expression of cavins in response to hypoxia is dependent on hypoxia-inducible factor-1. Indeed, the inhibition of hypoxia-inducible factor-1 restores the expression of cavins and caveolae formation. Expression of cavins regulates insulin signaling because the silencing of cavin-1 and cavin-2 impairs insulin signaling pathway. In human, cavin-1 and cavin-2 are decreased in the sc adipose tissue of obese diabetic patients compared with lean subjects. Moreover, the expression of cavin-2 correlates negatively with the homeostatic model assessment index of insulin resistance and glycated hemoglobin level. In conclusion, we propose a new mechanism in which hypoxia inhibits cavin-1 and cavin-2 expression, resulting in the disappearance of caveolae. This leads to the inhibition of insulin signaling and the establishment of insulin resistance. (*Endocrinology* 156: 789–801, 2015)

Oxygen homeostasis is required for normal cell and tissue function. During hypoxia, cells establish cellular and metabolic responses to limit their oxygen consumption. Hypoxia decreases cell proliferation, switches metabolism

from oxidative phosphorylation to glycolysis, switches from oxidative glucose metabolism to reductive glutamine metabolism to promote fatty acid synthesis, and promotes angiogenesis to increase oxygen supply to cells (1–6).

ISSN Print 0013-7227 ISSN Online 1945-7170

Printed in U.S.A.

Copyright © 2015 by the Endocrine Society

Received August 5, 2014. Accepted December 8, 2014.

First Published Online December 18, 2014

* C.R. and K.D. contributed equally to the work.

Abbreviations: Ct, cycle threshold; DRM, detergent-resistant membrane; EM, electron microscope; Glut, glucose transporter; HIF, hypoxia-inducible factor; IR, insulin receptor; REDD1, regulated in development and DNA damage responses; siRNA, small interfering RNA.

Hypoxia also plays an important role in the dysfunction of the adipose tissue during obesity and the development of insulin resistance. Indeed, the expansion of the adipose tissue during obesity is associated with the development of hypoxic areas in obese mice (*ob/ob* mice and dietary induced obesity) and in overweight/obese patients (7–12).

Adipose tissue hypoxia, mainly through the activation of its master transcription factor, hypoxia-inducible factor (HIF)-1, induces a dysregulation of adipokines secretion, (7, 9, 13, 14), and contributes to the development of inflammation, by promoting macrophages and T lymphocytes accumulation and by inducing inflammatory phenotype in macrophages (9–11, 13, 15, 16). Modulation of HIF-1 α expression has an impact on the development of obesity and insulin resistance. Overexpression of HIF-1 α in adipocytes leads to the development of adipose tissue inflammation associated with fibrosis and insulin resistance in mice (17). Inhibition of HIF-1 α or HIF-1 β expression protects mice from obesity-induced glucose intolerance and insulin resistance and ameliorates adipose tissue dysfunction (18–22).

At the cellular level, hypoxia inhibits insulin-induced signaling pathways and induces insulin resistance in adipocytes through an HIF-1-dependent mechanism (23, 24). However, the precise molecular mechanisms by which hypoxia induces insulin resistance remains to be identified.

The insulin receptor is mainly localized within caveolae at the plasma membrane (25–27). Caveolae are small invaginations of the plasma membrane localized in lipid raft area and are particularly abundant in adipocytes in which they can represent up to 50% of the plasma membrane surface (28–30). Caveolae are involved in protein endocytosis, intracellular trafficking, lipid homeostasis, and signal transduction (30). Caveolae formation depends on the presence of specific proteins, such as the structural proteins caveolins and peripheral proteins cavins (28, 31). Caveolins 1–3 are essential for the formation of caveolae, and the absence of caveolin-1 expression leads to the disappearance of caveolae structures (32, 33). However, caveolins are not the sole proteins implicated in caveolae formation, and multiple proteins ensure the formation of caveolae. Among these proteins, cavins (PTRF/cavin-1, SDPR/cavin-2, SRBC/cavin-3 and MURC/cavin-4) are crucial for caveolae processing. Cavin complex is recruited to caveolin at the plasma membrane through membrane lipids and proteins interactions. Cavin-1 is required for caveolae formation, whereas cavin-2 is involved in the generation of caveolar membrane curvature (31, 34–37). Cavin-3 regulates caveolae endocytosis, whereas the expression of cavin-4 is restricted to the muscle (29, 38). The expression levels and cellular localizations of each protein

are tightly regulated and are required for the correct formation of caveolae. The absence of caveolin-1 or cavins leads to the loss of caveolae (39, 40). This absence of caveolae results in a variety of disease such as lipodystrophy, muscular dystrophy, cardiovascular disease, and cancer (41–43).

Some studies have shown that insulin receptor is localized within caveolae (26, 44, 45). A functional role of caveolae in insulin signaling is suggested by the observation that some lipodystrophic patients with severe insulin resistance present mutations in caveolin-1 or Cavin-1 (41, 42) and that the caveolar localization of the insulin receptor is necessary for its activation in adipocytes because caveolin-1-deficient cells have impaired insulin signaling (46).

To identify mechanisms implicated in the development of insulin resistance in response to hypoxia, we have investigated the effect of hypoxia on caveolae formation. We show that *in vivo* and in intact cells, hypoxia decreases cavin-1 and cavin-2 expression in adipocytes, associated with a loss of caveolae. Cavin expression is also decreased in adipose tissue from obese diabetic patients and its down-regulation in mouse adipocytes inhibits insulin signaling. Together, these observations suggest that hypoxia participates in the establishment of insulin resistance in adipose tissue through a down-regulation of caveolae that leads to a decrease in insulin signaling pathway.

Materials and Methods

Materials

Insulin was obtained from Life Technologies. Antibodies were obtained from the following companies: regulated in development and DNA damage responses (REDD1) and cavin-2 from Proteintech; phosphotyrosine from Cell Signaling Technology; insulin receptor (IR) and ERK2 from Santa Cruz Biotechnology; tubulin from Sigma-Aldrich; cavin-1 and flotillin from BD Biosciences; and glucose transporter (Glut)-1 from Abcam. Control small interfering RNA (siRNA) and siRNA directed against cavin-1, cavin-2, or HIF-1 α were purchased from Thermo Scientific. The primer sets for real-time PCR were purchased from Eurogentec. Culture media were obtained from Life Technologies. Inhibitors were obtained from Calbiochem.

Cell culture

3T3-L1 fibroblasts were obtained from the American Type Culture Collection (CL-173) and grown and induced to differentiate in adipocytes as previously described (23). Briefly, 3 days after confluence, 3T3-L1 fibroblasts were treated for 2 days with DMEM and 10% fetal calf serum (vol/vol) supplemented with isobutyl methylxanthine (250 nmol/L), dexamethasone (250 nmol/L), rosiglitazone (10 μ mol/L), and insulin (800 nmol/L) and then for two additional days with DMEM and 10% fetal calf serum containing 800 nmol/L insulin. The adipocytes were used between days 2 and 7 after the end of the differentiation protocol when the adipocyte phenotype appeared in more than 90% of the cells.

The isolation and properties of hMADS cells have been described by Plaisant et al (47). Adipocyte differentiation was performed as described previously (48). Confluent cells were cultured in DMEM/Ham's F12 media supplemented with transferrin (10 $\mu\text{g}/\text{mL}$), insulin (0.86 μM), T_3 (0.2 nmol/L), dexamethasone (1 $\mu\text{mol}/\text{L}$), isobutyl-methylxanthine (100 $\mu\text{mol}/\text{L}$), and rosiglitazone (500 nmol/L). Three days later, the medium was changed (dexamethasone and isobutylmethylxanthine were omitted).

Hypoxia treatment

For hypoxic treatment, the medium was replaced by DMEM containing 0.5% BSA and incubated within hypoxystation H35 (AES Chemunex) calibrated at 1% O_2 , 94% nitrogen, and 5% CO_2 for 16 hours.

Cell fractionation

Plasma membranes were prepared as previously described (49). OptiPrep fractionation (Sigma-Aldrich) was realized as fol-

lows: 3T3-L1 adipocytes were lysed with lysis buffer [50 mmol/L HEPES (pH 7.4), 150 mmol/L NaCl, 10 mmol/L EDTA, 10 mmol/L $\text{Na}_4\text{P}_2\text{O}_7$, 100 mmol/L NaF, 2 mmol/L vanadate, protease inhibitor cocktail (Complete; Roche)] containing Triton X-100 (1 μL per 10 mg protein) for 1 hour at 4°C. After shaking, the lysate was centrifuged 10 minutes at $110 \times g$. Six hundred microliters of supernatant mixed with 400 μL of OptiPrep density gradient medium (Sigma-Aldrich) were placed at the bottom of an ultracentrifuge tube and overlaid with 2 mL of 30% sucrose and 1 mL of lysis buffer. The gradient was formed after 2 hours of ultracentrifugation at 33 000 rpm in a TLS50 rotor. The mixture was divided into 10 fractions collected from the top of the tube and analyzed by Western blot.

Transfection of siRNA

3T3-L1 adipocytes were used for reverse transfection 7 days after the induction of differentiation. 3T3-L1 adipocytes were trypsinized, and control siRNA, or siRNA directed against HIF-1 α , cavin-1, or cavin-2 (40 pmol) were transfected using INTERFERin (Polyplus Transfection) according to the protocol of Kilroy et al (50). Briefly, siRNA complexes (80 nmol/L final concentration) were incubated with INTERFERin and lay onto the wells. 3T3-L1 adipocytes were trypsinized and added to the siRNA/INTERFERin complex solution. The adipocyte phenotype after transfection was assessed by visualization of lipid droplets, staining with oil red O, and expression of peroxisomal proliferator-activated receptor- γ protein (Regazzetti, C., K. Dumas, unpublished data).

Western blot analysis

Serum-starved cells were treated with ligands, chilled to 4°C, and washed with ice-cold PBS (6 mmol/L Na_2HPO_4 ; 1 mmol/L KH_2PO_4 , pH 7.4; 140 mmol/L NaCl; 3 mmol/L KCl) and solubilized with RIPA buffer [50 mmol/L Tris, pH 7.5; 150 mmol/L NaCl; 1% Nonidet P40; 0.1% sodium dodecyl sulfate; 0.5% Na deoxycholate; 1 mmol/L orthovanadate; 5 mmol/L NaF; 2.5 mmol/L $\text{Na}_4\text{P}_2\text{O}_7$; and Complete protease inhibitor cocktail (Roche Diagnostics)] for 30 minutes at 4°C.

Epididymal fat pads were frozen in liquid nitrogen and stored at -80°C until they were used. Tissues were solubilized by sonification in ice-cold buffer containing 20 mmol/L Tris (pH 7.5), 150 mmol/L NaCl, 2 mmol/L orthovanadate, 100 mmol/L NaF, 10 mmol/L $\text{Na}_4\text{P}_2\text{O}_7$, and completed with 1% Triton X-100 and Complete protease inhibitor cocktail (Roche Diagnostics).

Lysates were centrifuged (14 000 rpm) for 10 minutes at 4°C, and the protein concentration was determined using BCA protein assay reagent (Thermo

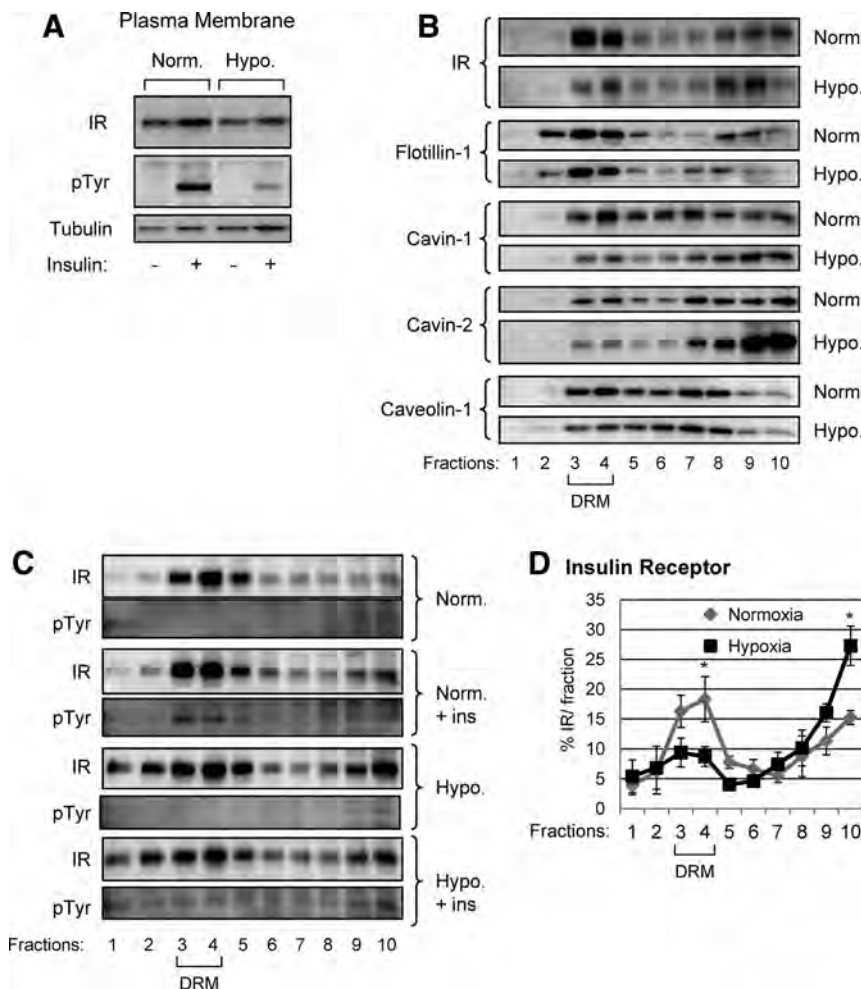


Figure 1. Hypoxia-induced delocalization of IR and caveolar proteins. A, 3T3-L1 adipocytes were incubated for 16 hours in normoxia or in hypoxia (1% O_2) before being stimulated with insulin (100 nM) for 5 minutes. Plasma membranes were analyzed by immunoblots with indicated antibodies. B, 3T3-L1 adipocytes were incubated for 16 hours in normoxia or in hypoxia (1% O_2). C, 3T3-L1 adipocytes were incubated for 16 hours in normoxia or in hypoxia (1% O_2) before being stimulated with insulin (100 nM) for 5 minutes. Cell lysates were separated into 10 fractions from the lightest (fraction 1) to the heaviest (fraction 10) using OptiPrep density gradient fractionation (Sigma-Aldrich) and analyzed by Western blots with indicated antibodies. D, Quantification of IR of three experiments is shown. *, $P < .05$. Hypo, hypoxia; Norm, normoxia.

Fisher Scientific). Cell lysates were analyzed by Western blot. Immunoblots were revealed using a Fujifilm LAS-3000 imaging system. Quantifications were realized using Fujifilm MultiGauge or ImageJ softwares (National Institutes of Health, Bethesda, Maryland).

Hypoxia of epididymal adipose tissue by ligation of spermatic artery

C57BL/6/J mice were exposed to a 12-hour light, 12-hour dark schedule and had free access to water and standard chow diet. Mice were anesthetized, and the left spermatic artery was ligated to induce hypoxia on the fat pad for indicated periods of time. The right spermatic artery was not ligated, and the fat pad was used as an internal control. Mice woke up from the surgery and were kept for indicated periods of time before being killed by cervical dislocation. Epididymal adipose tissues were removed, freeze clamped in liquid nitrogen, and stored at -80°C until used. The Principles of Laboratory Animal Care (National Institutes of Health publication number 85–23, revised 1985 (<http://grants1.nih.gov/grants/olaw/references/phspol.htm>) as well the European Union guidelines on animal laboratory care (<http://ec.europa.eu/>

environment/chemicals/lab_animals/legislation_en.htm) were followed. All procedures were approved by the Animal Care Committee of the Faculty of Medicine of the Nice-Sophia Antipolis University (Nice, France).

Obese patients

Morbidly obese patients ($n = 8$ obese and $n = 7$ obese diabetic) were recruited through the Department of Digestive Surgery and Liver Transplantation (Nice hospital) where they underwent bariatric surgery for their morbid obesity. Bariatric surgery was indicated for these patients in accordance with French guidelines. Exclusion criteria were the presence of a hepatitis B or hepatitis C infection, excessive alcohol consumption (>20 g/d) or another cause of chronic liver disease as previously described (51–53). The characteristics of the study groups are described in Supplemental Table 1. Before surgery, fasting blood samples were obtained and used to measure alanine amino transferase, aspartate aminotransaminase, glucose, and insulin. Insulin resistance was calculated using the homeostatic model assessment index for insulin resistance (HOMA-IR) (54). Abdominal sc adipose tissue was obtained during surgery. Control

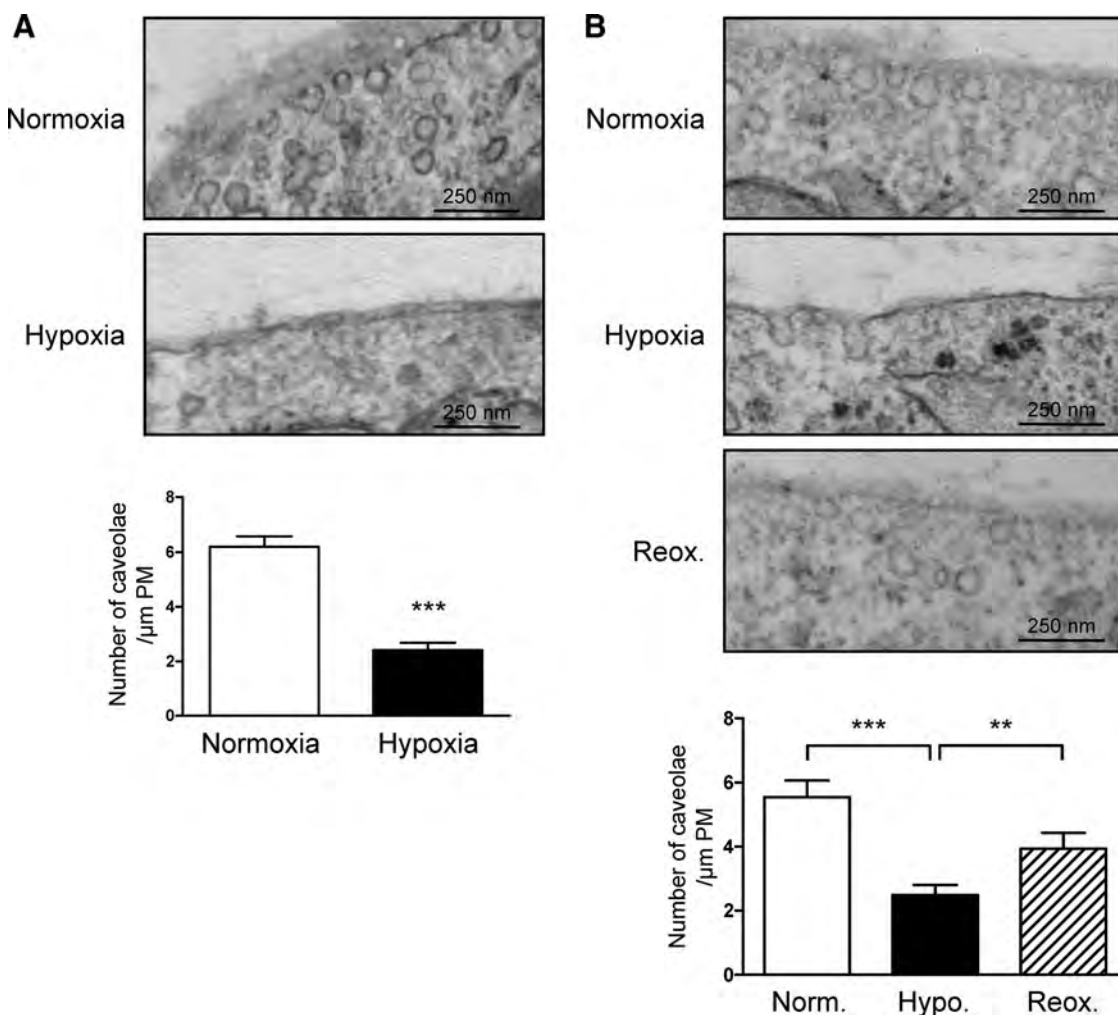


Figure 2. Hypoxia induced the loss of caveolae in 3T3-L1 adipocytes. 3T3-L1 adipocytes were incubated for 16 hours in normoxia or in hypoxia (1% O_2) (A) or reoxygenated (B) for 1 hour. Caveolae structure were identified by transmission EM. Quantification is performed after counting the number of caveolae and are expressed as number of caveolae per micrometer of plasma membrane (PM). ***, $P < .0001$; **, $P < .01$. Number of caveolae counted is as follows: normoxia: 1938, hypoxia: 1597 (A); normoxia: 1105, hypoxia: 1125, reox: 731 (B). Reox, reoxygenated.

sc adipose tissue was obtained from four lean subjects (two females and two males; aged 37.3 ± 11.5 y; body mass index of 20.9 ± 0.5 kg/m²) undergoing lipectomy for cosmetic purposes. Informed written consent was obtained from all subjects for this study, which was set up in accordance with French legislation regarding ethics and human research (Huriet-Serusclet). The Comité Consultatif de Protection des Personnes dans la Recherche Biomédicale de Nice approved the study (protocol 07/04:2003, number 03.017).

Real-time quantitative PCR analysis

Cells and murine tissues

RNA was isolated from adipocytes or epididymal fat pads (TRIZOL; Invitrogen), and cDNA was synthesized using Tran-

scriptor first-strand cDNA synthesis kit (Roche Diagnostics). Real-time quantitative PCR was performed with sequence detection systems (StepOne; Applied Biosystems) and SYBR Green dye. Gene expression values were calculated based on the comparative cycle threshold (Ct) method ($2^{-\Delta\Delta Ct}$). The levels of mRNA were normalized to the expression value of the housekeeping gene 36B4 and expressed relative to the mean of the group of normoxic controls. The primer sequence can be obtained upon request.

Human tissues

Total RNA was extracted from human tissues using RNeasy minikit (QIAGEN) and treated with Turbo DNA-free (Applied Biosystems) following the manufacturer's protocol. The quantity and quality of the RNA were determined using the Agilent 2100 Bioanalyzer with an RNA 6000 Nano kit (Agilent Technologies). Total RNA (1 μ g) was reverse transcribed with a high-capacity cDNA reverse transcription kit (Applied Biosystems). Real-time quantitative PCR was performed in duplicate for each sample using the StepOne real-time PCR system (Applied Biosystems). The TaqMan gene expression assays were purchased from Applied Biosystems: *Cavin-2* (serum deprivation response, cavin-2) (Hs00190538_m1); *Cavin-1* (polymerase I and transcript release factor, cavin-1) (Hs00396859_m1); *Glut4* (*SLC2A4*) (Hs00168966_m1); *HIF-1A* (hypoxia inducible factor-1) (Hs00153153_m1); and *RPLP0* (ribosomal phosphoprotein large P0) (Hs99999902_m1). Gene expression values were normalized to the expression value of the housekeeping gene *RPLP0* and calculated based on the comparative Ct method ($2^{-\Delta\Delta Ct}$) as described by the manufacturer's protocols.

Electron microscopy

For ultrastructural analysis, cells were fixed in 1.6% glutaraldehyde in 0.1 M phosphate buffer (pH 7.4) at 4°C, rinsed in 0.1 mol/L cacodylate buffer, and postfixed for 1 hour in 1% osmium tetroxide and 1% potassium ferrocyanide in 0.1 mol/L cacodylate buffer to enhance the staining of membranes. Cells were rinsed in cold distilled water, quickly dehydrated in cold ethanol, and lastly embedded in epoxy resin. Contrasted ultrathin sections (70 nm) were analyzed under a JEOL 1400 transmission electron microscope (EM) mounted with a Morada Olympus charge-coupled device camera.

Statistical analysis

The statistical significance of the differential gene expression between two

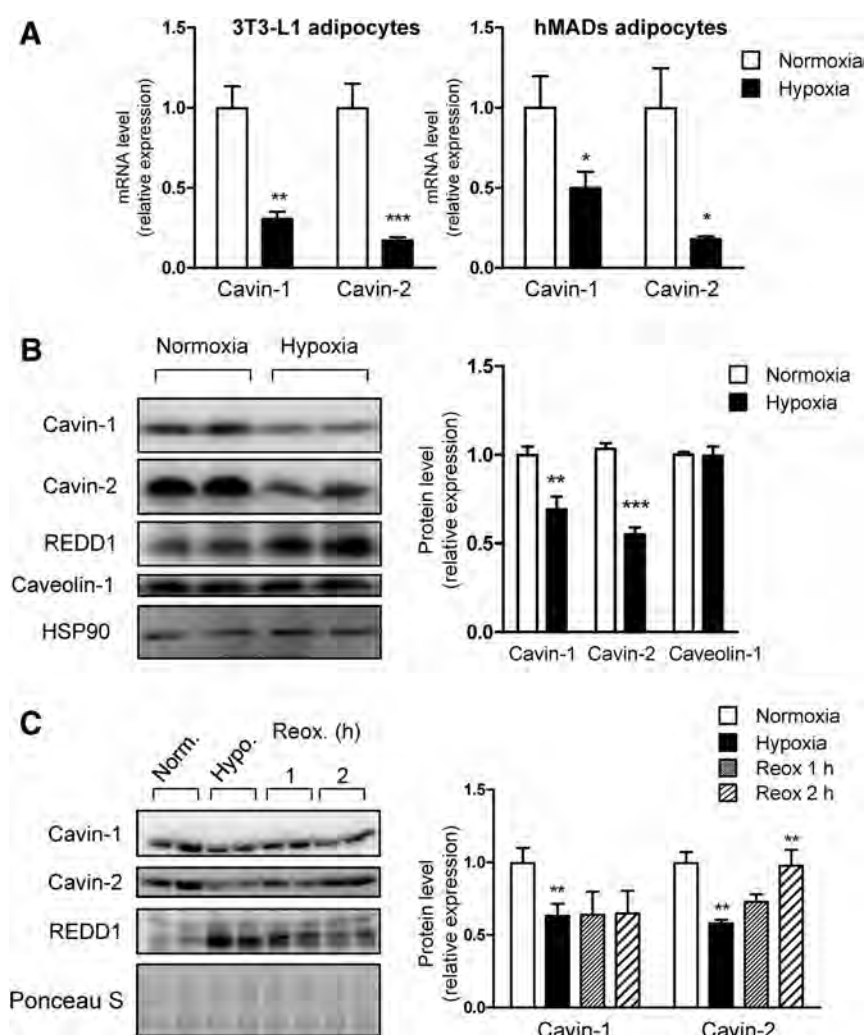


Figure 3. Hypoxia decreased cavin-1 and cavin-2 expression. A, 3T3-L1 adipocytes and hMADS adipocytes were incubated for 16 hours in normoxia or in hypoxia (1% O₂), and mRNA expression was determined by quantitative RT-PCR. B, 3T3-L1 adipocytes were incubated for 16 hours in normoxia or in hypoxia (1% O₂) and protein expression was analyzed by specific immunoblots. Quantification of relative expression of cavin-1, cavin-2, and caveolin-1 (normalized to tubulin protein level) is shown (n = 8). C, 3T3-L1 adipocytes were incubated for 16 hours in normoxia or in hypoxia (1% O₂), or reoxygenated for 1 or 2 hours, and protein expression was analyzed by specific immunoblots. Quantification of relative expression of cavin-1 and cavin-2 is shown (n = 3). Ponceau S is used as a loading control. ***, $P < .0001$; **, $P < .01$; *, $P < .05$. HSP, heat shock protein; Hypo, hypoxia; Norm, normoxia.

groups was determined using the nonparametric Mann-Whitney test with the δ Ct of each group. Correlations were analyzed using the Spearman's rank correlation test. $P < .05$ is considered as significant.

Results

Hypoxia-modulated insulin receptor localization in 3T3-L1 adipocytes

Hypoxia inhibited insulin-tyrosine phosphorylation of insulin receptor in adipocytes (23). Because the localization of

insulin receptor in caveolae microdomains in plasma membrane is required for its activation, we first evaluated its cellular localization and phosphorylation in normoxia and in response to hypoxia. 3T3-L1 adipocytes were stimulated with insulin, plasma membranes were extracted, and insulin receptor within this fraction was analyzed by Western blots. Hypoxia inhibited insulin receptor tyrosine phosphorylation without significantly modifying its amount at the plasma membrane (Figure 1A). The distribution of the IR was then evaluated by cellular fractionation [using the Opti-Prep density gradient method (Sigma-Aldrich)] in normoxia or in

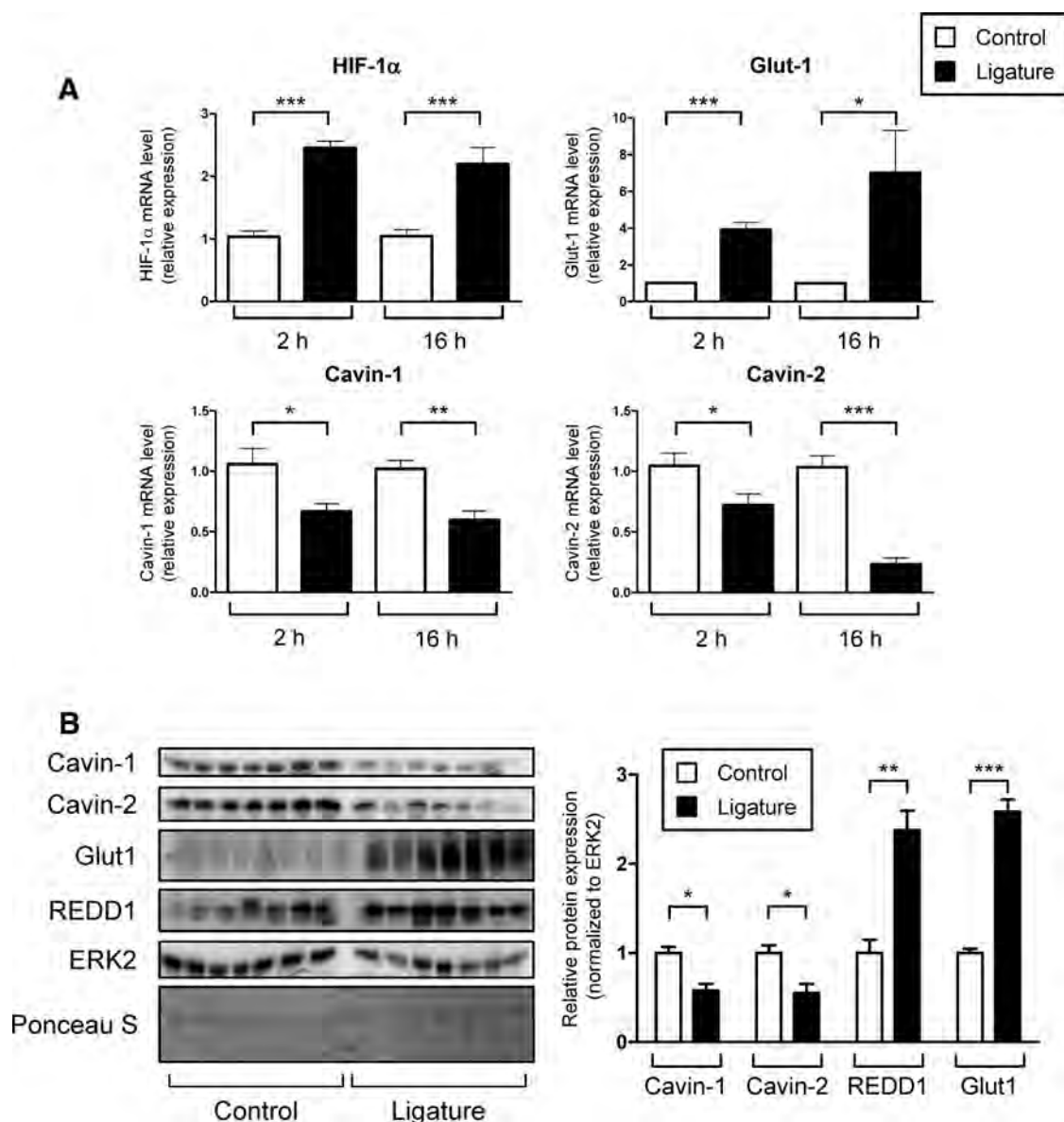


Figure 4. Ligature of spermatic artery induced hypoxia of epididymal adipose tissue and decreased cavin-1 and cavin-2 expression. Spermatic artery of mice were ligatured as described in *Materials and Methods*. Epididymal adipose tissues were removed and used to analyze mRNA expression after 2 and 16 hours (A) or protein expression after 16 hours (B). A, Results are expressed in a relative expression, with the control value taken as 1 and are the means \pm SE of eight mice in each group. B, Quantification of the relative expression of cavin-1, cavin-2, Glut-1, and REDD1 (normalized to ERK2) is shown (each point represents one mouse, $n = 7$). Ponceau S is shown as loading control. *, $P < .05$; **, $P < .01$; ***, $P < .001$.

hypoxia. Cell lysates were resolved into 10 fractions from the lightest (fraction 1) to the heaviest (fraction 10) and analyzed by Western blots (Figure 1B). Detergent-resistant membrane (DRM) fractions were identified by immunoblotting of flotillin-1. Flotillins were initially discovered as caveolae-associated integral proteins (55), but they still localize to lipid-raft membranes in the absence of caveolins (56, 57). Therefore, although they are not exclusively located in caveolar domains, flotillins are considered as a good marker for total lipid rafts, biochemically preserved, and recovered in DRMs. In normoxia, IR was mainly located within the DRM fractions (3 and 4) to heavier fractions (Figure 1B). In Figure 1C, 3T3-L1 adipocytes were stimulated with insulin prior to cellular fractionation. In normoxia, insulin stimulated the tyrosine phosphorylation of its receptor located in DRM fractions. In hypoxia, the IR in fractions 3 and 4 was no longer phosphorylated in response to insulin.

Hypoxia induced the disappearance of caveolae in 3T3-L1 adipocytes

Because hypoxia inhibited IR phosphorylation and distribution at the plasma membrane, we evaluated the effect of

hypoxia on the integrity of caveolae. We evaluated the distribution of cavins proteins, cavin-1 and cavin-2, in response to hypoxia by cell fractionation (Figure 1B). In normoxia, cavin-1 and cavin-2 were mainly detected in fractions 3 and 4 and in fewer amount in heavier fractions. Hypoxia induced a change in the distribution of these proteins. Indeed, cavin-1 and cavin-2 amounts shifted from lightest fractions to heavier fractions (fractions 9 and 10). This modification of protein distribution suggests that hypoxia could affect the formation of caveolae in adipocytes.

The integrity of caveolae in 3T3-L1 adipocytes incubated in normoxia or hypoxia was determined by transmission EM. In Figure 2A, caveolae were detected near the plasma membrane in 3T3-L1 adipocytes. Hypoxia incubation induced the disappearance of caveolae in this region. We have previously demonstrated that the inhibition of the insulin signaling pathway by hypoxia can be reversed after cell reoxygenation (23). Accordingly, the reoxygenation of adipocytes restored the presence of caveolae at the cell surface (Figure 2B).

Hypoxia decreased expression of cavin-1 and cavin-2

Cell fractionation is not a reflection of the quantity of proteins within the cell, but it rather reflects their cellular localization. Because a decrease in cavins and caveolin has been shown to alter caveolae structure (39, 40, 58), we investigated whether the expression of these proteins was modified by hypoxia in murine (3T3-L1) and human (hMADS) adipocytes. In 3T3-L1 and hMADS adipocytes, hypoxia inhibited the expression of mRNA of cavin-1 and cavin-2 (Figure 3A). In 3T3-L1 adipocytes, hypoxia decreased significantly the protein expression of cavin-1 and cavin-2 (Figure 3B). In contrast, the expression of caveolin-1 was not modified after hypoxia treatment (Figure 3B). Because reoxygenation restored caveolae at the cell surface, we have determined the effect of reoxygenation on cavin-1 and cavin-2 expression in 3T3-L1 adipocytes. As shown in Figure 3C, reoxygenation restored cavin-2 expression without any significant effect on cavin-1 protein expression.

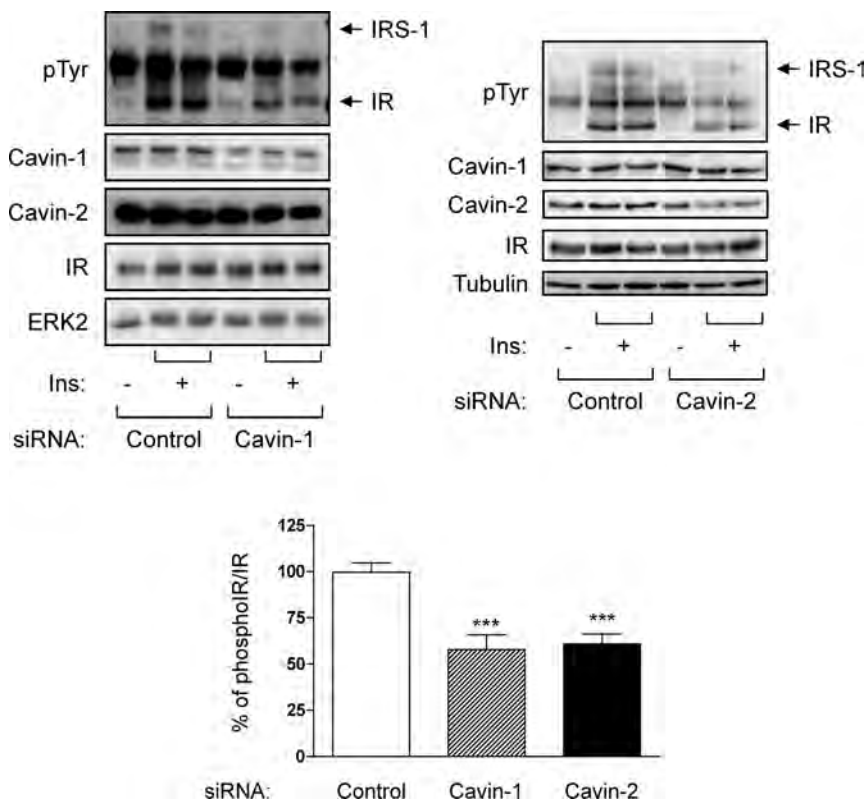


Figure 5. Inhibition of cavin-1 and cavin-2 expression inhibited insulin receptor phosphorylation. 3T3-L1 adipocytes were transfected with control or siRNA against cavin-1 or cavin-2. Forty-eight hours after transfection, 3T3-L1 adipocytes were stimulated with insulin (100 nM) for 5 minutes. Proteins were analyzed by immunoblots using indicated antibodies. Phosphorylation of insulin receptor is normalized using insulin receptor, and quantification of three independent experiments in duplicate is shown. ***, $P < .001$. Ins, insulin.

To study the effect of hypoxia on protein expression in mice, we have set up a protocol to induce hypoxia in epididymal adipose tissue by the ligation of spermatic artery. The left spermatic artery of C57BL6/J mice was ligated to induce hypoxia on the fat pad for the indicated periods of time. The right spermatic artery was not ligated, and the fat pad was used as an internal control. Ligation of spermatic artery induced hypoxia of the epididymal adipose tissue, detected by the increase of HIF-1 α and Glut-1 mRNA expression (Figure 4A). Hypoxia decreased cavin-1 and cavin-2 mRNA expression in epididymal fat pads as soon as after 2 hours of ligation. Protein expression was also studied, and we observed that hypoxia inhibited cavin-1 and cavin-2 expression in hypoxic fat pads (Figure 4B). As control, the expression of REDD1, a hypoxia-induced protein (59, 60), and Glut-1 was increased. ERK2 and Ponceau S are shown as loading control.

Decrease in expression of cavin-1 and cavin-2 inhibited insulin signaling pathway in adipocytes

Because cavins are key components of caveolae, we investigated the outcome of the decrease in expression of cavin-1 and cavin-2 on insulin receptor activity. 3T3-L1 adipocytes were transfected with siRNA against cavin-1 or cavin-2 and stimulated with insulin (Figure 5). Transfection of cavins siRNA decreases the expression of cavins to a level similar to hypoxia treatment. Down-regulation

of the expression of cavin-1 or cavin-2 inhibited IR tyrosine phosphorylation (respectively, 43% \pm 8% and 40% \pm 5% of inhibition).

Hypoxia decreased the expression of cavin-1 and cavin-2 through a HIF-1 α dependent mechanism

Because the expression of cavin-1 and cavin-2 is regulated by hypoxia, we investigated the implication of HIF-1 transcription factor in this mechanism. Indeed, we previously reported that HIF-1 is implicated in the inhibition of insulin signaling in response to hypoxia (23). 3T3-L1 adipocytes were transfected with siRNA against HIF-1 α or treated with echinomycin, a HIF-1 α inhibitor, prior to being exposed to hypoxia for 16 hours (Figure 6).

The decrease of expression of cavin-1 and cavin-2 induced by hypoxia was reversed after inhibition of HIF-1. Efficiency of echinomycin and silencing of HIF-1 α was evaluated by the down-regulation of REDD1 at the protein level (Figure 6) as previously reported (61). These results demonstrate that the expression of cavin-1 and cavin-2 was regulated by HIF-1 dependent mechanisms.

We then determined the involvement of HIF-1 in caveolae formation (Figure 7). Inhibition of HIF-1 α by siRNA restored the number of caveolae at the cell surface in hypoxia (Figure 7A). In parallel, the activation of HIF-1 by

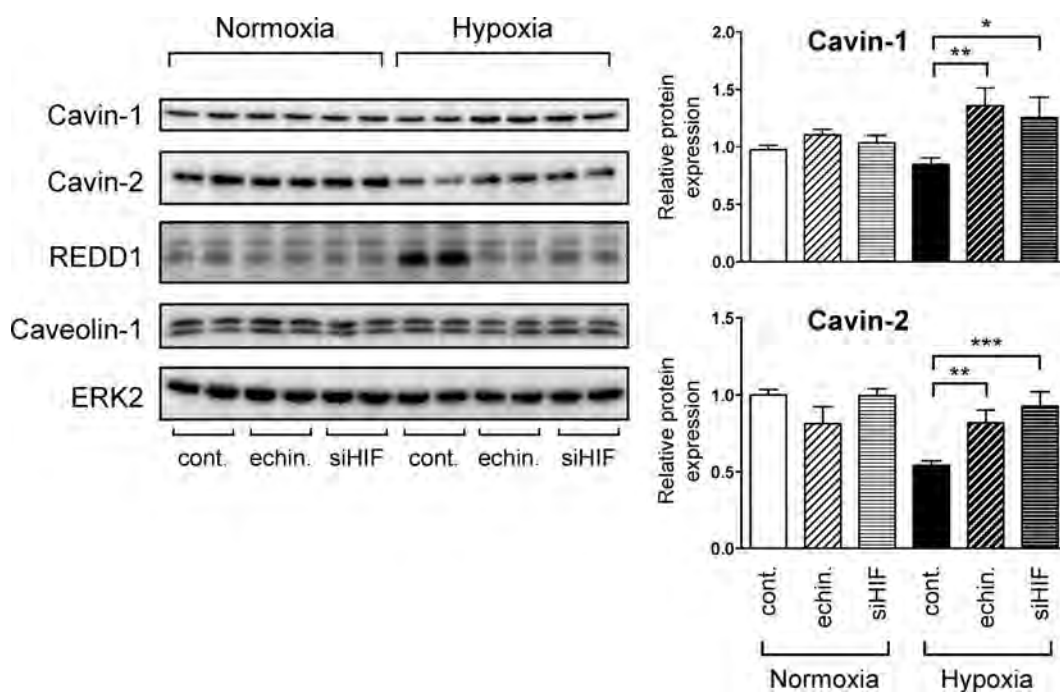


Figure 6. Inhibition of HIF-1 α restored cavin-1 and cavin-2 expression in hypoxia in 3T3-L1 adipocytes. 3T3-L1 adipocytes were transfected with control or HIF-1 α siRNA. Forty-eight hours after transfection, 3T3-L1 adipocytes were treated without or with echinomycin (20 nM) for 16 hours and incubated in normoxia or in hypoxia (1% O₂). Proteins were analyzed by immunoblots using the indicated antibodies. Quantification of expression of proteins is normalized using tubulin (n = 3 independent experiments in duplicate). *, P < .05; **, P < .01; ***, P < .001. cont, control.

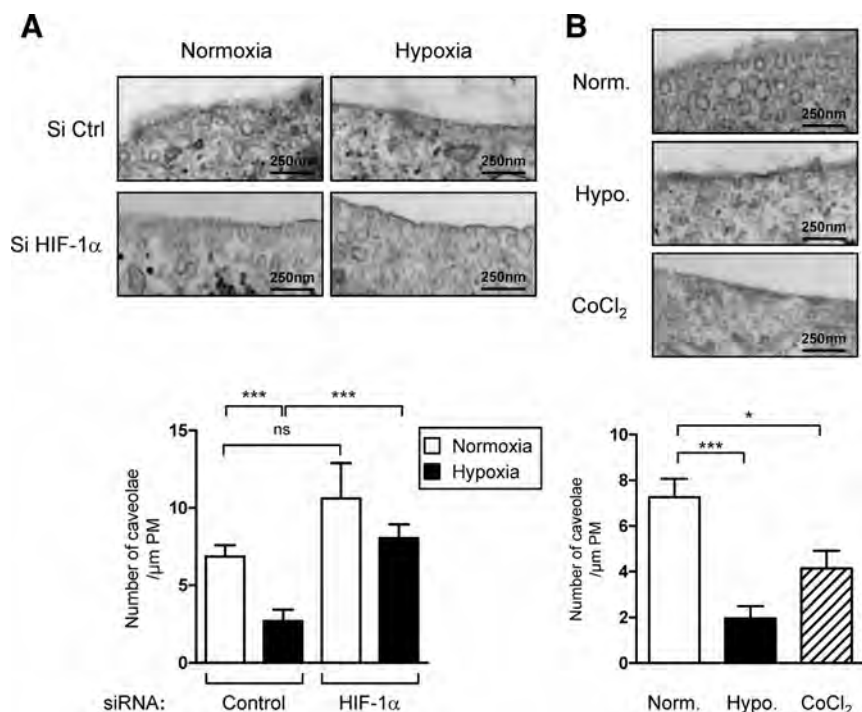


Figure 7. Hypoxia induced the loss of caveolae through HIF-1 activity in 3T3-L1 adipocytes. A, 3T3-L1 adipocytes were transfected with control or HIF-1 α siRNA before being incubated in normoxia or in hypoxia for 16 hours. B, 3T3-L1 adipocytes were incubated for 16 hours in normoxia or in hypoxia (1% O₂) or treated with CoCl₂ (200 μ M). Caveolae structures were identified by transmission EM. Quantification is performed after counting the number of caveolae and are expressed as the number of caveolae per micrometer of plasma membrane (PM). ***, $P < .0001$; *, $P < .05$. Numbers of caveolae counted are as follows: control siRNA normoxia, 431; hypoxia, 245; HIF-1 siRNA normoxia, 614; hypoxia, 728 (A); normoxia, 401; hypoxia, 226; CoCl₂, 1241 (B). Hypo, hypoxia; Norm, normoxia.

CoCl₂ inhibited the caveolae at the cell surface (Figure 7B). Taken together, these observations suggest that hypoxia decreased caveolae formation through a HIF-1-dependent pathway.

Insulin resistance is associated with a decreased in the expression of cavin-1 and 2 in adipose tissue of obese patients

Because obesity is associated with the hypoxia of the adipose tissue and insulin resistance, we evaluated the expression of HIF-1 α , cavin-1, and cavin-2 in sc adipose tissue of lean subjects and obese patients without or with type 2 diabetes. As shown in Figure 8A, HIF-1 α mRNA expression was increased in the adipose tissues of obese and obese diabetic patients. In contrast, cavin-1 and cavin-2 were decreased only in sc adipose tissue of obese diabetic patients compared with lean subjects (Figure 8A). Furthermore, cavin-2 correlated positively with cavin-1 level and negatively with HOMA-IR (index used to evaluate insulin resistance) and glycated hemoglobin level (evaluating the average plasma glucose concentration over prolonged periods of time), which reflect the risk of developing diabetes-related complications.

This indicates that the decreased expression of cavin in adipose tissue could be associated with insulin resistance.

Discussion

Hypoxia promotes inflammation, impairs adipose tissue endocrine function, and contributes to insulin resistance (7–10, 12, 13, 62). We and others (23, 24) have demonstrated that hypoxia induces insulin resistance in adipocytes through the inhibition of the insulin receptor autophosphorylation and signaling pathway. In the attempt to understand the mechanisms implicated, we demonstrate that hypoxia inhibits the expression of caveolar proteins cavin-1 and cavin-2 in adipocytes, which is accompanied by the loss of caveolae at the plasma membrane. Moreover, cavin-1 and cavin-2 expression is decreased in adipose tissue from obese diabetic patients. These observations prompt us to propose that hypoxia induces insulin resistance through the down-regulation of caveolae, leading to the impaired insulin signaling pathway.

Caveolae are abundant in adipocytes in which they play a major role in insulin signaling (27, 44). IRs are mainly localized at the plasma membrane in caveolae, with little insulin receptors found outside from the caveolae (26, 44, 45, 63). Caveolar localization of insulin receptor is required for its activation. Indeed, the modulation of caveolin-1 expression and caveolae structures affects insulin signaling pathway (27, 45, 63). Moreover, the absence of cavin-1 and cavin-2 in 3T3-L1 adipocytes inhibits insulin-induced activation of its receptor. This is in accordance with the observation that the deficiency of cavin-1 generates mice without caveolae and resistant to diet-induced obesity with an abnormal lipid metabolism and insulin signaling pathway (39). Hypoxia regulates only cavin expression but not the expression of caveolin-1. The expression and distribution of cavin might be affected, whereas the caveolin-1 distribution or expression seems unaltered but still leads to caveolae disassembly. Briand et al (64) have recently reported that during extreme fat cell shrinkage in adipocytes, caveolin-1 expression was unaffected, whereas cavin-1 and cavin-2 were targeted to degradation, resulting in caveolae disassembly. The deletion of cavin-2 in endothe-

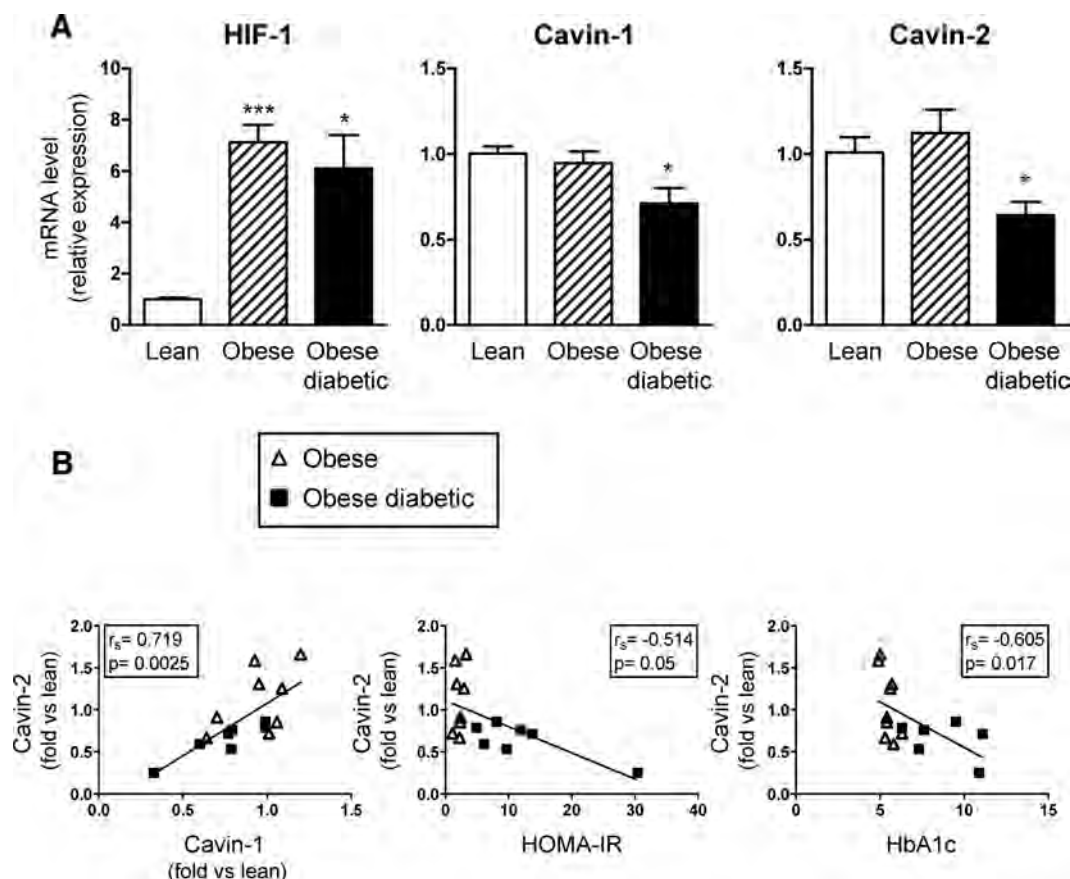


Figure 8. Cavin-1 and cavin-2 expression was decreased in adipose tissue of obese diabetic patients. A, Biopsies of sc adipose tissues from lean ($n = 4$), obese without ($n = 8$), or obese with diabetes ($n = 7$) were collected. Total RNAs were extracted and the relative amount of cavin-1, cavin-2, and HIF-1 α were determined by real-time quantitative PCR. Results are expressed in arbitrary units with the control value (lean subjects) taken as 1 and are the means \pm SE of the number of subjects in each group. *, $P < .05$; ***, $P < .0001$. B, Correlations between cavin-2 and cavin-1 expression levels, cavin-2 and HOMA-IR, and HbA1c were analyzed using a Spearman's rank correlation test (white triangle, obese patients; black square, obese diabetic patients). HbA1c, glycated hemoglobin.

lial cells causes flattening of caveolae perturbing neither caveolin-1 expression nor oligomerization (65). Therefore, cavins can be viewed as critical caveolar organizers whose distribution or expression would influence caveolae integrity. In this regard, cavins appear as early sensors of physiological events of caveolae dynamics. Moreover, our observations clearly demonstrate that insulin receptor localization within caveolae is mandatory for its activation.

During obesity, adipose tissue oxygen tension is decreased to reach 2% (8–11). Hypoxia regulates inflammation and angiogenesis but also general cellular metabolism including glucose use. In the present study, we demonstrate that hypoxia can regulate caveolae formation through the regulation of cavin proteins expression. Indeed, hypoxia decreases the expression of cavin-1 and cavin-2, in murine and human adipocytes, and also in a model of ligation of the spermatic artery to induce hypoxia of the epididymal adipose tissue. Moreover, this inhibition of the expression of cavins is accompanied by the loss of caveolae at the surface of 3T3-L1 adipocytes. Cavins con-

tribute to the stability of caveolae because the down-regulation of cavin-1 shortens the half-life of caveolin-1, likely targeting caveolin-1 for lysosomal degradation (36, 37). Cavin proteins might also serve as a bridge for other caveolar proteins such as EH domain containing 2 (66) and organize cytoskeleton connection (39). Cavin redistribution to cytosolic compartments might be linked to cavin degradation, an event reported in adipocytes and in others cells to signal caveolae disassembly (40, 64).

Hypoxia has been shown to regulate gene expression in human adipocytes. Among 1346 genes differently regulated by hypoxia, cavin-2 expression is decreased (3.76-fold change) compared with the normoxic conditions (67). Inhibition of cavin-1 and cavin-2 expression is dependent on the HIF-1 transcription factor. The molecular mechanisms implicated in the regulation of cavin-1 and cavin-2 expression remain unknown. A sequence analysis reveals that cavin-2 promoter contains HRE sequences, but we cannot rule out that other transcription factors could participate in the regulation of the expression of cavins. For instance, Krüppel-like factor-7, activating transcription

factor, Fos-like antigen 2, and Jun transcription factors are involved in the regulation of gene expression in response to hypoxia in adipocytes, and this activation requires HIF-1 α (68).

Insulin resistance and type 2 diabetes are linked to obesity. Hypoxia has been proposed to play a crucial role in the establishment of adipose tissue insulin resistance, and we found that HIF-1 α expression is increased in adipose tissue during obesity. This is in agreement with previous studies showing an up-regulation of the expression of HIF-1 α mRNA in adipose tissue during obesity in mice (genetic obesity or high fat diet) (10, 11, 24, 69) and in humans (70). Because the expression of HIF-1 α is not different between obese and obese diabetic patients, we cannot rule out that the activity of HIF-1 will be modified between obese and obese diabetic patients because HIF-1 α regulation mainly requires posttranslational mechanisms (3). The expression of cavin-1 and cavin-2 is significantly inhibited in adipose tissue of obese patients with type 2 diabetes. The decrease in cavin-2 expression correlated with insulin resistance as evaluated by HOMA-IR. Dysfunctional caveolae results in insulin resistance because patients with mutations of caveolin-1 or cavin-1 display lipodystrophy phenotype characterized by insulin resistance development (41, 42, 71, 72). Caveolae dysfunction is also implicated in several pathologies, such as muscular dystrophies, pulmonary hypertension in chronic obstructive pulmonary disease, bladder smooth muscle hypertrophy, and cancer (73, 74). Even if the role of caveolae in cancer development remains unclear, expression of cavin-1, cavin-2, and cavin-3 is down-regulated in breast cancer (75, 76). Because no correlation between HIF-1 α and cavin-2 has been revealed, this suggest that others factors, in addition to HIF-1, could participate the regulation of the expression of cavins during diabetes.

In conclusion, we propose that during obesity, hypoxia induces insulin resistance through the regulation of cavins expression. Inhibition of cavin-1 and cavin-2 expression induces the disappearance of caveolae leading to the inhibition of insulin signaling and establishment of insulin resistance.

Acknowledgments

We acknowledge Frédéric Bost (INSERM Unité 1065) for careful reading, Jerome Gilleron (INSERM Unité 1065) for helpful discussions, and Johanna Chiche (INSERM Unité 1065) for reagents. We gratefully acknowledge Veronique Corcelle and the C3M animal facility team for their valuable assistance with animal care. We also greatly acknowledge the Centre Commun de

Microscopie Appliquée (Université de Nice Sophia Antipolis, Microscopy and Imaging Platform, Côte d'Azur).

Address all correspondence and requests for reprints to: Sophie Giorgetti-Peraldi, PhD, INSERM Unité 1065, Centre Méditerranéen de Médecine Moléculaire, Bâtiment ARCHIMED, 151 Route Saint Antoine de Ginestière, BP 2 3094, F-06204 Nice Cedex 3, France. E-mail: peraldis@unice.fr.

Author contributions include the following: C.R. and K.D., designed and performed the experiments, researched and analyzed the data, contributed to the discussion, and reviewed the manuscript. S.L.-G., F.P., and S.B. contributed to the experiments and discussed the data. I.D., S.L.L., P.V., Y.L.M.-B., A.T., P.G., J.F.T., and M.C. analyzed the data, contributed to the discussion, and reviewed the manuscript. P.P. contributed to the experiments, discussed the data, and wrote and reviewed the manuscript. S.G.P. designed and performed the experiments, analyzed the data, and wrote and edited the manuscript. S.G.P. is the guarantor of this work, had full access to all the data, and takes full responsibility for the integrity of data and the accuracy of the data analysis.

This work was supported by INSERM (France), Société Francophone du Diabète, SFD/Roche Pharma, European Foundation for the study of Diabetes/Lilly European Diabetes Research Programme, Agence Nationale de la Recherche (Grant ANR-09-GENO-036 and "Investments for the Future" Labex Signalife Grant ANR-11-LABX-0028-01), the University of Nice-Sophia Antipolis, Region Provence-Alpes-Cote-d'Azur, Conseil Général des Alpes Maritimes, and the Programme Hospitalier de Recherche Clinique (Centre Hospitalier Universitaire of Nice). C.R. is a recipient of a fellowship of the Société Francophone du Diabète, and F.P. is a recipient of a fellowship from the Ministère de la Recherche et de l'Éducation.

Disclosure Summary: The authors have nothing to disclose.

References

1. Wise DR, Ward PS, Shay JE, et al. Hypoxia promotes isocitrate dehydrogenase-dependent carboxylation of α -ketoglutarate to citrate to support cell growth and viability. *Proc Natl Acad Sci USA*. 2011;108(49):19611–19616.
2. Metallo CM, Gameiro PA, Bell EL, et al. Reductive glutamine metabolism by IDH1 mediates lipogenesis under hypoxia. *Nature*. 2012;481(7381):380–384.
3. Semenza GL. HIF-1 mediates metabolic responses to intratumoral hypoxia and oncogenic mutations. *J Clin Invest*. 2013;123(9):3664–3671.
4. Forsythe JA, Jiang BH, Iyer NV, et al. Activation of vascular endothelial growth factor gene transcription by hypoxia-inducible factor 1. *Mol Cell Biol*. 1996;16(9):4604–4613.
5. Kim JW, Tchernyshyov I, Semenza GL, Dang CV. HIF-1-mediated expression of pyruvate dehydrogenase kinase: a metabolic switch required for cellular adaptation to hypoxia. *Cell Metab*. 2006;3(3):177–185.
6. Papandreou I, Cairns RA, Fontana L, Lim AL, Denko NC. HIF-1 mediates adaptation to hypoxia by actively downregulating mitochondrial oxygen consumption. *Cell Metab*. 2006;3(3):187–197.
7. Trayhurn P. Hypoxia and adipose tissue function and dysfunction in obesity. *Physiol Rev*. 2013;93(1):1–21.

8. **Pasarica M, Sereda OR, Redman LM, et al.** Reduced adipose tissue oxygenation in human obesity—evidence for rarefaction, macrophage chemotaxis and inflammation without an angiogenic response. *Diabetes*. 2008;58:718–725.
9. **Hosogai N, Fukuhara A, Oshima K, et al.** Adipose tissue hypoxia in obesity and its impact on adipocytokine dysregulation. *Diabetes*. 2007;56(4):901–911.
10. **Rausch ME, Weisberg S, Vardhana P, Tortoriello DV.** Obesity in C57BL/6J mice is characterized by adipose tissue hypoxia and cytotoxic T-cell infiltration. *Int J Obes (Lond)*. 2008;32:451–463.
11. **Ye J, Gao Z, Yin J, He Q.** Hypoxia is a potential risk factor for chronic inflammation and adiponectin reduction in adipose tissue of ob/ob and dietary obese mice. *Am J Physiol Endocrinol Metab*. 2007;293(4):E1118–E1128.
12. **He Q, Gao Z, Yin J, Zhang J, Yun Z, Ye J.** Regulation of HIF-1 α activity in adipose tissue by obesity-associated factors: adipogenesis, insulin, and hypoxia. *Am J Physiol Endocrinol Metab*. 2011;300(5):E877–E885.
13. **Wang B, Wood IS, Trayhurn P.** Dysregulation of the expression and secretion of inflammation-related adipokines by hypoxia in human adipocytes. *Pflugers Arch*. 2007;455(3):479–492.
14. **Trayhurn P, Wang B, Wood IS.** Hypoxia in adipose tissue: a basis for the dysregulation of tissue function in obesity? *Br J Nutr*. 2008;100(2):227–235.
15. **Fujisaka S, Usui I, Ikutani M, et al.** Adipose tissue hypoxia induces inflammatory M1 polarity of macrophages in an HIF-1 α -dependent and HIF-1 α -independent manner in obese mice. *Diabetologia*. 2013;56(6):1403–1412.
16. **Wood IS, de Heredia FP, Wang B, Trayhurn P.** Cellular hypoxia and adipose tissue dysfunction in obesity. *Proc Nutr Soc*. 2009;68(4):370–377.
17. **Halberg N, Khan T, Trujillo ME, et al.** Hypoxia-inducible factor 1 α induces fibrosis and insulin resistance in white adipose tissue. *Mol Cell Biol*. 2009;29(16):4467–4483.
18. **Sun K, Halberg N, Khan M, Magalang UJ, Scherer PE.** Selective inhibition of hypoxia-inducible factor 1 α ameliorates adipose tissue dysfunction. *Mol Cell Biol*. 2013;33(5):904–917.
19. **Jiang C, Qu A, Matsubara T, et al.** Disruption of hypoxia-inducible factor 1 in adipocytes improves insulin sensitivity and decreases adiposity in high-fat diet-fed mice. *Diabetes*. 2011;60(10):2484–2495.
20. **Krishnan J, Danzer C, Simka T, et al.** Dietary obesity-associated Hif1 α activation in adipocytes restricts fatty acid oxidation and energy expenditure via suppression of the Sirt2-NAD⁺ system. *Genes Dev*. 2012;26(3):259–270.
21. **Lee KY, Gesta S, Boucher J, Wang XL, Kahn CR.** The differential role of Hif1 β /Arnt and the hypoxic response in adipose function, fibrosis, and inflammation. *Cell Metab*. 2011;14(4):491–503.
22. **Lee YS, Kim JW, Osborne O, et al.** Increased adipocyte O₂ consumption triggers HIF-1 α , causing inflammation and insulin resistance in obesity. *Cell*. 2014;157(6):1339–1352.
23. **Regazzetti C, Peraldi P, Gremeaux T, et al.** Hypoxia decreases insulin signaling pathways in adipocytes. *Diabetes*. 2009;58(1):95–103.
24. **Yin J, Gao Z, He Q, Zhou D, Guo Z, Ye J.** Role of hypoxia in obesity-induced disorders of glucose and lipid metabolism in adipose tissue. *Am J Physiol Endocrinol Metab*. 2009;296(2):E333–E342.
25. **Kabayama K, Sato T, Saito K, et al.** Dissociation of the insulin receptor and caveolin-1 complex by ganglioside GM3 in the state of insulin resistance. The neck of caveolae is a distinct plasma membrane subdomain that concentrates insulin receptors in 3T3-L1 adipocytes. *Proc Natl Acad Sci USA*. 2007;104(34):13678–13683.
26. **Foti M, Porcheron G, Fournier M, Maeder C, Carpentier JL.** The neck of caveolae is a distinct plasma membrane subdomain that concentrates insulin receptors in 3T3-L1 adipocytes. *Proc Natl Acad Sci USA*. 2007;104(4):1242–1247.
27. **Stralfors P.** Caveolins and caveolae, roles in insulin signalling and diabetes. *Adv Exp Med Biol*. 2012;729:111–126.
28. **Hansen CG, Nichols BJ.** Exploring the caves: cavins, caveolins and caveolae. *Trends Cell Biol*. 2010;20(4):177–186.
29. **Bastiani M, Parton RG.** Caveolae at a glance. *J Cell Sci*. 2010;123(Pt 22):3831–3836.
30. **Parton RG, del Pozo MA.** Caveolae as plasma membrane sensors, protectors and organizers. *Nat Rev Mol Cell Biol*. 2013;14(2):98–112.
31. **Briand N, Dugail I, Le Lay S.** Cavin proteins: new players in the caveolae field. *Biochimie*. 2011;93(1):71–77.
32. **Razani B, Combs TP, Wang XB, et al.** Caveolin-1-deficient mice are lean, resistant to diet-induced obesity, and show hypertriglyceridemia with adipocyte abnormalities. *J Biol Chem*. 2002;277(10):8635–8647.
33. **Drab M, Verkade P, Elger M, et al.** Loss of caveolae, vascular dysfunction, and pulmonary defects in caveolin-1 gene-disrupted mice. *Science*. 2001;293(5539):2449–2452.
34. **Chadda R, Mayor S.** PTRF triggers a cave in. *Cell*. 2008;132(1):23–24.
35. **Hayer A, Stoeber M, Bissig C, Helenius A.** Biogenesis of caveolae: stepwise assembly of large caveolin and cavin complexes. *Traffic*. 2010;11(3):361–382.
36. **Hansen CG, Bright NA, Howard G, Nichols BJ.** SDPR induces membrane curvature and functions in the formation of caveolae. *Nat Cell Biol*. 2009;11(7):807–814.
37. **Hill MM, Bastiani M, Luetterforst R, et al.** PTRF-cavin, a conserved cytoplasmic protein required for caveola formation and function. *Cell*. 2008;132(1):113–124.
38. **McMahon KA, Zajicek H, Li WP, et al.** SRBC/cavin-3 is a caveolin adapter protein that regulates caveolae function. *EMBO J*. 2009;28(8):1001–1015.
39. **Liu L, Brown D, McKee M, et al.** Deletion of cavin/PTRF causes global loss of caveolae, dyslipidemia, and glucose intolerance. *Cell Metab*. 2008;8(4):310–317.
40. **Breen MR, Camps M, Carvalho-Simoes F, Zorzano A, Pilch PF.** Cholesterol depletion in adipocytes causes caveolae collapse concomitant with proteosomal degradation of cavin-2 in a switch-like fashion. *Plos One*. 2012;7(4):e34516.
41. **Kim CA, Delepine M, Boutet E, et al.** Association of a homozygous nonsense caveolin-1 mutation with Berardinelli-Seip congenital lipodystrophy. *J Clin Endocrinol Metab*. 2008;93(4):1129–1134.
42. **Hayashi YK, Matsuda C, Ogawa M, et al.** Human PTRF mutations cause secondary deficiency of caveolins resulting in muscular dystrophy with generalized lipodystrophy. *J Clin Invest*. 2009;119(9):2623–2633.
43. **Ding SY, Lee MJ, Summer R, Liu L, Fried SK, Pilch PF.** Pleiotropic effects of cavin-1 deficiency on lipid metabolism. *J Biol Chem*. 2014;289(12):8473–8483.
44. **Gustavsson J, Parpal S, Karlsson M, et al.** Localization of the insulin receptor in caveolae of adipocyte plasma membrane. *FASEB J*. 1999;13(14):1961–1971.
45. **Kimura A, Mora S, Shigematsu S, Pessin JE, Saltiel AR.** The insulin receptor catalyzes the tyrosine phosphorylation of caveolin-1. *J Biol Chem*. 2002;277(33):30153–30158.
46. **Cohen AW, Razani B, Wang XB, et al.** Caveolin-1-deficient mice show insulin resistance and defective insulin receptor protein expression in adipose tissue. *Am J Physiol Cell Physiol*. 2003;285(1):C222–C235.
47. **Plaisant M, Fontaine C, Cousin W, Rochet N, Dani C, Peraldi P.** Activation of hedgehog signaling inhibits osteoblast differentiation of human mesenchymal stem cells. *Stem Cells*. 2009;27(3):703–713.
48. **Rodriguez AM, Elabd C, Delteil F, et al.** Adipocyte differentiation of multipotent cells established from human adipose tissue. *Biochem Biophys Res Commun*. 2004;315(2):255–263.
49. **Cormont M, Tanti JF, Zahraoui A, Van Obberghen E, Tavitian A, Le Marchand-Brustel Y.** Insulin and okadaic acid induce Rab4 re-

- distribution in adipocytes. *J Biol Chem.* 1993;268(26):19491–19497.
50. Kilroy G, Burk DH, Floyd ZE. High efficiency lipid-based siRNA transfection of adipocytes in suspension. *PLoS One.* 2009;4(9):e6940.
 51. Bertola A, Bonnafous S, Anty R, et al. Hepatic expression patterns of inflammatory and immune response genes associated with obesity and NASH in morbidly obese patients. *Plos One.* 2010;5(10):e13577.
 52. Anty R, Bekri S, Luciani N, et al. The inflammatory C-reactive protein is increased in both liver and adipose tissue in severely obese patients independently from metabolic syndrome, type 2 diabetes, and NASH. *Am J Gastroenterol.* 2006;101(8):1824–1833.
 53. Anty R, Iannelli A, Patouraux S, et al. A new composite model including metabolic syndrome, alanine aminotransferase and cyto-keratin-18 for the diagnosis of non-alcoholic steatohepatitis in morbidly obese patients. *Aliment Pharmacol Ther.* 2010;32(11–12):1315–1322.
 54. Wallace TM, Levy JC, Matthews DR. Use and abuse of HOMA modeling. *Diabetes Care.* 2004;27(6):1487–1495.
 55. Bickel PE, Scherer PE, Schnitzer JE, OH P, Lisanti MP, Lodish HF. Flotillin and epidermal surface antigen define a new family of caveolae-associated integral membrane proteins. *J Biol Chem.* 1997;272(21):13793–13802.
 56. Rajendran L, Le Lay S, Illges H. Raft association and lipid droplet targeting of flotillins are independent of caveolin. *Biol Chem.* 2007;388(3):307–314.
 57. Rajendran L, Masilamani M, Solomon S, et al. Asymmetric localization of flotillins/reggies in preassembled platforms confers inherent polarity to hematopoietic cells. *Proc Natl Acad Sci USA.* 2003;100(14):8241–8246.
 58. Bastiani M, Liu L, Hill MM, et al. MURC/cavin-4 and cavin family members form tissue-specific caveolar complexes. *J Cell Biol.* 2009;185(7):1259–1273.
 59. Shoshani T, Faerman A, Mett I, et al. Identification of a novel hypoxia-inducible factor 1-responsive gene, RTP801, involved in apoptosis. *Mol Cell Biol.* 2002;22(7):2283–2293.
 60. Ellisen LW, Ramsayer KD, Johannessen CM, et al. REDD1, a developmentally regulated transcriptional target of p63 and p53, links p63 to regulation of reactive oxygen species. *Mol Cell.* 2002;10(5):995–1005.
 61. Regazzetti C, Bost F, Le Marchand-Brustel Y, Tanti JF, Giorgetti-Peraldi S. Insulin induces REDD1 expression through hypoxia-inducible factor 1 activation in adipocytes. *J Biol Chem.* 2010;285(8):5157–5164.
 62. Ye J. Emerging role of adipose tissue hypoxia in obesity and insulin resistance. *Int J Obes (Lond).* 2009;33(1):54–66.
 63. Parpal S, Karlsson M, Thorn H, Stralfors P. Cholesterol depletion disrupts caveolae and insulin receptor signaling for metabolic control via insulin receptor substrate-1, but not for mitogen-activated protein kinase control. *J Biol Chem.* 2001;276(13):9670–9678.
 64. Briand N, Prado C, Mabillet G, et al. Caveolin-1 expression and cavin stability regulate caveolae dynamics in adipocyte lipid store fluctuation. *Diabetes.* 2014;63(12):4032–4044.
 65. Hansen CG, Shvets E, Howard G, Riento K, Nichols BJ. Deletion of cavin genes reveals tissue-specific mechanisms for morphogenesis of endothelial caveolae. *Nat Commun.* 2013;4:1831.
 66. Moren B, Shah C, Howes MT, et al. EHD2 regulates caveolar dynamics via ATP-driven targeting and oligomerization. *Mol Biol Cell.* 2012;23(7):1316–1329.
 67. Geiger K, Leiberer A, Muendlein A, et al. Identification of hypoxia-induced genes in human SGBS adipocytes by microarray analysis. *Plos One.* 2011;6(10):e26465.
 68. Leiberer A, Geiger K, Muendlein A, Drexel H. Hypoxia induces a HIF-1 α dependent signaling cascade to make a complex metabolic switch in SGBS-adipocytes. *Mol Cell Endocrinol.* 2014;383(1–2):21–31.
 69. Linden MA, Pincu Y, Martin SA, Woods JA, Baynard T. Moderate exercise training provides modest protection against adipose tissue inflammatory gene expression in response to high-fat feeding. *Physiol Rep.* 2014;2(7).
 70. Canello R, Henegar C, Viguerie N, et al. Reduction of macrophage infiltration and chemoattractant gene expression changes in white adipose tissue of morbidly obese subjects after surgery-induced weight loss. *Diabetes.* 2005;54(8):2277–2286.
 71. Rajab A, Straub V, McCann LJ, et al. Fatal cardiac arrhythmia and long-QT syndrome in a new form of congenital generalized lipodystrophy with muscle rippling (CGL4) due to PTRF-CAVIN mutations. *PLoS Genet.* 2010;6(3):e1000874.
 72. Cao H, Alston L, Ruschman J, Hegele RA. Heterozygous CAV1 frameshift mutations (MIM 601047) in patients with atypical partial lipodystrophy and hypertriglyceridemia. *Lipids Health Dis.* 2008;7:3.
 73. Gupta R, Toufaily C, Annabi B. Caveolin and cavin family members: dual roles in cancer. *Biochimie.* 2014;107PB:188–202.
 74. Shastry S, Delgado MR, Dirik E, Turkmen M, Agarwal AK, Garg A. Congenital generalized lipodystrophy, type 4 (CGL4) associated with myopathy due to novel PTRF mutations. *Am J Med Genet A.* 2010;152A(9):2245–2253.
 75. Nassoy P, Lamaze C. Stressing caveolae new role in cell mechanics. *Trends Cell Biol.* 2012;22(7):381–389.
 76. Bai L, Deng X, Li Q, et al. Down-regulation of the cavin family proteins in breast cancer. *J Cell Biochem.* 2012;113(1):322–328.

Letter

The Promyelocytic Leukemia Protein Is Upregulated in Conditions of Obesity and Liver Steatosis

Arkaitz Carracedo^{1,2,3,4,*}, Déborah Rousseau^{5,6*}, Nicholas Douris^{7*}, Sonia Fernández-Ruiz², Natalia Martín-Martín², Dror Weiss¹, Kaitlyn Webster¹, Andrew C. Adams^{7,8}, Mercedes Vazquez-Chantada², Maria L. Martinez-Chantar^{2,9}, Rodolphe Anty^{5,6,10}, Albert Tran^{5,6,10}, Eleftheria Maratos-Flier⁷, Philippe Gual^{5,6}, Pier Paolo Pandolfi¹

1. Cancer Research Institute, Beth Israel Deaconess Cancer Center, Department of Medicine and Pathology, Beth Israel Deaconess Medical Center, Harvard Medical School, Boston, MA, USA
2. CIC bioGUNE, Bizkaia Technology Park, Derio, Spain
3. IKERBASQUE, Basque foundation for science, Bilbao, Spain
4. Biochemistry and Molecular Biology Department, University of the Basque Country (UPV/EHU), P. O. Box 644, E-48080 Bilbao, Spain
5. INSERM, U1065, Team 8, "Hepatic Complications in Obesity", Nice, F-06204, Cedex 3, France
6. University of Nice-Sophia-Antipolis, Faculty of Medicine, Nice, F-06107, Cedex 2, France
7. Division of Endocrinology; Department of Medicine, Beth Israel Deaconess Medical Center, Harvard Medical School, Boston MA 02215, USA
8. Lilly Research Laboratories, Lilly Corporate Center, Indianapolis, Indiana, USA
9. Centro de Investigación Biomédica en Red de Enfermedades Hepáticas y Digestivas (Ciberehd)
10. CHU of Nice, Digestive Center, Nice, F-06202, Cedex 3, France

* Equal contribution

✉ Corresponding authors: acarracedo@cicbiogune.es and ppandolf@bidmc.harvard.edu

© 2015 Ivyspring International Publisher. Reproduction is permitted for personal, noncommercial use, provided that the article is in whole, unmodified, and properly cited. See <http://ivyspring.com/terms> for terms and conditions.

Received: 2015.01.16; Accepted: 2015.02.24; Published: 2015.04.11

The promyelocytic leukemia protein (PML) is the essential component of multi-protein sub-nuclear structures, the PML-Nuclear bodies (PML-NB, [1]). The PML-NBs regulate a variety of nuclear functions, including post-translational modifications in nuclear proteins (acetylation, SUMOylation, ubiquitylation) [1]. This function has led to the current notion that PML is a modulator of cell responses, which might not be essential in steady-state conditions (under lack of stress) but plays a critical role when the cell and organism is challenged. This notion is supported by the fact that the lack of PML in mice does not result in embryonic lethality or overt physiological alterations in adulthood, but it alters the response to oncogenic insults or dietary alterations [1-4].

The activity of PML has been mostly investigated in the context of suppression, pathogenesis and progression of tumorigenesis. However, evidence of the function of this protein beyond malignant transformation are quickly accumulating. We and others have recently reported that the expression of PML is relevant for the response to metabolic insults, nutritional disorders and obesity [4-8]. In this study, we aimed at extending and defining the status of PML in

conditions of nutritional challenge. To this end, we evaluated PML transcript abundance in a cohort of human liver biopsies from lean or morbidly obese subjects. Liver material from lean patients was obtained from 3 subjects (3 women; age, 46±12 years; BMI, 21±2 kg/m²) undergoing partial hepatectomy for benign tumors (neighbor tissues from four adenoma and one focal nodular hyperplasia) and did not display any hepatic steatosis, inflammation or fibrosis. For obese patients, bariatric surgery was indicated in accordance with French guidelines (the study was approved by "Comité Consultatif de Protection des Personnes dans la Recherche Biomédicale de Nice" 07/04:2003, N° 03.017) (Fig. 1A). Quantitative real time RT-PCR (q-RT-PCR) analysis (references from Applied biosystems Hs99999902_m1 for housekeeping *RPLP0* (Ribosomal protein, large subunit, P0) and Hs00231241_m1 for *PML* and as previously described [9, 10]), revealed a significant PML up-regulation in obese individuals (Fig. 1B). Further, hepatic PML expression increased in obese patients without liver complications (n=5) versus lean subjects (+2.49±0.28, P=0.036). We next decided to extend this observation to diet-induced (Research Diets D12451 as obesogenic

diet; LabDiet 5008 (Pharmaserv, Framingham, MA, USA) as chow, following the procedure in Ref. [11]) or genetic (Agouti mutant heterozygous) mouse models of obesity (the mouse experiments were approved by IACUC, USA). Q-RT-PCR analysis in high-fat diet fed mice demonstrated the up-regulation of Pml in livers from obese mice (murine Pml primers, Pml_F: GATCTCCGCGACAATTCAGT, Pml_R: ATGCCACT GCTGAATCTCCT; Cyclophilin was used as house-keeping gene; Cyclo_F: GGTGGAGAGCACCAAG ACAGA, Cyclo_R: GCCGGAGTCGACAATGATG; Fig. 1C). Importantly, transcriptional up-regulation of this gene was accompanied by the detection of Pml

immunoreactive nuclear bodies by immunohistochemistry in <5% of hepatocytes in livers from HFD mice (using Millipore Pml antibody), but rarely in those from lean individuals (Fig. 1D), similar to our prior observations in another mouse model [4]. Of note, Pml immunoreactivity was often restricted to a single or few large nuclear bodies of doughnut shape, a structural conformation prior described for PML nuclear bodies. We also confirmed the increase Pml immunoreactivity in a second murine model of obesity, driven by the heterozygous mutation in the *Agouti* gene (Jackson laboratory ref. KK.Cg-*A^y*/J; Ref. [12]; Fig. 1E).

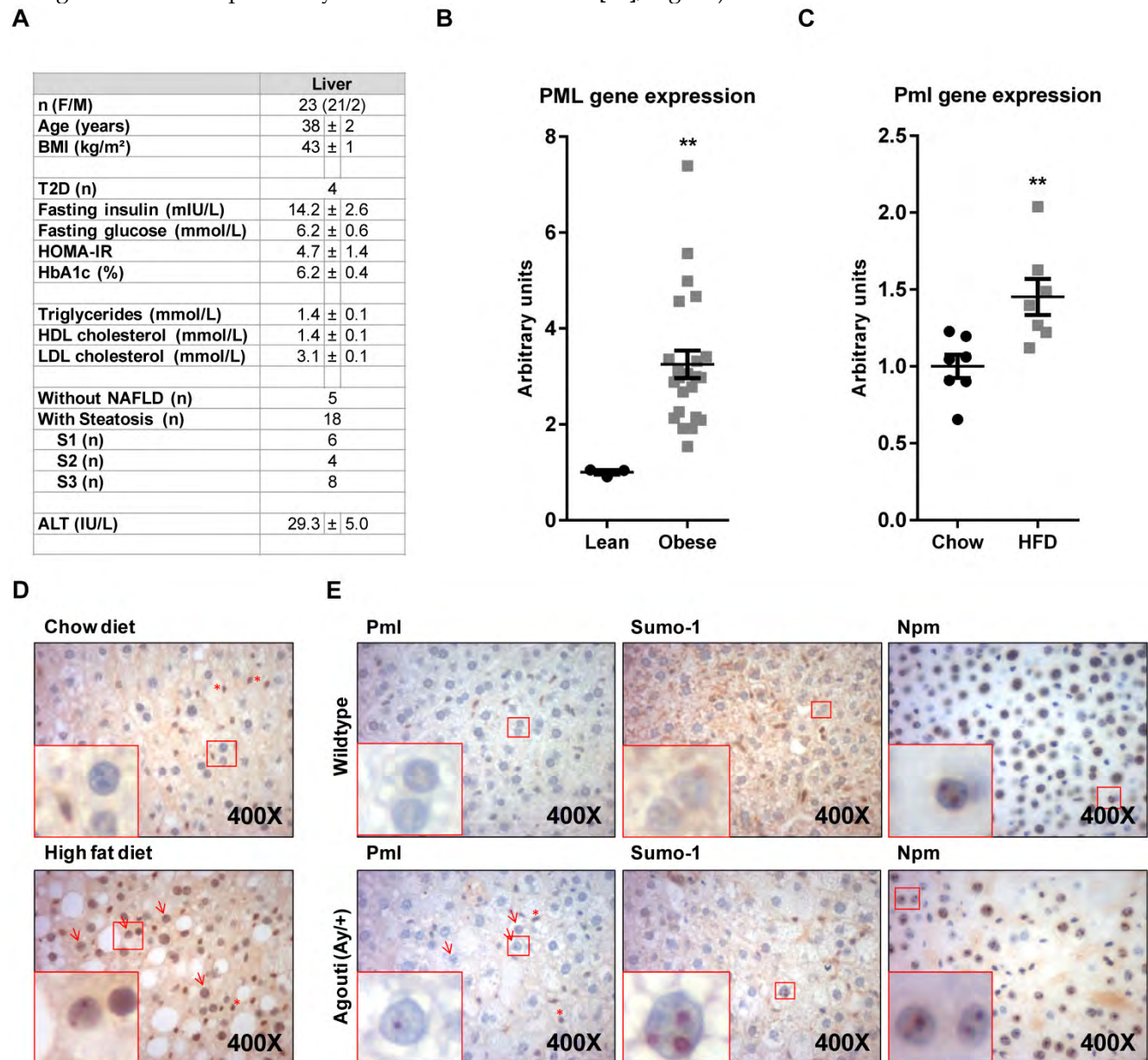


Figure 1. PML is up-regulated in hepatocytes from obese individuals. (A-B) Description of the clinical features of obese subjects (A) in which PML transcript abundance (q-RT-PCR) was measured (B). (C-D). Pml transcript abundance (q-RT-PCR) (C) and immunoreactivity (D) in mice subjected to standard (chow) or obesity-inducing high-fat diets (HFD) (representative micrographs from n=4-5; squares represent zoomed region; red arrows depict PML immunoreactive hepatocytes; red asterisks depict PML immunoreactive non-hepatocyte cells). **, p<0.01 calculated by non-parametric Mann-Whitney test. (E) Pml, Sumo-1 and Nucleophosmin (Npm) immunoreactivity in livers from wild type or agouti heterozygous mutant mice (representative micrographs from n=3; squares, arrows and asterisks as described in D).

PML nuclear bodies are enriched in SUMO-1 (Santa Cruz BioTechnology). Immunohistochemical analysis confirmed similar nuclear distribution of Sumo-1 into nuclear bodies at a similar rate of Pml, which strongly suggests that the staining of Pml corresponds to functional nuclear bodies (Fig. 1E). It is worth noting that this altered pattern of nuclear localization was not observed in other non PML-NB resident proteins such as nucleophosmin (a nucleolar protein; Cell Signaling Technology; Fig. 1E). In summary, our results demonstrate that PML accumulates in hepatocytes in conditions of obesity.

Obesity is associated to lipid accumulation in hepatocytes, termed steatosis [13]. Since there are pathological conditions where steatosis can be triggered in the absence of obesity, we sought to ascertain whether PML accumulation was related to obesity or it was a consequence of the steatosis associated to weight increase. To this end, we first evaluated PML expression in obese patients with different degree of steatosis (0, <5%; 1, 5%-30%; 2, >30%-60%; 3, >60%) [14]. The results clearly demonstrated that PML expression significantly correlated with the extent of steatosis (Fig. 2A).

In addition, we took advantage of a dietary regime that results in weight loss and liver lipid accumulation, namely ketogenic diet (KD; Ref. Bio-Serv F3666, [11]). The results confirmed that Pml transcript and immunoreactivity were increased (Fig. 2B-C).

Fatty liver disease is a rapidly increasing pathology that, albeit tightly associated with obesity, is also observed in a fraction of lean individuals, where it is thought to be related to nutrition and life style factors [13]. Our results conclusively demonstrate that PML expression is increased in livers from obese individuals, and is particularly associated to a steatotic phenotype. These findings are of relevance for the characterization of PML non-tumoral functions. Importantly, this observation might open an interesting mean of regulation of PML in the context of cancerous lesions, in which nutrient availability might impact on the expression of this protein and hence on the biology of the disease. In particular, they extend our knowledge regarding the patho-physiological regulation of PML in metabolism. In this respect, it is tempting to speculate that PML induction may represent a failsafe response to steatosis in view of the positive role it plays in the activation fatty acid oxidation pathways [4, 5].

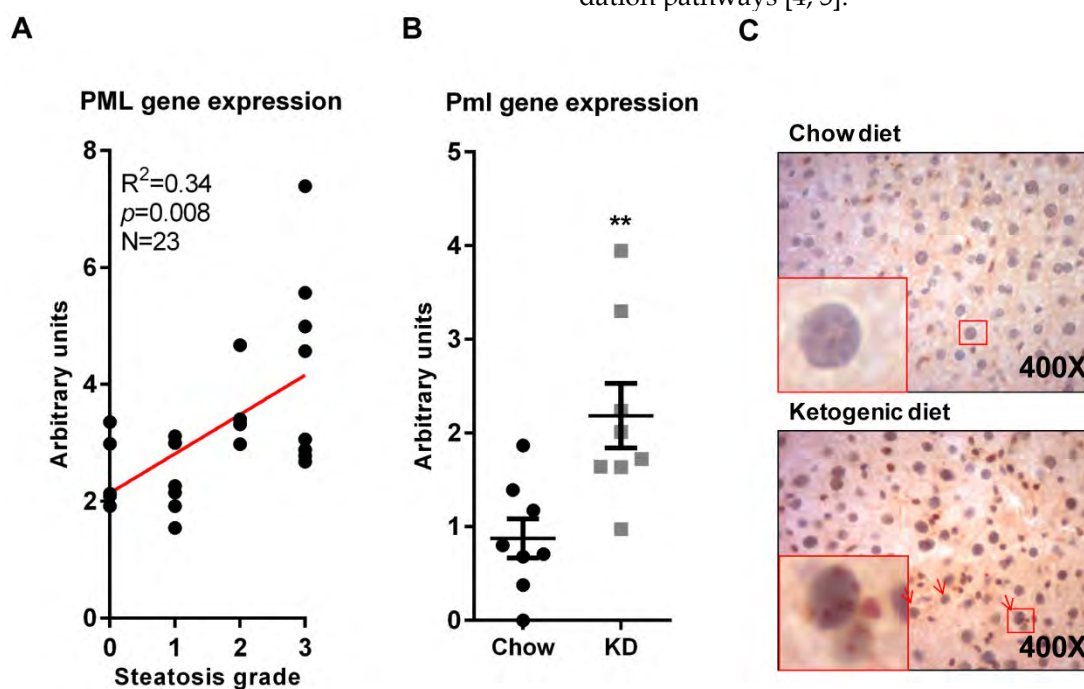


Figure 2. PML liver mRNA expression increases in steatosis. (A) PML mRNA expression (q-RT-PCR) in individuals with defined degree of liver steatosis; the correlation of PML and steatotic grade (S0-S3) was calculated by non-parametric Spearman test. (B-C) Pml transcript expression (q-RT-PCR) (B) and immunoreactivity (C) in livers from mice subjected to chow or ketogenic diet (KD). Representative micrographs from n=4-5; squares represent zoomed region; red arrows depict PML immunoreactive hepatocytes; red asterisks depict PML immunoreactive non-hepatocyte cells **, p<0.01 calculated by non-parametric Mann-Whitney test.

Acknowledgements

Apologies to those whose related publications were not cited due to space limitations. The work of AC is supported by the Ramón y Cajal award, the

Basque Department of Industry, Tourism and Trade (Etortek), health (2012111086) and education (PI2012-03), Marie Curie (277043), Movember, ISCIII (PI10/01484, PI13/00031) and ERC (336343). N.M-M. is supported by the Spanish Association Against

Cancer (AECC). The work of P.G. was supported by grants from INSERM (France), the University of Nice, the Programme Hospitalier de Recherche Clinique (Centre Hospitalier Universitaire of Nice), and charities (Association Française pour l'Etude du Foie, Société Francophone du Diabète and SFD/Roche Pharma, European Foundation for the study of Diabetes/Lilly European Diabetes Research Program and the French Government (National Research Agency, ANR) through the "Investments for the Future" (LABEX SIGNALIFE: program reference #ANR-11-LABX-0028-01). The work of P.P.P. and A.C. was supported by the National Institutes of Health (NIH, USA) grants. N.D. was supported by NRSA 5T32DK751627 (NIH, USA). M.L.M.-C was funded by Sanidad Gobierno Vasco 2013, FIS PI11/01588.

Competing Interests

The authors declare no competing financial interest.

References

1. Bernardi R, Pandolfi PP. Structure, dynamics and functions of promyelocytic leukaemia nuclear bodies. *Nat Rev Mol Cell Biol.* 2007; 8: 1006-16. doi:nrm2277 [pii]10.1038/nrm2277.
2. Bernardi R, Pandolfi PP. Role of PML and the PML-nuclear body in the control of programmed cell death. *Oncogene.* 2003; 22: 9048-57. doi:10.1038/sj.onc.12071061207106 [pii].
3. Carracedo A, Ito K, Pandolfi PP. The nuclear bodies inside out: PML conquers the cytoplasm. *Curr Opin Cell Biol.* 2011; 23: 360-6. doi:S0955-0674(11)00028-7 [pii]10.1016/j.ccb.2011.03.011.
4. Carracedo A, Weiss D, Leliant AK, Bhasin M, de Boer VC, Laurent G, et al. A metabolic pro-survival role for PML in breast cancer. *The Journal of clinical investigation.* 2012; 122: 3088-100. doi:62129 [pii]10.1172/JCI62129.
5. Ito K, Carracedo A, Weiss D, Arai F, Ala U, Avigan DE, et al. A PML-PPAR- δ pathway for fatty acid oxidation regulates hematopoietic stem cell maintenance. *Nat Med.* 2012; 18: 1350-8. doi:nm.2882 [pii]10.1038/nm.2882.
6. Kim MK, Yang S, Lee KH, Um JH, Liu M, Kang H, et al. Promyelocytic Leukemia (PML) Inhibits Adipogenesis and Loss of PML Results in Fat Accumulation in Mice. *Am J Physiol Endocrinol Metab.* 2011 Dec;301(6):E1130-42.
7. Cheng X, Guo S, Liu Y, Chu H, Hakimi P, Berger NA, et al. Ablation of promyelocytic leukemia protein (PML) re-patterns energy balance and protects mice from obesity induced by a Western diet. *J Biol Chem.* 2013; 288: 29746-59. doi:10.1074/jbc.M113.487595.
8. Kitamura YI, Kitamura T, Kruse JP, Raum JC, Stein R, Gu W, et al. FoxO1 protects against pancreatic beta cell failure through NeuroD and MafA induction. *Cell Metab.* 2005; 2: 153-63. doi:S1550-4131(05)00232-9 [pii]10.1016/j.cmet.2005.08.004.
9. Anty R, Bekri S, Luciani N, Saint-Paul MC, Dahman M, Iannelli A, et al. The inflammatory C-reactive protein is increased in both liver and adipose tissue in severely obese patients independently from metabolic syndrome, Type 2 diabetes, and NASH. *Am J Gastroenterol.* 2006; 101: 1824-33. doi:10.1111/j.1572-0241.2006.00724.x.
10. Bekri S, Gual P, Anty R, Luciani N, Dahman M, Ramesh B, et al. Increased adipose tissue expression of hepcidin in severe obesity is independent from diabetes and NASH. *Gastroenterology.* 2006; 131: 788-96. doi:10.1053/j.gastro.2006.07.007.
11. Kennedy AR, Pissios P, Otu H, Roberson R, Xue B, Asakura K, et al. A high-fat, ketogenic diet induces a unique metabolic state in mice. *Am J Physiol Endocrinol Metab.* 2007; 292: E1724-39. doi:10.1152/ajpendo.00717.2006.
12. Bultman SJ, Michaud EJ, Woychik RP. Molecular characterization of the mouse agouti locus. *Cell.* 1992; 71: 1195-204.
13. Fracanzani AL, Valenti L, Bugianesi E, Vanni E, Grieco A, Miele L, et al. Risk of nonalcoholic steatohepatitis and fibrosis in patients with nonalcoholic fatty liver disease and low visceral adiposity. *J Hepatol.* 2011; 54: 1244-9. doi:10.1016/j.jhep.2010.09.037.
14. Kleiner DE, Brunt EM, Van Natta M, Behling C, Contos MJ, Cummings OW, et al. Design and validation of a histological scoring system for nonalcoholic fatty liver disease. *Hepatology.* 2005; 41: 1313-21. doi:10.1002/hep.20701.

ER stress induces NLRP3 inflammasome activation and hepatocyte death

C Lebeau^{1,2}, E Proics^{1,2}, CHD de Bievil^{1,2}, D Rousseau^{1,2}, S Bonnafous^{1,2,3}, S Patouraux^{1,2,4}, G Adam^{1,2}, VJ Lavallard^{1,2}, C Rovere⁵, O Le Thuc⁵, MC Saint-Paul^{1,2,3}, R Anty^{1,2,3}, AS Schneck^{1,2,3}, A Iannelli^{1,2,3}, J Gugenheim^{1,2,3}, A Tran^{1,2,3}, P Gual^{1,2} and B Bailly-Maitre^{*1,2}

The incidence of chronic liver disease is constantly increasing, owing to the obesity epidemic. However, the causes and mechanisms of inflammation-mediated liver damage remain poorly understood. Endoplasmic reticulum (ER) stress is an initiator of cell death and inflammatory mechanisms. Although obesity induces ER stress, the interplay between hepatic ER stress, NLRP3 inflammasome activation and hepatocyte death signaling has not yet been explored during the etiology of chronic liver diseases. Steatosis is a common disorder affecting obese patients; moreover, 25% of these patients develop steatohepatitis with an inherent risk for progression to hepatocarcinoma. Increased plasma LPS levels have been detected in the serum of patients with steatohepatitis. We hypothesized that, as a consequence of increased plasma LPS, ER stress could be induced and lead to NLRP3 inflammasome activation and hepatocyte death associated with steatohepatitis progression. In livers from obese mice, administration of LPS or tunicamycin results in IRE1 α and PERK activation, leading to the overexpression of CHOP. This, in turn, activates the NLRP3 inflammasome, subsequently initiating hepatocyte pyroptosis (caspase-1, -11, interleukin-1 β secretion) and apoptosis (caspase-3, BH3-only proteins). In contrast, the LPS challenge is blocked by the ER stress inhibitor TUDCA, resulting in: CHOP downregulation, reduced caspase-1, caspase-11, caspase-3 activities, lowered interleukin-1 β secretion and rescue from cell death. The central role of CHOP in mediating the activation of proinflammatory caspases and cell death was characterized by performing knockdown experiments in primary mouse hepatocytes. Finally, the analysis of human steatohepatitis liver biopsies showed a correlation between the upregulation of inflammasome and ER stress markers, as well as liver injury. We demonstrate here that ER stress leads to hepatic NLRP3 inflammasome pyroptotic death, thus contributing as a novel mechanism of inflammation-mediated liver injury in chronic liver diseases. Inhibition of ER-dependent inflammasome activation and cell death pathways may represent a potential therapeutic approach in chronic liver diseases.

Cell Death and Disease (2015) 6, e1879; doi:10.1038/cddis.2015.248; published online 10 September 2015

Nonalcoholic fatty liver disease (NAFLD) has become the most common form of chronic liver disease, currently affecting 20–30% of the general population and 75–100% of obese individuals.¹ The spectrum of NAFLD is wide ranging: from hepatic steatosis to nonalcoholic steatohepatitis (NASH) and hepatocellular carcinoma. Hepatic steatosis is characterized by triglyceride accumulation in hepatocytes and follows a benign non-progressive clinical course. Nonalcoholic steatohepatitis (NASH), a progressive form, is defined as a combination of lipid accumulation, hepatocyte death, inflammation and fibrosis. As the probability of developing advanced fibrosis and hepatocellular carcinoma² is significantly greater in patients with steatohepatitis than in those with simple steatosis, it is important to elucidate the mechanism underlying the progression from steatosis to steatohepatitis.

The endoplasmic reticulum (ER) stress response has been linked to obesity, type 2 diabetes and liver cancer.^{3,4} Under stress conditions, the ER initiates the unfolded protein response (UPR) to restore homeostasis. The UPR involves three transmembrane sensors: inositol-requiring enzyme 1 (IRE1 α), PKR-like ER kinase (PERK) and activating transcription factor (ATF6).⁵ Each pathway culminates in the transcriptional regulation of gene expression, which first seeks to reestablish ER homeostasis. Failure of the UPR to decrease ER stress leads to apoptosis, notably via CHOP, a proapoptotic transcription factor whose expression is highly induced by ER stress.⁶

Increased activation of the ER stress response has been reported in obese mice and humans.^{3,4,7,8} Obesity results in liver ER stress, which promotes insulin resistance and hepatosteatosis through the IRE1 α branch.³ Moreover, PERK

¹INSERM, U1065, Equipe 8 « Complications hépatiques de l'obésité », Bâtiment Universitaire ARCHIMED, Nice, France; ²Université de Nice Sophia Antipolis, Faculté de Médecine, Nice, France; ³Centre Hospitalier Universitaire Nice, Hôpital l'Archet, Département Digestif, Nice, France; ⁴Centre Hospitalier Universitaire Nice, Hôpital l'Archet, Département Biologie, Nice, France and ⁵Institut de Pharmacologie Moléculaire et Cellulaire, CNRS, UMR7275, Valbonne, France

*Corresponding author: B Bailly-Maitre, INSERM, U1065, Team 8 "Hepatic complications in obesity", Bâtiment Universitaire ARCHIMED, 151 route Saint Antoine de Ginestière, BP 2 3194, 06204 Nice, France. Tel: +33 (0)4 89 06 42 38; Fax: +33 (0)4 89 06 42 21; E-mail: beatrice.bailly-maitre@unice.fr

Abbreviations: NAFLD, nonalcoholic fatty liver disease; NASH, nonalcoholic steatohepatitis; ER stress, endoplasmic reticulum stress; UPR, unfolded protein response; IRE1 α , inositol-requiring enzyme 1; PERK, PKR-like ER kinase; ATF6, activating transcription factor 6; CHOP, C/EBP homologous protein; GRP78, glucose-regulated protein 78; XBP-1, X-box binding protein 1; NLRP3, NOD-like receptor family, pyrin domain containing 3; TLR-4, toll-like receptor-4; HFD, high-fat diet; MCD, methionine- and choline-deficient diet; TUDCA, tauroursodeoxycholic acid; AST and ALT, aspartate and alanine aminotransferases; ATF4, activating transcription factor 4; eIF2, eukaryotic initiation factor 2; TUN1, tunicamycin

Received 11.5.2015; revised 17.7.2015; accepted 21.7.2015; Edited by G Raschella'

and IRE1 α can regulate lipid stores in the liver, enforcing the hepatic metabolic disorders associated with obesity.^{9,10} It is well established that apoptosis and inflammation are increased in patients with NASH, correlating with histological severity. Because the ER stress response is a critical mediator of inflammation, apoptosis and insulin resistance, it could have a central role in the progression from steatosis to NASH. However, the evidence for activation of hepatic ER stress in patients with NASH needs to be clarified. Gonzalez-Rodriguez *et al.*¹¹ observed that NASH patients displayed more elevated ER stress markers, namely CHOP and GRP78, reinforcing the notion that enhanced ER stress within liver cells may be relevant in the progression from steatosis to NASH.^{12–14}

In addition, while studies indicated a contribution of NF- κ B in the inflammatory responses triggered as a consequence of hepatic ER stress associated with NASH,¹⁵ the potential interplay between ER stress and inflammasome engagement has yet to be explored in NASH progression. The NLRP3 inflammasome is a multi-protein complex which instigates the inflammatory response and contributes to insulin resistance. The NLRP3 inflammasome senses obesity-associated danger signals, namely endotoxin (LPS),¹⁶ hyperglycemia and free fatty acids (FFAs), and mediates caspase-1-dependent maturation of the proinflammatory cytokines interleukin-1 β (IL-1 β) and IL-18.¹⁷ Importantly, increased plasma LPS levels have been detected in mice models of NAFLD¹⁸ and in humans with NASH.^{19–21} Studies have suggested that the NLRP3 inflammasome may have a deleterious role in steatosis and NASH pathogenesis. Indeed, a deficiency in *caspase-1*, *Nlrp3* or *ASC* in mice results in protection from high-fat diet (HFD)-induced steatosis and insulin resistance.^{16,22,23} Similarly, a deficiency in *IL-1 β* , *IL-1 Receptor* or *TLR4*²⁴ protects mice from methionine- and choline-deficient (MCD) diet-induced steatohepatitis. Moreover, the NLRP3 inflammasome also triggers pyroptosis, a form of programmed cell death. Pyroptosis is defined as a caspase-1 or caspase-11-dependent cell death subroutine that is associated with the generation of pyrogenic mediators such as IL-1 β and IL-18.^{25,26} Therefore, the NLRP3 inflammasome could be a major cause of cell death and inflammation in NASH progression.

A 'two hit' mechanism has been proposed to drive NASH pathogenesis.²⁷ The first hit is associated with steatosis and sensitizes the liver to additional proinflammatory insults (second hit), such as LPS, which aggravate liver injury and contribute to the development of NASH.^{28,29} We hypothesized that, as a consequence of increased plasma LPS, ER stress could be induced and lead to NLRP3 inflammasome activation and hepatocyte death associated with NASH. To address this issue, we explored *in vivo* whether the administration of LPS could trigger exaggerated hepatic ER stress signaling, and compared the response with that of tunicamycin, a chemical ER stress inducer, in steatotic livers from genetically obese (*ob/ob*) mice. We analyzed the potential benefit of TUDCA, an ER stress inhibitor, in the prevention and treatment of hepatic inflammation and death caused by an LPS challenge. We found that PERK and IRE1 α pathways cooperate to activate CHOP, and that this appears to be a critical link between inflammasome activation and hepatocyte death in NASH. Importantly, the upregulation of transcripts of ER stress

correlated with inflammasome priming and liver injury in NASH patients, which highlights their relevance in disease progression.

Results

TUDCA protects the liver from LPS-induced injury, apoptosis and inflammasome priming. In genetically obese mice (*ob/ob*) with severe steatosis and challenged with LPS, we investigated the *in vivo* effects of TUDCA treatment. Liver histological analysis revealed severe inflammation with many inflammatory foci and areas of cell death in LPS-injected mice compared with PBS-injected mice (Figure 1a). Five days of TUDCA treatment dramatically reduced the number of steatohepatitis foci (presence of inflammatory foci and ballooned hepatocytes) induced by LPS (Figure 1a). TUDCA treatment also resulted in partial resolution of hepatic steatosis (Figure 1a and Supplementary Figure S1A). As expected, inflammatory foci were absent in PBS- and TUDCA-injected mice (Supplementary Figure S1A). Consistent with these observations, serum levels of aspartate (AST) and alanine (ALT) aminotransferases were significantly lower in [TUDCA+LPS]-treated *ob/ob* mice compared with LPS-treated mice (Figure 1b). TUDCA-treated mice also displayed a reduction in AST and ALT levels compared with those receiving PBS. Thus, in *ob/ob* mice, LPS challenge induced NASH-like pathological features: ballooned hepatocytes, liver damage and inflammation. TUDCA treatment prevented these effects. After LPS injection, liver sections of TUDCA-treated mice also contained less TUNEL-positive hepatocytes compared with untreated animals. TUNEL staining showed that both apoptosis (nuclear fragmentation, Figure 1c) and necrosis (diffuse cytoplasmic staining, Supplementary Figure S1A) were significantly reduced after TUDCA treatment. Furthermore, the levels of active caspase-3 and substrate CAD were markedly reduced in [TUDCA+LPS]-treated mice in comparison with LPS-treated ones (Figure 1c). In accordance with inflammatory cell infiltration, the hepatic levels of *TNF α* , *IL-1 β* , *IFN γ* and *iNOS* messenger mRNA were significantly increased in LPS-injected mice (Figure 1d). TUDCA treatment decreased the hepatic levels of these markers upon LPS challenge. Notably, IL-1 β is matured by proinflammatory caspases (caspase-1 and caspase-11).¹⁷ Interestingly, the analysis of mRNA levels showed that *caspase-1* and *caspase-11* were significantly decreased in the livers of [TUDCA+LPS]-treated mice in comparison with LPS-treated ones (Figure 1d). We concluded that TUDCA treatment suppresses hepatocyte ballooning, apoptosis and inflammasome priming upon LPS challenge in *ob/ob* mice.

TUDCA provides protection against LPS-induced ER stress and inflammasome pyroptotic death. As TUDCA treatment prevented LPS-induced upregulation of *IL-1 β* , *caspase-1* and *caspase-11* gene expression (Figure 1d) and TUNEL positivity (Figure 1c), we hypothesized that LPS could induce hepatic ER stress pyroptosis. As in apoptotic cell death, cells undergoing pyroptosis incur DNA damage and become positive in the terminal deoxynucleotidyl

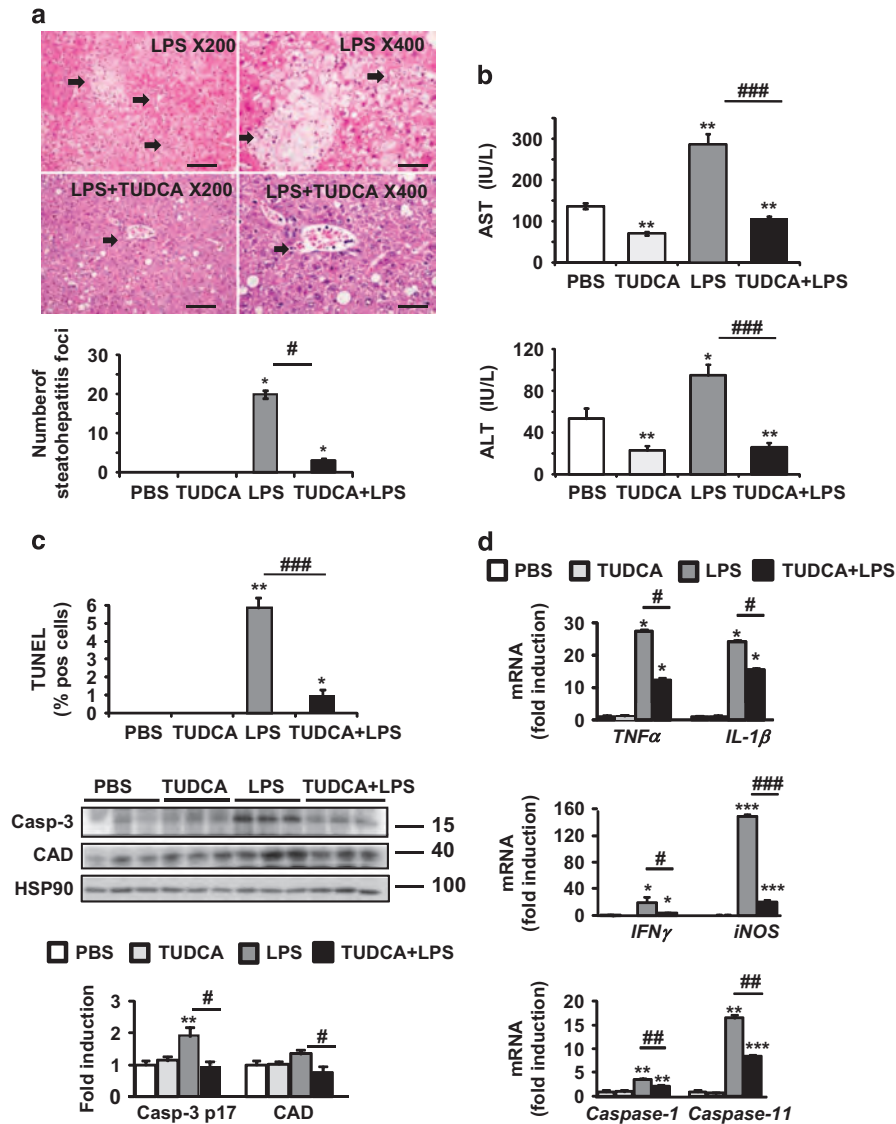


Figure 1 Tudca protected against LPS-induced liver injury, apoptosis and inflammasome priming in *ob/ob* mice. Tudca was injected intraperitoneally (500 μ g/g) for 5 days. An LPS challenge (2 μ g/g) was performed 6-h before killing. (a) Shown are photomicrographs of sections of murine liver stained with H&E (scale bar = 50 μ m at \times 200 or 25 μ m at \times 400 magnification). The number of steatohepatitis foci (number of inflammatory foci in contact with ballooned hepatocytes, identified by arrows) was evaluated. (b) Serum AST and ALT transaminase levels were measured ($n=9-12$). (c) Apoptotic hepatocytes were visualized with TUNEL assay. The expression of active caspase-3 and CAD was evaluated in total liver lysates. Quantification was performed from the immunoblot analysis and expressed as fold induction ($n=6$). (d) Relative expression of hepatic *TNF α* , *IL-1 β* , *caspase-1* and *caspase-11* mRNA (normalized to *36B4* mRNA). Data were expressed as fold induction ($n=7$). Data are expressed as mean \pm standard error of the mean. Statistical significance from controls is denoted by * $P \leq 0.05$, ** $P \leq 0.01$, *** $P \leq 0.001$

transferase dUTP nick-end labeling (TUNEL) assay. Also, Figure 2a shows that LPS-treated *ob/ob* mice exhibited marked increases in both active caspase-11 and -1, whereas Tudca strongly prevented activation. As reported,¹⁶ hepatic steatosis was already associated with increased levels of both active inflammatory caspases in the liver. We observed that NLRP3 expression was induced upon LPS stimulation at the protein and mRNA levels, whereas it was decreased with Tudca, as shown in Figures 2a and b, respectively. Accordingly, hepatic activation of another specific inflammasome substrate, *IL-18*, was reduced at the mRNA level (Figure 2b). Importantly, in agreement with increased caspase-11 and -1 activation, the serum levels of systemic

mature *IL-1 β* rose after LPS injury, whereas Tudca treatment completely abolished *IL-1 β* secretion in these mice (Figure 2c). Tudca treatment also decreased the circulating levels of global inflammatory markers such as *TNF α* , *IFN γ* (Figure 2c), *MCP-1* and *IL-6* (Supplementary Figure S1B) in response to LPS. It should be acknowledged that the circulating inflammatory markers could be derived from adipose tissue in addition to the liver and contribute to inflammatory responses.

Together, these data reveal that upon LPS treatment, ER-dependent NLRP3 inflammasome and hepatocyte death pathways were induced in the livers of *ob/ob* mice, whereas Tudca blocked both pathways. We next decided to

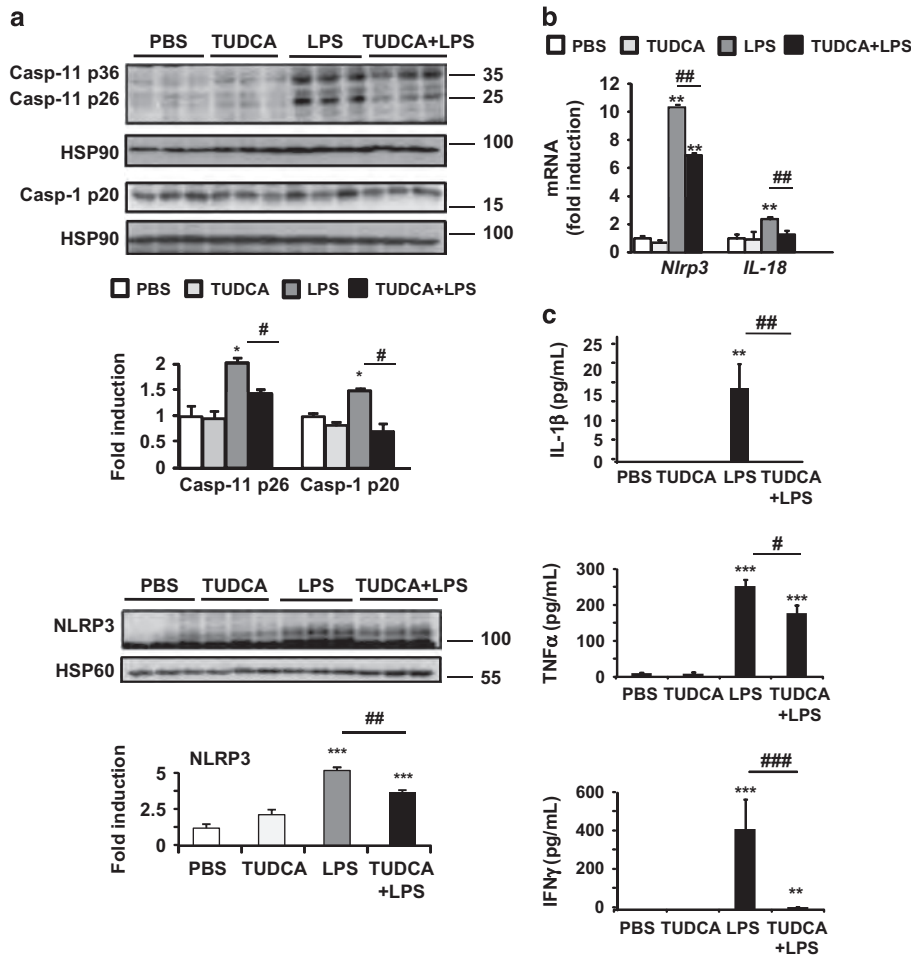


Figure 2 TUDCA treatment prevented hepatic activation of the NLRP3 inflammasome in *ob/ob* mice challenged with LPS. (a) Analysis of whole-liver samples from PBS-, TUDCA-, LPS- and [TUDCA+LPS]-treated mice. Immunoblot analysis of active caspase-11, active caspase-1 and NLRP3 protein levels are shown ($n=4-6$). (b) Real-time quantitative PCR analysis was performed to compare relative hepatic levels of *Nlrp3* and *IL-18* mRNAs. (c) Plasma cytokine levels were quantified for IL-1 β , TNF α and IFN γ ($n=7-9$). Statistical significance from controls is denoted by * $P \leq 0.05$, ** $P \leq 0.01$, *** $P \leq 0.001$

administer the TUDCA treatment with LPS for the duration of the 6-h treatment. Importantly, we observed that a unique dose of TUDCA was still capable of protecting the liver against LPS-induced steatohepatitis foci formation and necrosis (Supplementary Figure S2A), liver injury (Supplementary Figure S2B) and apoptosis (Supplementary Figure S2C) independently of the grade of steatosis (Supplementary Figure S2A). TUDCA 6-h co-treatment decreased the activation of inflammatory caspases in the liver at the protein and mRNA levels (Supplementary Figure S3A, top and bottom, respectively). The increase in circulating levels of IL-1 β , TNF α and IFN γ in response to LPS was also limited by TUDCA (Supplementary Figure S3B). Thus, the hepatoprotective and anti-inflammatory properties of TUDCA against LPS are independent of its ability to improve steatosis.

TUDCA reduces LPS-induced hepatic IRE1 α and PERK activation. During ER stress, IRE1 α initiates an unconventional splicing of the mRNA encoding an isoform of the XBP-1 protein (sXBP-1).⁵ PERK phosphorylates eIF2 α , which results in the translational induction of ATF4. ATF6 is cleaved and its cytosolic domain translocates to the nucleus.

We examined the hepatic status of sXBP-1, phospho-eIF2 α , ATF4 and total ATF6 in *ob/ob* mice. The levels of the sXBP-1 protein (Figure 3a) and target gene *DnaJ9* (Supplementary Figure S4a) increased significantly in LPS-treated mice, whereas they were barely detected in [TUDCA+LPS]-treated mice. In addition, the hepatic levels of phosphorylated eIF2 α and ATF4 protein expression were slightly enhanced with LPS, while TUDCA pretreatment protected from LPS-induced eIF2 α activation (Figure 3a). Interestingly, 5 days of TUDCA treatment reduced the basal state of phosphorylation of eIF2 α . In contrast, total ATF6 expression remained unchanged irrespective of LPS stimulation (Figure 3a). The GRP78 protein was markedly increased in the livers of TUDCA-treated *ob/ob* mice, whereas the CHOP protein was barely detectable. TUDCA further increased the [GRP78/CHOP] ratio, thereby promoting potential protection against LPS stimulation (Figure 3b). Importantly, we found similar results on an mRNA level when TUDCA and LPS were administrated together for the duration of the 6-h treatment (Supplementary Figure S3C).

As reported,³ the basal levels of phospho-JNK were already elevated in the steatotic liver as a consequence of IRE1 α

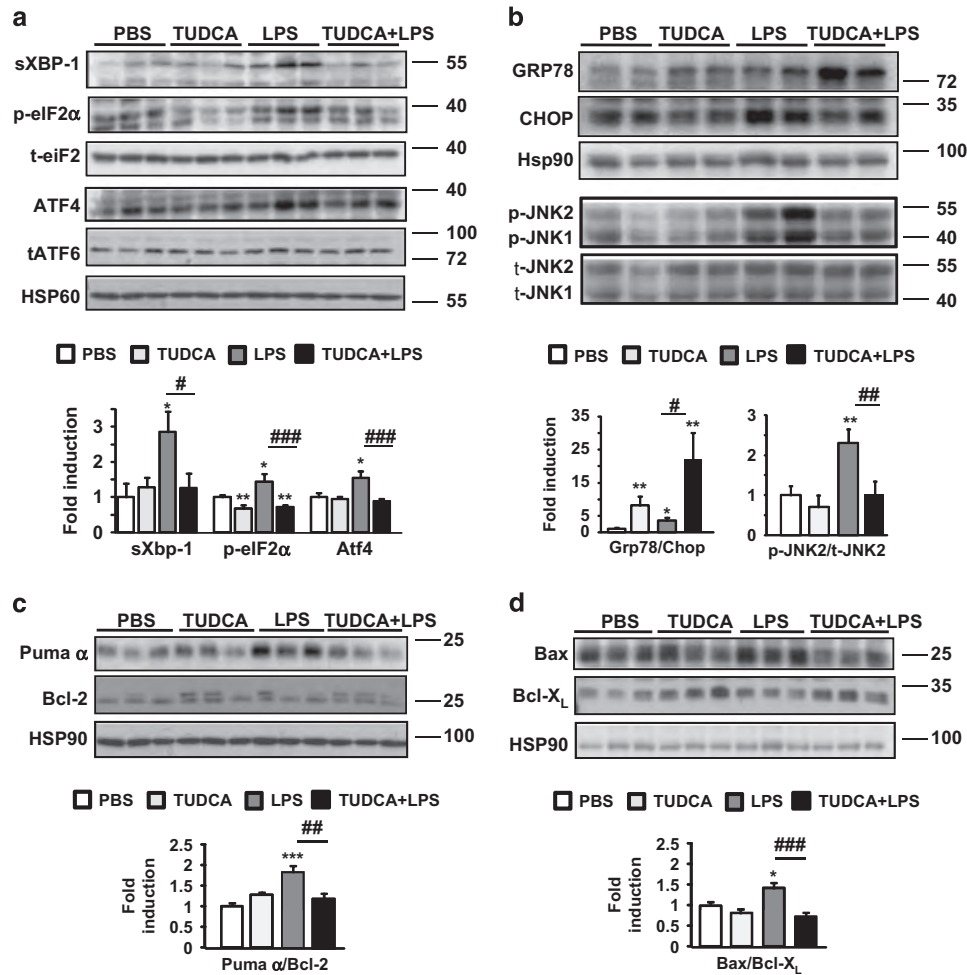


Figure 3 TUDCA inhibited the LPS-induced IRE1 α and PERK hepatic activities by favoring anti-apoptotic signaling pathways in *ob/ob* mice. The expression of ER stress (a and b) and apoptotic proteins, presented as Bcl-2 family pro-apoptotic/anti-apoptotic ratios (c and d), was compared by immunoblotting and quantified ($n = 6-9$). Data are expressed as mean \pm standard error of the mean. Statistical significance from controls is denoted by * $^{\#}P \leq 0.05$, ** $^{\#}P \leq 0.01$, *** $^{\#}P \leq 0.001$

activation compared with lean control livers (Supplementary Figures S5A–C). Upon LPS challenge, the levels of phospho-JNK rose further, whereas TUDCA treatment prevented exaggerated JNK activation (Figure 3b). CHOP mediates its pro-apoptotic effects by positively regulating pro-apoptotic Puma and Bax proteins, while negatively regulating the anti-apoptotic Bcl-2 protein.⁵ Importantly, LPS stimulation increased Puma and Bax protein expression (Figures 3c and d). TUDCA blocked this upregulation and slightly increased the levels of Bcl-X_L and Bcl-2 proteins. Thus, TUDCA treatment inhibited the increase in Bax and Puma protein levels, thereby promoting a protective Bcl-X_L- and Bcl-2-dependent mechanism against LPS-induced liver injury.

These data revealed that in livers from obese mice, administration of LPS results in the activation of IRE1 α and PERK, as well as CHOP overexpression. This, in turn, activates the NLRP3 inflammasome, initiating hepatocyte apoptosis and, more specifically, pyroptosis. In contrast, the LPS challenge is blocked by the ER stress inhibitor TUDCA. In light of the data, we addressed whether feeding mice with a methionine- and choline-deficient (MCD) diet, a nutritional model of steatohepatitis, would induce a similar phenotype.

As expected, the MCD-fed mice developed a typical feature of NASH: increased liver injury (Supplementary Figure S6A). All these parameters correlated with an increased hepatic priming of the NLRP3 inflammasome and ER stress markers, specifically CHOP, in the MCD-fed mice (Supplementary Figures S6B and C).

Tunicamycin treatment leads to hepatic apoptosis, exacerbated NLRP3 inflammasome activation and overwhelmed IRE1 α and PERK activities. We questioned whether ER stress activation with tunicamycin (TUNI), a specific ER stress inducer, would lead to increased liver injury and NLRP3 inflammasome activation in the livers of obese mice. As shown in Figure 4a, the serum levels of AST were significantly increased in TUNI-injected mice compared with control animals, indicative of additional hepatocyte death, and we observed a strong increase in the number of steatohepatitis foci. Furthermore, these mice present a marked increase in TUNEL-positive hepatocytes, activated hepatic caspase-3, Puma α and active Bax in response to TUNI (Figure 4b). These results clearly indicate that ER

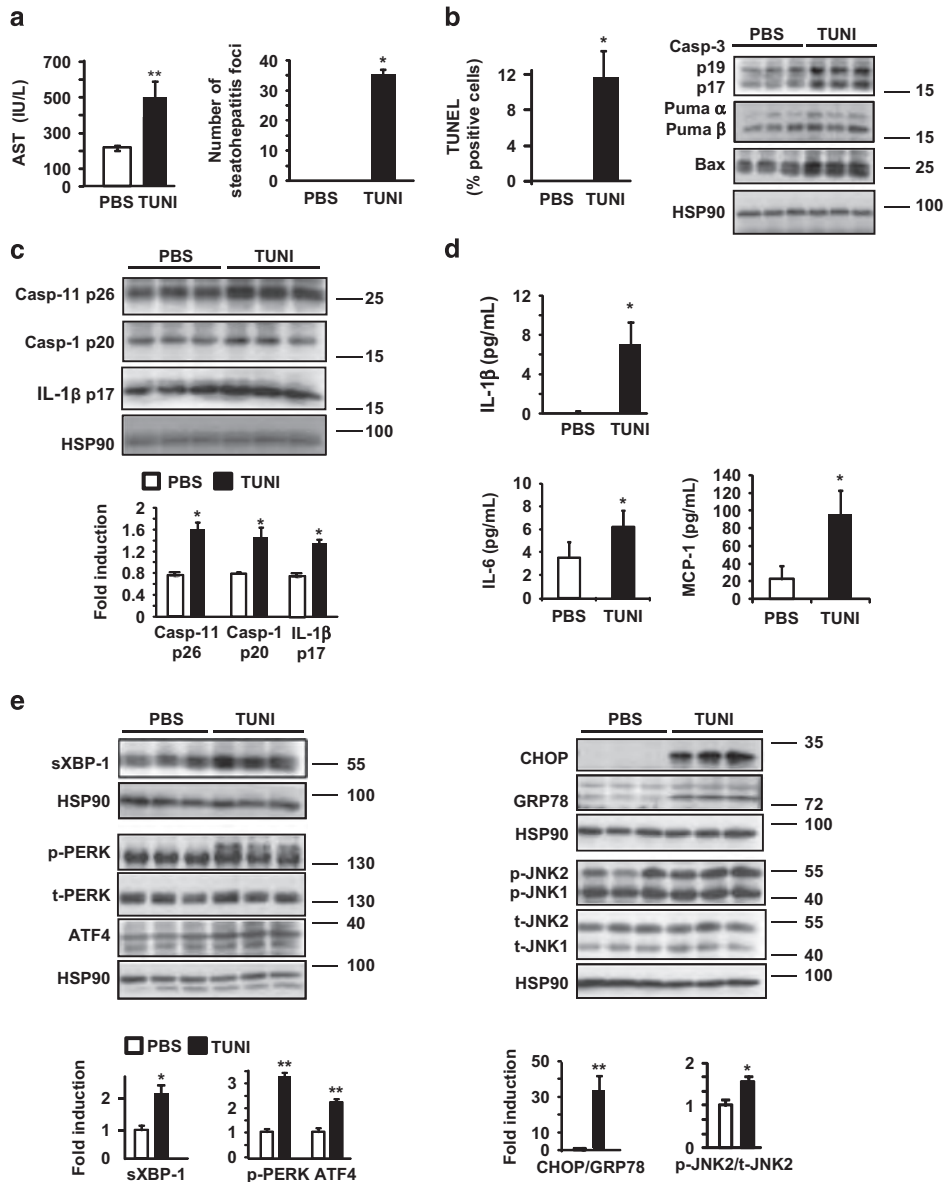


Figure 4 Challenge with tunicamycin in *ob/ob* mice increased apoptosis and activation of the NLRP3 inflammasome, and was associated with hepatic IRE1 α and PERK activities. Mice were injected with TUNI (2 μ g/g) 6 h before killing. (a) Serum AST (IU/l) levels were measured and the number of steatohepatitis foci was determined ($n=5$). (b) The number of apoptotic hepatocytes was monitored by TUNEL staining. Immunoblotting of active caspase-3, Puma- α , Puma- β and Bax was performed from whole-liver lysates. (c) Immunoblot analysis of the protein levels of active caspase-11, caspase-1 and IL-1 β are shown ($n=5$). (d) Plasma levels of the cytokines IL-1 β , IL-6 and MCP-1 are represented ($n=5$). (e) The expression of ER stress proteins was compared in TUNI- and PBS-injected mice ($n=5$). Data are expressed as mean \pm standard error of the mean. Statistical significance from controls is denoted by * $P \leq 0.05$, ** $P \leq 0.01$

stress by TUNI led to liver injury associated with hepatocyte apoptosis in *ob/ob* mice.

Regarding inflammasome activation, we found that TUNI exacerbated hepatic caspase-11, caspase-1 and production of IL-1 β compared with control mice (Figure 4c). Importantly, in agreement with increased caspase-11 and -1 activation, the serum levels of systemic mature IL-1 β increased after TUNI injection (Figure 4d). TUNI treatment also increased the circulating levels of the proinflammatory cytokines IL-6 and MCP-1 (Figure 4d). The mRNA level of *Nlrp3* was also specifically increased with TUNI (Supplementary Figure S4B).

Hence, the induction of ER stress by TUNI administration not only triggered apoptosis, but also led to an increase in hepatocyte pyroptosis in *ob/ob* mice.

We thus analyzed the activity of UPR effectors in response to TUNI. The level of sXBP-1, a target of IRE1 α , was significantly increased after TUNI treatment (Figure 4e). Consequently, the mRNA levels of *sXBP-1* and the target gene *DnaJ9* (Supplementary Figure S4B) were increased in response to TUNI. Simultaneously, levels of hepatic phospho-PERK increased in TUNI-challenged mice compared with control mice. Accordingly, we detected a marked increase in

the protein (Figure 4e) and mRNA levels (Supplementary Figure S4B) of ATF4. Finally, a strong upregulation in CHOP protein expression, a downstream target of sXBP-1 and ATF4,⁵ was detected after TUNI challenge, alongside an increase in phospho-JNK expression (Figure 4e). Accordingly, TUNI increased the [CHOP/GRP78] ratio at the protein (Figure 4e) and the mRNA levels (Supplementary Figure S4B), thus favoring programmed hepatocyte death.

CHOP mediates ER-stress-induced pyroptosis and apoptosis in mouse primary hepatocytes. We evaluated cell viability, pyroptosis and apoptosis in primary mouse hepatocytes treated with LPS or TUNI, or co-treated with TUNI and LPS [TUNI+LPS], in the absence or presence of the ER stress inhibitor TUDCA. Although LPS and TUDCA alone did not alter hepatocyte viability (MTT test, Figure 5a) or positivity for TUNEL staining (Figure 5b), primary hepatocytes displayed enhanced sensitivity to co-treatment with TUNI+LPS, compared with TUNI alone, with a marked decrease in viability and a higher percentage of TUNEL-positive hepatocytes (Figures 5a and b). Furthermore, hepatocyte death induced by TUNI+LPS was partially suppressed by TUDCA. We also confirmed these results in AML12 hepatocytes (Supplementary Figure S7). We also tested whether Z-YVAD-fmk, a caspase-1 and caspase-11 inhibitor, could block the hepatocyte death induced by TUNI+LPS. The cell death caused by TUNI+LPS was indeed attenuated by Z-YVAD-fmk

(Supplementary Figure S7). These results suggest that loss of viability was dependent on proinflammatory caspase-1 and caspase-11 activities. We next monitored the protein levels of proinflammatory caspases, IL-1 β and CHOP by immunoblotting. Expression of the CHOP protein was enhanced in TUNI-treated hepatocytes, whereas it was barely detectable in controls (Figure 5c). Strikingly, CHOP protein expression was further increased in hepatocytes treated with TUNI+LPS. Importantly, this pattern of CHOP activation mirrored the increase in the active forms of caspase-11, caspase-1 and IL-1 β . These effects were strongly inhibited by TUDCA (Figure 5c). We hypothesized that CHOP could induce the activation of inflammatory caspases, but not apoptotic caspase-3. We then performed similar experiments in primary hepatocytes by knocking-down *Chop* using siRNA. As shown in Figure 5d, the knockdown of endogenous *Chop* strongly prevented the accumulation of active caspase-11, caspase-1 and their substrate IL-1 β in response to TUNI or TUNI+LPS, but not active caspase-3 (data not shown). This result indicated that TUNI and LPS act synergistically to induce CHOP-dependent inflammasome pyroptotic death.

NASH patients show increased hepatic ER stress, inflammasome priming and liver injury. In line with our results, we hypothesized that progression from steatosis to NASH could be associated with enhanced hepatic ER stress and inflammasome activation in obese patients. This was

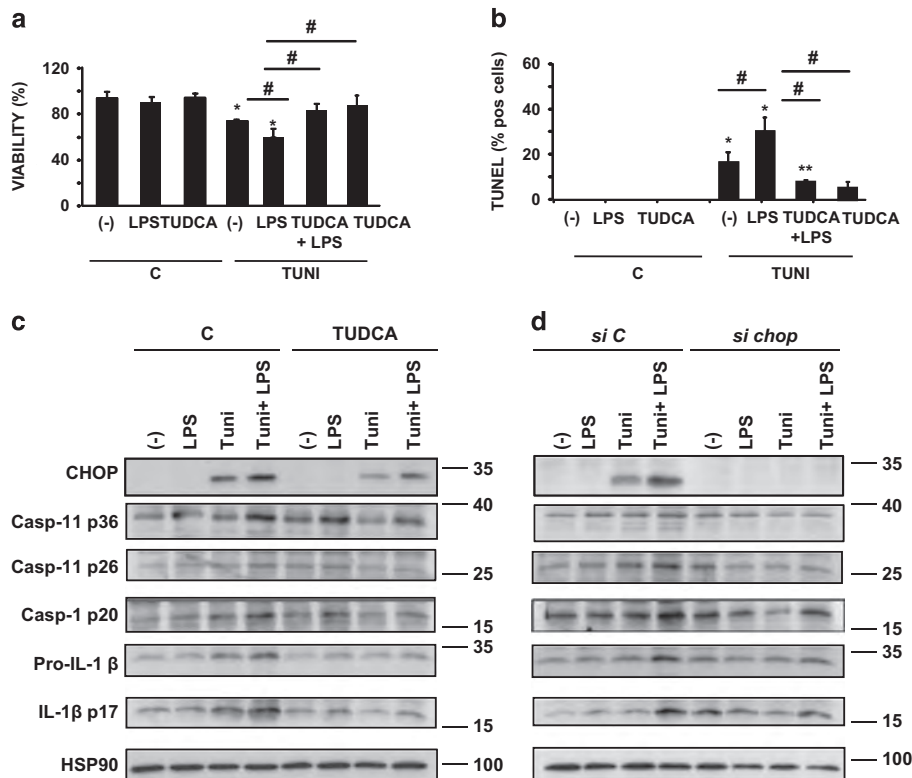


Figure 5 TUDCA inhibited CHOP-induced apoptosis and activation of the inflammasome in response to LPS and tunicamycin co-treatment in primary mouse hepatocytes. (a and b) Hepatocytes were pretreated for 48 h with 500 μ g/ml TUDCA followed by culture for 24 h in normal medium (c) or 100 ng/ml LPS, 1 μ g/ml TUNI or both (LPS+TUNI). After treatment, the percentage of viable cells quantified by MTT assay (a) (relative to control) and TUNEL-positive hepatocytes (b) was quantified ($n=4-6$). (c and d) Immunoblot analysis of CHOP, active caspase-11, caspase-1, pro-IL-1 β and IL-1 β protein levels assessed from hepatocytes pretreated either with TUDCA (c) or *Chop* siRNA (d) before stimulation ($n=3$). Data are expressed as mean \pm standard error of the mean. Statistical significance from controls is denoted by * $P \leq 0.05$, ** $P \leq 0.01$

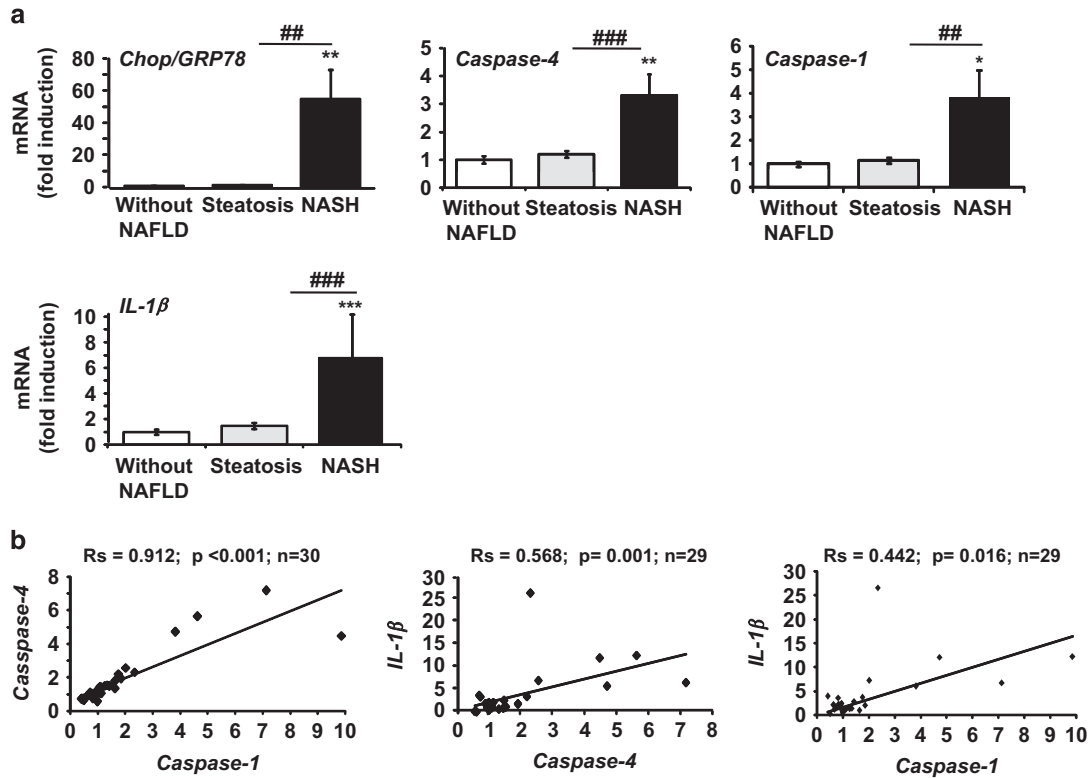


Figure 6 Increased expression of ER stress and inflammasome gene expression in human NASH. (a) The mRNA expression of *Chop*, *Grp78*, *caspase-4*, *caspase-1* and *IL-1β* (normalized to *RPLPO* mRNA) was measured in the livers of massively obese patients without NAFLD ($n=6$), with steatosis ($n=15$) or with NASH ($n=9$). Statistical significance of controls (patients without NAFLD) was determined with the Mann–Whitney test. (b) Correlation between NLRP3 inflammasome components at the relative mRNA expression level is shown. Correlation was evaluated using the Spearman's rank correlation test. Statistical significance from controls is denoted by * $P \leq 0.05$, ** $P \leq 0.01$, *** $P \leq 0.001$, **** $P \leq 0.0001$, ***** $P \leq 0.00001$.

tested by evaluating the expression of ER stress markers (*Chop* and *Grp78*) and inflammasome priming (*caspase-4*, which shares 60% homology with murine *caspase-11*), *caspase-1* and *IL-1β* in 30 obese subjects (Supplementary Table 1). The analysis of the mRNA levels showed a significant increase in both the deleterious [*Chop/Grp78*] ratio (54-fold increase), and inflammasome components (*caspase-4*, *caspase-1* and *IL-1β*) in NASH patients ($n=9$) compared with patients without NAFLD ($n=6$) and with steatosis ($n=15$, Figure 6a). These markers of ER stress and the inflammasome also correlated with the NAFLD Activity Score and liver injury, as evaluated by transaminase levels (Supplementary Table 2). In addition, we also found a positive correlation between the ER stress and level of inflammasome transcripts (Supplementary Table 2). The [*Chop/Grp78*] ratio correlated with the levels of *caspase-4* ($R_s=0.414$, $P=0.029$, $n=28$), *caspase-1* ($R_s=0.421$, $P=0.026$, $n=28$) and *IL-1β* ($R_s=0.46$, $P=0.016$, $n=27$) transcripts, which also correlated with each other (Figure 6b). These results indicate that ER stress and inflammasome platforms may cooperate in the progression from steatosis to NASH.

Discussion

Steatosis is an extremely common disorder affecting nearly 30% of the US population, among which 25% develop NASH with an inherent risk for progression to cirrhosis and

hepatocarcinoma. Although the function of the NLRP3 inflammasome in myeloid immune cells has been well characterized, increasing evidence shows that the NLRP3 inflammasome activation also occurs in non-myeloid cells, namely hepatocytes,³⁰ in normal and pathogenic states. Nevertheless, studies have not examined whether the ER stress response stimulates hepatic NLRP3 inflammasome activation and associated cell death in NASH. Our studies suggest several potential mechanisms related to ER stress and inflammasome activation that cooperate to induce NASH development.

We first found that exaggerated ER stress obtained with LPS or TUNI in the steatotic liver leads to a transient state of NASH-like disease and the presence of hepatocyte pyroptotic cell death. Remarkably, in livers from *ob/ob* mice, challenge with LPS resulted in a degree of steatohepatitis that closely resembled human NASH, and two of the main pathological features, steatohepatitis foci and hepatocyte apoptosis, were also rapidly induced by the administration of TUNI to *ob/ob* mice. In addition, we demonstrated in these animal models that the ER stress effectors PERK and IRE1 α converge on CHOP activation, thus increasing the activity of the NLRP3 inflammasome (*caspase-11*, *caspase-1*, *IL-1β*) and hepatic apoptosis (TUNEL positivity, *caspase-3*, BH3-only proteins). Second, a treatment with TUDCA dramatically reduces NLRP3 inflammasome activation and improves the NASH-pathological features in these models. Indeed, we have shown

that TUDCA, administered as a protective 5-day pretreatment or as a potential 6-h treatment in *ob/ob* LPS-injected mice, exhibits anti-inflammatory and hepatoprotective properties. Third, CHOP is a critical signaling node that links ER stress-induced cell death and inflammasome activation in hepatocytes. The level of CHOP activation was robust after LPS and TUNI co-treatment, which correlated with increased cell death and activation of caspase-11 and caspase-1. Genetic silencing of *Chop* strongly reduced the activation of caspase-11, -1 and IL-1 β production, suggesting that *Chop* modulates caspase-11 and caspase-1 activation at the transcriptional level in hepatocytes. We also observed that TUDCA protected hepatocytes from LPS- and TUNI-induced inflammasome activation and cell death, thus phenocopying the effects observed in mice with TUDCA treatment. Importantly, we reported a significant increase in gene expression of *Chop* in the livers of NASH patients, which correlated with priming of the inflammasome markers *caspase-1*, *caspase-4* and *IL-1 β* . These markers significantly correlated with liver injury (transaminases) and inflammation (presence of inflammatory foci and NAS score) suggesting that the cross-talk between ER stress and inflammasome is an important mediator in the pathophysiology of NASH.

Sustained inflammasome activation can trigger apoptosis and pyroptosis, resulting in DNA damage with positivity for TUNEL staining. We found an increase in TUNEL-positive hepatocytes in both livers from LPS- and TUNI-injected mice, which correlated with increased production of active caspase-1, caspase-11, IL-1 β and of caspase-3, PERK and IRE1 α activities. These results suggest that LPS and TUNI induce ER-dependent pyroptosis and apoptosis in the livers of *ob/ob* mice, whereas Z-YVAD-fmk and TUDCA blocked both pathways.

Our current data demonstrate for the first time a connection between ER stress activation and the presence of pyroptotic cell death in hepatocytes with a hyperactivated NLRP3 inflammasome. Importantly, we confirmed our results in a frequently used nutritional model of steatohepatitis by feeding mice with the MCD diet.

The role of CHOP in NAFLD remains unclear, as evidence demonstrated that MCD-diet-induced steatohepatitis was reduced in *Chop* knockout mice and that inflammation was exacerbated in macrophages from *Chop*-deficient mice¹³ arguing for a cell autonomous effect of the *Chop* deficiency. Our results support a deleterious role of CHOP, driving both ER stress-induced hepatocyte death through the activation of BH3-only proteins³¹ and the NLRP3 inflammasome activation in our experimental models. Herein, we demonstrated that CHOP expression correlated with Puma and Bax induction. These results are consistent with the concept that the induction of Puma is necessary for ER stress-induced apoptosis and can be linked to direct Bax activation, initiating mitochondrial dysfunction as a downstream consequence of ER stress.³² These results are in accordance with the high hepatic expression levels of Puma and Bax found in patients with NASH contributing to hepatocyte lipoapoptosis.³³ Interestingly under stress conditions, Bax and Bak can activate IRE1 α .³⁴ They could act as retro-positive controls amplifying ER stress apoptosis, inflammasome activation and downstream mitochondrial dysfunction in NASH models.

Transcriptionally, CHOP expression is regulated by ATF4, sXBP-1 and cATF6.³⁵ Therefore, the increase in CHOP expression observed in the steatotic livers of mice treated with LPS and TUNI could be a reflection of both PERK and IRE1 α /sXBP1 activation, as ATF6 remained unchanged. The increase in phospho-JNK observed in these mice could also reflect IRE1 α /TRAF2/ASK1 activation.⁵ Interestingly, JNK is speculated to promote CHOP activity through phosphorylation,^{5,6} thereby potentially reinforcing the PERK pathway and the IRE1 α /sXBP-1-dependent pathway that increases CHOP production, inflammasome activation and hepatocyte death.

Such a connection between ER stress and inflammasome pathways has been recently suggested through the thioredoxin-interacting protein (TXNIP) which associates PERK and IRE1 α with the NLRP3 inflammasome, thus activating β -cell death and contributing to diabetes.^{36,37} We did not observe any variation of TXNIP protein expression in our experimental conditions suggesting that TXNIP does not seem to be a target of hepatic IRE1 α and PERK, at least in our models (Supplementary Figure S8). Hyperactivated IRE1 α or irremediable ER stress would also spontaneously generate ROS.³⁶ We found that the level of ROS production was slightly increased after LPS and TUNI co-treatment (Supplementary Figure S8). As ROS enhance the activation of NLRP3 inflammasome, they may further amplify effects of the IRE1 α -PERK-CHOP axes to increase pyroptosis in our experimental conditions. Future studies seeking to characterize the tight link between ER stress and NLRP3 pathways and its contribution to liver inflammation and cell death are worth considering.

As other inflammasome pathways have been described,³⁸ our results support a model in which the severity of the ER stress response could activate these pathways, in hepatocytes and nonparenchymal cells, resulting in the induction of proinflammatory signaling, hepatocyte pyroptotic death and fibrosis in various liver pathologies, such as NASH, ASH and HCC. For example, AIM2 could be an attractive candidate as it senses damage-associated molecular patterns, such as cytoplasmic and mitochondrial DNA, which are increased in NASH patients.³⁹ AIM2 could form an NLRP3-independent inflammasome with Pycard and caspase-1, contributing to the pathological features of these liver diseases.

A therapeutic strategy that aims to target these common processes might be effective; TUDCA could provide such a strategy. In our animal models, it is possible that TUDCA decreases the amount of inflammatory mediators produced by activating inflammatory macrophages and the inflammatory microenvironment. Studies have reported that TUDCA decreases the amount of TNF α produced by inflammatory macrophages in a model of HCC.⁴⁰ TUDCA could also decrease the expression of TLR4, the receptor of LPS. In the liver, TLR4 is expressed in both hepatocytes and immune cells such as macrophages. TLR4 specifically activates IRE1 α to increase cytokine production (IL-6 and TNF α) in macrophages.⁴¹ Such a mechanism could also occur in hepatocytes contributing to amplify the inflammatory responses provoked by an LPS challenge

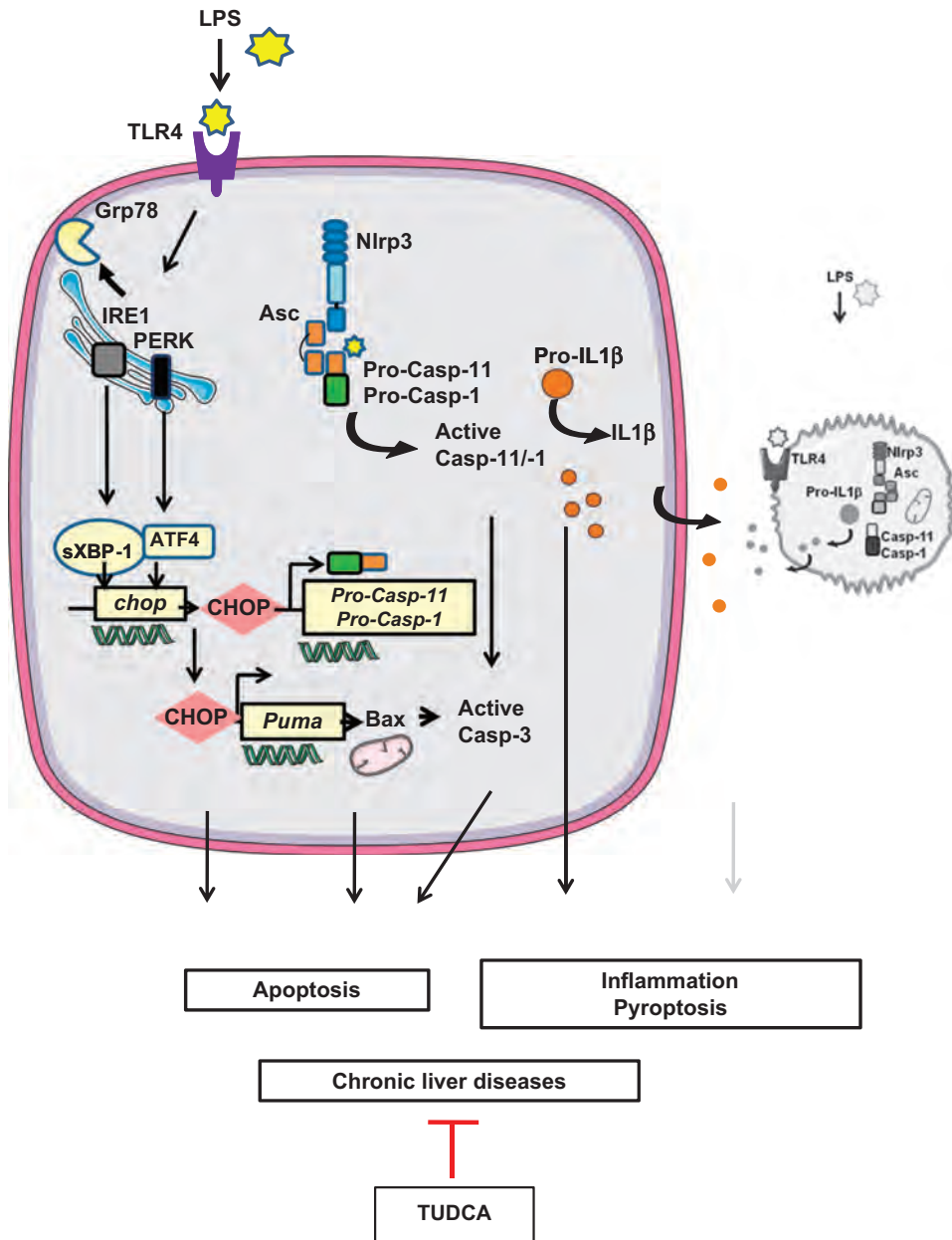


Figure 7 ER stress activates NLRP3 inflammasome and hepatocyte death in liver disorders. Endotoxemia (LPS), a pathological condition found in chronic liver diseases, overwhelms hepatic IRE1 α and PERK activities, leading to the overexpression of CHOP, which regulates the expression of *caspase-1*, *caspase-11* and Puma, and triggers hepatocyte pyroptosis and apoptosis. TUDCA increased the [GRP78/CHOP] ratio, promoting protection against ER-dependent NLRP3 inflammasome and cell death pathways. Using TUDCA, either alone or combined with hepatoprotective and anti-inflammatory interventions, could be a valid therapeutic strategy for the treatment of liver disorders

(Figure 7). Further studies are needed to fully answer this question.

In summary, we have demonstrated that ER stress leads to NLRP3 inflammasome activation, thus resulting in severe liver inflammation and hepatocyte pyroptotic death, and contributing as a novel mechanism of ER-mediated liver damage (Figure 7). In this way, blocking ER-dependent NLRP3 inflammasome and cell death pathways, with TUDCA alone, or combined with other hepatoprotective and anti-inflammatory interventions, may represent a valid therapeutic strategy for the treatment of liver disorders.

Materials and Methods

Animal care, mouse model and treatments. All the animal procedures were conducted in compliance with protocols approved by local ethical government authorities. Male, *ob/ob* mice (C57BL/6J-*ob/ob*), at 6 weeks of age were purchased from Janvier Laboratories (Saint-Berthevin, France). Experiments were started 2 weeks after the arrival of the mice in our animal facility. Four different treatment protocols were administered: (1) TUDCA was injected intraperitoneally (250 μ g/g twice a day, total 500 μ g/g/day) for 5 days. Control mice received the same volume of vehicle (PBS). Mice were subjected to a single LPS injection (2 μ g/g) 6 h before being killed. (2) TUDCA and LPS were co-injected intraperitoneally at the above-mentioned concentrations for the duration of the 6-h treatment. Other mice were either injected with PBS, TUDCA or LPS 6 h before being killed, at the

concentrations stated previously. (3) Mice were intraperitoneally injected with tunicamycin (2 $\mu\text{g/g}$) or vehicle control (PBS) 6 h before being killed. All the mice were fed a normal chow diet (A04, Safe Diet, Augy, France). (4) Wild-type C57BL/6 male mice (16–18 weeks of age), from Janvier were fed a methionine- and choline-deficient diet (MCD, ref 960439) or control diet (ND) (ref 960440, MP BIO) for 2 weeks. Water was available *ad libitum*.

Biochemical analysis and cytokine measurement. Serum levels of aspartate aminotransferase (AST) and alanine aminotransferase (ALT) were determined using a standardized UV test after activation with pyridoxal-phosphate (Roche-Hitachi analyzer, ASTPM, ALTPM, Cobas, Meylan, France). The BD Cytometric Bead Array (CBA) Mouse Inflammation Kit was used to quantitatively measure cytokines by flow cytometry as described previously.⁴²

Histological evaluation. Liver tissue specimens were fixed in 10% buffered formalin, embedded in paraffin, sectioned (5 μm thick), stained with hematoxylin-eosin, and then analyzed blindly by a liver pathologist.

TUNEL assay. Liver tissue specimens were embedded in paraffin and sectioned at 5 μm for processing by the TUNEL method using a commercial kit, using DAB peroxidase substrate (Roche Molecular Biochemicals, Meylan, France) and counterstained with methyl green. Specimens were evaluated by microscopy at high power magnification ($\times 100$) in a blinded manner. A total of 30 random fields were counted for each TUNEL-stained tissue sample. TUNEL assays on primary hepatocytes were performed following exactly the same procedure as we previously described.^{43,44}

In vitro assay for viability. Cell viability was determined by a colorimetric assay based on the ability of viable cells to reduce 3-(4,5-dimethylthiazol-2-yl)-2,5-diphenyl tetrazolium bromide (MTT) as described,^{45,46} generating a dark blue formazan product. Dissolved MTT was added to each well of the plate and the plate was incubated at 37 °C for 1 h. The absorbance at 550 nm was measured using a microplate spectrophotometer system (ELX800, Bio-TEK Instruments, Colmar, France). Results are presented as a percentage of the control values.

Real-time quantitative PCR analysis. Total RNA was extracted from liver tissue using an RNeasy Mini Kit (Qiagen, Courtaboeuf, France). The samples were treated with Turbo DNA-free (Applied Biosystems, Courtaboeuf, France) or RNase-free DNase kit (Qiagen) following the manufacturer's protocols. The quality of the isolated RNA was determined using the Agilent 2100 Bioanalyser with RNA 6000 Nano Kit (Agilent Technologies, Massy, France). Total RNA was reverse-transcribed with the High Capacity cDNA Reverse Transcription Kit (Applied Biosystems). Real-time quantitative PCR was performed using the ABI PRISM 7500/Step-One Fast Real Time PCR System following the manufacturer's protocols in C3M genomics facilities. The TaqMan gene expression assays were purchased from Applied Biosystems (Supplementary Materials and Methods). Gene expression values were normalized to the value of the housekeeping gene 36B4 (mice conditions) or RPLP0 (human conditions) and calculated on the basis of the comparative cycle threshold Ct method (2 $\Delta\Delta\text{Ct}$) as we described previously.^{44,46}

Immunoblot analysis. Total liver protein was isolated from snap-frozen tissues, homogenized in detergent-containing buffer, normalized for the protein content (50 μg per sample), and analyzed by SDS-PAGE (8–15% gels) immunoblotting as previously described for ER stress studies^{42,46} and for inflammasome studies.⁴⁷ Equal loading was assured by Ponceau S staining. Western blot analyses were performed using the primary antibodies described in Supplementary Materials and Methods. Antibody detection was accomplished using horseradish peroxidase-conjugated secondary antibodies (Supplementary Materials and Methods) and an enhanced chemiluminescence method (Amersham Biosciences, Piscataway, NJ, USA). Immunoblots were scanned, and the signals were quantified using ImageJ software.

Cellular models and treatments. Hepatocytes from mouse liver were isolated by a two-step collagenase procedure, as we previously described.⁴⁶ Isolated cells were resuspended in Medium I (Williams' Medium E) supplemented with 10% fetal bovine serum (PAA Laboratories, Villacoublay, France), 100 units/ml penicillin, 100 $\mu\text{g/ml}$ streptomycin, 2 mM L-glutamine, 0.02 U/ml insulin (Humulin, Lilly, Fegersheim, France). Viability was evaluated by trypan blue exclusion (Sigma, St. Louis, MO, USA). Hepatocytes were incubated for 4 h at 37 °C in a humidified

atmosphere with 5% CO₂. For culture, Medium I was renewed with Medium II (a fetal bovine serum-free Medium I, supplemented instead with 0.5% bovine serum albumin). Hepatocytes were also pretreated with TUDCA (500 $\mu\text{g/ml}$) for 48 h or with Z-YVAD-fmk (25 μM) for 1 h in Medium II. Following these incubation times, tunicamycin (TUNI; 1 $\mu\text{g/ml}$), LPS (100 ng/ml) or [TUNI+LPS] was gently added to the culture for 24 h in Medium II. AML12 hepatocytes (CRL-2254, ATCC) were cultured in medium (DMEM, 4.5 g/l glucose, 100 units/ml penicillin, 100 $\mu\text{g/ml}$ streptomycin and 2 mM L-glutamine) supplemented with 10% fetal bovine serum (PAA Laboratories), under 5% CO₂ at 37 °C. The conditions for stimulation were the same.

siRNA transfection. Primary hepatocytes were transfected with *chop* (*ddit3*) siRNA (MSS273951, Invitrogen, Carlsbad, CA, USA) or control siRNA (Invitrogen, Low) at 30 nM using Lipofectamine RNAiMAX (Invitrogen) according to the manufacturer's instructions. After 48 h of transfection, the cells were then treated as indicated above.

Human studies. Morbidly obese patients ($n=30$) were recruited through the Department of Digestive Surgery and Liver Transplantation (Nice Hospital) where they underwent bariatric surgery for their morbid obesity. Bariatric surgery was indicated for these patients in accordance with the French guidelines. Exclusion criteria were: presence of a hepatitis B or hepatitis C infection, excessive alcohol consumption (> 20 g/day) or another cause of chronic liver disease, as previously described.⁴⁸ The characteristics of the study groups are given in Supplementary Table 1. Before surgery, fasting blood samples were obtained and used to measure ALT and AST aminotransaminases; glucose and insulin resistance were calculated using the homeostatic model assessment (HOMA-IR) index. Surgical liver biopsies were obtained during surgery and no ischemic preconditioning had been performed. Histopathological analysis was performed according to the scoring system of Kleiner *et al.*⁴⁹ Four histopathological features were semi-quantitatively evaluated: grade of steatosis (0, < 5%; 1, 5–30%; 2, > 30–60%; 3, > 60%), lobular inflammation (0, no inflammatory foci; 1, < 2 inflammatory foci per $\times 200$ field; 2, 2–4 inflammatory foci per $\times 200$ field; 3, > 4 inflammatory foci per $\times 200$ field), hepatocellular ballooning (0, none; 1, few ballooned cells; 2, many cells/prominent ballooning) and stage of fibrosis (from none = 0, to cirrhosis = 4). All the subjects gave their informed written consent to participate in this study in accordance with the French legislation regarding Ethics and Human Research (Huriet-Serusclet law). The "Comité Consultatif de Protection des Personnes dans la Recherche Biomédicale de Nice" approved the study (07/04:2003, N°03.017).

Statistical analysis. Statistical significance of differential gene expression between the two study groups was determined using the non-parametric Mann-Whitney test with the ΔCt of each group. Correlations were analyzed using the Spearman's rank correlation test. Other data from mice and cells were statistically analyzed by Student's *t*-test or ANOVA and *post hoc* analysis for multiple group comparison. Data are expressed as mean \pm S.E.M. Statistical significance from controls is denoted by * $P \leq 0.05$, ** $P \leq 0.01$, *** $P \leq 0.001$. Following the same pattern, # denotes statistical significance between specified groups.

Conflict of Interest

The authors declare no conflict of interest.

Acknowledgements. This work was supported by grants from INSERM (France), the University of Nice, the Programme Hospitalier de Recherche Clinique (Centre Hospitalier Universitaire Nice) and charities (Association Française pour l'Etude du Foie (AFEF)/Aptalis, Société Francophone du Diabète (SFD/MSD), Benjamin Delessert, Fondation Recherche Médicale (FRM) to BBM; EFS/Lilly European Diabetes Research Programme, SFD, SFD/Roche Pharma, AFEF/LFB to PG). This work and CL were funded by the French Government (National Research Agency, ANR) through the 'Investments for the Future' LABEX SIGNALIFE: program reference #ANR-11-LABX-0028-01. We thank Dr. Sandrine Marchetti and Dr. Jean-Louis Nahon for scientific discussions. We thank the C3M Animal Facility team for their assistance with animal care.

1. Henao-Mejia J, Elinav E, Jin C, Hao L, Mehal WZ, Strowig T *et al*. Inflammasome-mediated dysbiosis regulates progression of NAFLD and obesity. *Nature* 2012; **482**: 179–185.
2. Angulo P. Nonalcoholic fatty liver disease. *N Engl J Med* 2002; **346**: 1221–1231.

3. Ozcan U, Cao Q, Yilmaz E, Lee AH, Iwakoshi NN, Ozdelen E *et al*. Endoplasmic reticulum stress links obesity, insulin action, and type 2 diabetes. *Science* 2004; **306**: 457–461.
4. Puri P, Mirshahi F, Cheung O, Natarajan R, Maher JW, Kellum JM *et al*. Activation and dysregulation of the unfolded protein response in nonalcoholic fatty liver disease. *Gastroenterology* 2008; **134**: 568–576.
5. Xu C, Bailly-Maitre B, Reed JC. Endoplasmic reticulum stress: cell life and death decisions. *J Clin Invest* 2005; **115**: 2656–2664.
6. McCullough KD, Martindale JL, Klott LO, Aw TY, Holbrook NJ. Gadd153 sensitizes cells to endoplasmic reticulum stress by down-regulating Bcl2 and perturbing the cellular redox state. *Mol Cell Biol* 2001; **21**: 1249–1259.
7. Nakatani Y, Kaneto H, Kawamori D, Yoshiuchi K, Hatazaki M, Matsuoka TA *et al*. Involvement of endoplasmic reticulum stress in insulin resistance and diabetes. *J Biol Chem* 2005; **280**: 847–851.
8. Gregor MF, Yang L, Fabbrini E, Mohammed BS, Eagon JC, Hotamisligil GS *et al*. Endoplasmic reticulum stress is reduced in tissues of obese subjects after weight loss. *Diabetes* 2009; **58**: 693–700.
9. Lee AH, Scapa EF, Cohen DE, Glimcher LH. Regulation of hepatic lipogenesis by the transcription factor XBP1. *Science* 2008; **320**: 1492–1496.
10. Oyadomari S, Harding HP, Zhang Y, Oyadomari M, Ron D. Dephosphorylation of translation initiation factor 2 α enhances glucose tolerance and attenuates hepatosteatosis in mice. *Cell Metab* 2008; **7**: 520–532.
11. Gonzalez-Rodriguez A, Mayoral R, Agra N, Valdecantos MP, Pardo V, Miquilena-Colina ME *et al*. Impaired autophagic flux is associated with increased endoplasmic reticulum stress during the development of NAFLD. *Cell Death Dis* 2014; **5**: e1179.
12. Toriguchi K, Hatano E, Tanabe K, Takemoto K, Nakamura K, Koyama Y *et al*. CHOP deficiency attenuates steatohepatitis, fibrosis and carcinogenesis in mice fed an MCD diet. *J Gastroenterol Hepatol* 2014; **29**: 1109–1118.
13. Malhi H, Kropp EM, Clavo VF, Kobrossi CR, Han J, Mauer AS *et al*. C/EBP homologous protein-induced macrophage apoptosis protects mice from steatohepatitis. *J Biol Chem* 2013; **288**: 18624–18642.
14. Goodall JC, Wu C, Zhang Y, McNeill L, Ellis L, Saudek V *et al*. Endoplasmic reticulum stress-induced transcription factor, CHOP, is crucial for dendritic cell IL-23 expression. *Proc Natl Acad Sci USA* 2010; **107**: 17698–17703.
15. Ribeiro PS, Cortez-Pinto H, Sola S, Castro RE, Ramalho RM, Baptista A *et al*. Hepatocyte apoptosis, expression of death receptors, and activation of NF- κ B in the liver of nonalcoholic and alcoholic steatohepatitis patients. *Am J Gastroenterol* 2004; **99**: 1708–1717.
16. Vandannagsar B, Youm YH, Ravussin A, Galgani JE, Stadler K, Mynatt RL *et al*. The NLRP3 inflammasome instigates obesity-induced inflammation and insulin resistance. *Nat Med* 2011; **17**: 179–188.
17. Lamkanfi M, Dixit VM. Inflammasomes: guardians of cytosolic sanctity. *Immunol Rev* 2009; **227**: 95–105.
18. Cani PD, Amar J, Iglesias MA, Poggi M, Knauf C, Bastelica D *et al*. Metabolic endotoxemia initiates obesity and insulin resistance. *Diabetes* 2007; **56**: 1761–1772.
19. Ruiz AG, Casafont F, Crespo J, Cayon A, Mayorga M, Estebanez A *et al*. Lipopolysaccharide-binding protein plasma levels and liver TNF- α gene expression in obese patients: evidence for the potential role of endotoxin in the pathogenesis of non-alcoholic steatohepatitis. *Obes Surg* 2007; **17**: 1374–1380.
20. Vyberg M, Ravn V, Andersen B. Pattern of progression in liver injury following jejunoileal bypass for morbid obesity. *Liver* 1987; **7**: 271–276.
21. Shanab AA, Scully P, Crosbie O, Buckley M, O'Mahony L, Shanahan F *et al*. Small intestinal bacterial overgrowth in nonalcoholic steatohepatitis: association with toll-like receptor 4 expression and plasma levels of interleukin 8. *Dig Dis Sci* 2011; **56**: 1524–1534.
22. Stienstra R, Joosten LA, Koenen T, van Tits B, van Diepen JA, van den Berg SA *et al*. The inflammasome-mediated caspase-1 activation controls adipocyte differentiation and insulin sensitivity. *Cell Metab* 2010; **12**: 593–605.
23. Stienstra R, van Diepen JA, Tack CJ, Zaki MH, van de Veerdonk FL, Perera D *et al*. Inflammasome is a central player in the induction of obesity and insulin resistance. *Proc Natl Acad Sci USA* 2011; **108**: 15324–15329.
24. Shi H, Kokoeva MV, Inouye K, Tzamelis I, Yin H, Flier JS. TLR4 links innate immunity and fatty acid-induced insulin resistance. *J Clin Invest* 2006; **116**: 3015–3025.
25. Galluzzi L, Vitale I, Abrams JM, Alnemri ES, Baehrecke EH, Blagosklonny MV *et al*. Molecular definitions of cell death subroutines: recommendations of the Nomenclature Committee on Cell Death 2012. *Cell Death Differ* 2012; **19**: 107–120.
26. Galluzzi L, Bravo-San Pedro JM, Vitale I, Aaronson SA, Abrams JM, Adam D *et al*. Essential versus accessory aspects of cell death: recommendations of the NCCD 2015. *Cell Death Differ* 2015; **22**: 58–73.
27. Day CP, James OF. *Steatohepatitis: a tale of two 'h's'?* *Gastroenterology* 1998; **114**: 842–845.
28. Yang SQ, Lin HZ, Lane MD, Clemens M, Diehl AM. Obesity increases sensitivity to endotoxin liver injury: implications for the pathogenesis of steatohepatitis. *Proc Natl Acad Sci USA* 1997; **94**: 2557–2562.
29. Kudo H, Takahara T, Yata Y, Kawai K, Zhang W, Sugiyama T. Lipopolysaccharide triggered TNF- α -induced hepatocyte apoptosis in a murine non-alcoholic steatohepatitis model. *J Hepatol* 2009; **51**: 168–175.
30. Wree A, Eguchi A, McGeough MD, Pena CA, Johnson CD, Canbay A *et al*. NLRP3 inflammasome activation results in hepatocyte pyroptosis, liver inflammation and fibrosis. *Hepatology* 2014; **59**: 898–910.
31. Li J, Lee B, Lee AS. Endoplasmic reticulum stress-induced apoptosis: multiple pathways and activation of p53-up-regulated modulator of apoptosis (PUMA) and NOXA by p53. *J Biol Chem* 2006; **281**: 7260–7270.
32. Kim H, Tu HC, Ren D, Takeuchi O, Jeffers JR, Zambetti GP *et al*. Stepwise activation of BAX and BAK by tBID, BIM, and PUMA initiates mitochondrial apoptosis. *Mol Cell* 2009; **36**: 487–499.
33. Cazanave SC, Elmi NA, Akazawa Y, Bronk SF, Mott JL, Gores GJ. CHOP and AP-1 cooperatively mediate PUMA expression during lipoapoptosis. *Am J Physiol Gastrointest Liver Physiol* 2010; **299**: G236–G243.
34. Hetz C, Bernasconi P, Fisher J, Lee AH, Bassik MC, Antonsson B *et al*. Proapoptotic BAX and BAK modulate the unfolded protein response by a direct interaction with IRE1 α . *Science* 2006; **312**: 572–576.
35. Oyadomari S, Mori M. Roles of CHOP/GADD153 in endoplasmic reticulum stress. *Cell Death Differ* 2004; **11**: 381–389.
36. Lerner AG, Upton JP, Praveen PV, Ghosh R, Nakagawa Y, Igbaria A *et al*. IRE1 α induces thioredoxin-interacting protein to activate the NLRP3 inflammasome and promote programmed cell death under irremediable ER stress. *Cell Metab* 2012; **16**: 250–264.
37. Osowski CM, Hara T, O'Sullivan-Murphy B, Kanekura K, Lu S, Hara M *et al*. Thioredoxin-interacting protein mediates ER stress-induced beta cell death through initiation of the inflammasome. *Cell Metab* 2012; **16**: 265–273.
38. Lamkanfi M, Dixit VM. The inflammasomes. *PLoS Pathog* 2009; **5**: e1000510.
39. Brunt EM. Pathology of nonalcoholic steatohepatitis. *Hepatol Res* 2005; **33**: 68–71.
40. Nakagawa H, Umemura A, Taniguchi K, Font-Burgada J, Dhar D, Ogata H *et al*. ER stress cooperates with hypernutrition to trigger TNF-dependent spontaneous HCC development. *Cancer Cell* 2014; **26**: 331–343.
41. Martinon F, Chen X, Lee AH, Glimcher LH. TLR activation of the transcription factor XBP1 regulates innate immune responses in macrophages. *Nat Immunol* 2010; **11**: 411–418.
42. Bailly-Maitre B, Belgardt BF, Jordan SD, Coornaert B, von Freyend MJ, Kleinriders A *et al*. Hepatic Bax inhibitor-1 inhibits IRE1 α and protects from obesity-associated insulin resistance and glucose intolerance. *J Biol Chem* 2010; **285**: 6198–6207.
43. Bailly-Maitre B, de Sousa G, Zucchini N, Gugenheim J, Bouloukos KE, Rahmani R. Spontaneous apoptosis in primary cultures of human and rat hepatocytes: molecular mechanisms and regulation by dexamethasone. *Cell Death Differ* 2002; **9**: 945–955.
44. Patouraux S, Rousseau D, Rubio A, Bonnafous S, Lavallard VJ, Lauron J *et al*. Osteopontin deficiency aggravates hepatic injury induced by ischemia-reperfusion in mice. *Cell Death Dis* 2014; **5**: e1208.
45. Bailly-Maitre B, de Sousa G, Bouloukos K, Gugenheim J, Rahmani R. Dexamethasone inhibits spontaneous apoptosis in primary cultures of human and rat hepatocytes via Bcl-2 and Bcl-XL induction. *Cell Death Differ* 2001; **8**: 279–288.
46. Bailly-Maitre B, Fondevila C, Kaldas F, Droin N, Luciano F, Ricci JE *et al*. Cytoprotective gene bi-1 is required for intrinsic protection from endoplasmic reticulum stress and ischemia-reperfusion injury. *Proc Natl Acad Sci USA* 2006; **103**: 2809–2814.
47. Bruey JM, Bruey-Sedano N, Luciano F, Zhai D, Balpai R, Xu C *et al*. Bcl-2 and Bcl-XL regulate proinflammatory caspase-1 activation by interaction with NALP1. *Cell* 2007; **129**: 45–56.
48. Anty R, Marjoux S, Iannelli A, Patouraux S, Schneck AS, Bonnafous S *et al*. Regular coffee but not espresso drinking is protective against fibrosis in a cohort mainly composed of morbidly obese European women with NAFLD undergoing bariatric surgery. *J Hepatol* 2012; **57**: 1090–1096.
49. Kleiner DE, Brunt EM, Van Natta M, Behling C, Contos MJ, Cummings OW *et al*. Design and validation of a histological scoring system for nonalcoholic fatty liver disease. *Hepatology* 2005; **41**: 1313–1321.



Cell Death and Disease is an open-access journal published by Nature Publishing Group. This work is licensed under a Creative Commons Attribution 4.0 Unported License. The images or other third party material in this article are included in the article's Creative Commons license, unless indicated otherwise in the credit line; if the material is not included under the Creative Commons license, users will need to obtain permission from the license holder to reproduce the material. To view a copy of this license, visit <http://creativecommons.org/licenses/by/4.0/>

Supplementary Information accompanies this paper on Cell Death and Disease website (<http://www.nature.com/cddis>)



Roux-En Y Gastric Bypass Results in Long-Term Remission of Hepatocyte Apoptosis and Hepatic Histological Features of Non-alcoholic Steatohepatitis

Anne-Sophie Schneck^{1,2,3}, Rodolphe Anty^{1,2,3}, Stéphanie Patouraux^{1,2,4}, Stéphanie Bonnafous^{1,2,3}, Déborah Rousseau^{1,2}, Cynthia Lebeauvin^{1,2}, Beatrice Bailly-Maitre^{1,2}, Arnaud Sans¹, Albert Tran^{1,2,3}, Jean Gugenheim^{1,2,3}, Antonio Iannelli^{1,2,3*†} and Philippe Gual^{1,2*†}

OPEN ACCESS

Edited by:

Honglei Weng,
Heidelberg University, Germany

Reviewed by:

Jun Li,
University Medical Center
Hamburg-Eppendorf, Germany
Mazen Nouredin,
Cedars-Sinai Medical Center, USA

*Correspondence:

Antonio Iannelli
iannelli.a@chu-nice.fr
Philippe Gual
gual@unice.fr

†These authors have contributed
equally to this work.

Specialty section:

This article was submitted to
Gastrointestinal Sciences,
a section of the journal
Frontiers in Physiology

Received: 02 June 2016

Accepted: 27 July 2016

Published: 19 August 2016

Citation:

Schneck A-S, Anty R, Patouraux S,
Bonnafous S, Rousseau D,
Lebeauvin C, Bailly-Maitre B, Sans A,
Tran A, Gugenheim J, Iannelli A and
Gual P (2016) Roux-En Y Gastric
Bypass Results in Long-Term
Remission of Hepatocyte Apoptosis
and Hepatic Histological Features of
Non-alcoholic Steatohepatitis.
Front. Physiol. 7:344.
doi: 10.3389/fphys.2016.00344

¹ Institut Nationale de la Santé et de Recherche Médicale, U1065, C3M, Team 8 "Hepatic Complications in obesity", Nice, France, ² Institut Nationale de la Santé et de Recherche Médicale, C3M, Université Côte d'Azur, Nice, France, ³ Digestive Centre, Archet Hospital Nice, Centre Hospitalier Universitaire de Nice, Nice, France, ⁴ Biological Centre, Pasteur Hospital, Centre Hospitalier Universitaire de Nice, Nice, France

The long-term effects of bariatric surgery on non-alcoholic steatohepatitis (NASH), focusing on liver injury and hepatocyte apoptosis, are not well-established. We here performed a longitudinal study with paired liver biopsies of nine morbidly obese women (median BMI: 42 [38.7; 45.1] kg/m²) with NASH with a median follow-up of 55 [44; 75] months after laparoscopic Roux-en-Y gastric bypass (LRYGB) surgery. LRYGB surgery was associated with significant weight loss (median BMI loss −13.7 [−16.4; −9.5] kg/m²), improved hepatic steatosis in all patients (55.5% with total resolution), and resolution of hepatic inflammation and hepatocyte ballooning in 100 and 88.8% of cases, respectively. Alanine aminotransferase levels dropped to normal values while hepatic activated cleaved caspase-3 levels strongly decreased after a median follow-up of 55 months. Hepatocyte apoptosis, as evaluated by serum caspase-generated keratin-18 fragment, improved within the first year following LRYGB and these improvements persisted for at least 55 months. LRYGB in morbidly obese patients with NASH is thus associated with a long-lasting beneficial impact on hepatic steatohepatitis and hepatocyte death.

Keywords: liver, NASH, bariatric surgery, NAFLD, steatosis, obesity

INTRODUCTION

Obesity represents a major health burden, as it is associated with a growing number of comorbidities (Must et al., 1999; Stevens et al., 2012). As the prevalence of obesity increases, so does the prevalence of non-alcoholic fatty liver disease (NAFLD), which is now the leading cause of chronic liver disease in the Western world (Younossi et al., 2011, 2016; Setiawan et al., 2016). NAFLD includes a spectrum of liver abnormalities, ranging from simple steatosis to non-alcoholic steatohepatitis (NASH) and to liver cirrhosis, eventually leading to hepatocellular carcinoma (Tran and Gual, 2013; Yeh and Brunt, 2014). Regarding NASH, which is characterized by the presence of liver inflammation and injury (hepatocyte ballooning and apoptosis), recent reports indicate

that it is the second most common indication for liver transplantation in the United States (Wong et al., 2015). To counter the obesity epidemic, bariatric surgery has emerged as the only therapeutic treatment that results in long-term weight loss and improvement or resolution of most obesity-related comorbidities (Mitka, 2012; Schauer et al., 2014). However, evidence of the long-term efficacy of bariatric surgery against NASH is not well-established. A recent report, including a cohort of 109 morbidly obese patients with biopsy-proven NASH, has shown that bariatric surgery induced the disappearance of NASH in nearly 85% of patients and reduced the pathological features of the disease after 12 months of follow-up (Lassailly et al., 2015). Other results reported in the literature are more disparate and focus on various liver complications (mainly steatosis and fibrosis) with differing bariatric procedures and with a follow-up never exceeding 24 months (Silverman et al., 1995; Clark et al., 2005; Mattar et al., 2005; Mottin et al., 2005; Barker et al., 2006; Csendes et al., 2006; de Almeida et al., 2006; Klein et al., 2006; Furuya et al., 2007; Liu et al., 2007; Mathurin et al., 2009; Chavez-Tapia et al., 2010). In this study, we evaluated the long-term effects (median follow-up biopsy at 55 months) of laparoscopic Roux-en-Y gastric bypass (LRYGB) surgery on hepatic NASH features and liver injury (mainly hepatocyte apoptosis) in morbidly obese women with biopsy-proven NASH at the time of the surgery.

MATERIALS AND METHODS

Study Design

Five hundred and sixty-eight consecutive severely and morbidly obese patients, referred for bariatric surgery, were included between December 2002 and December 2009. The study protocol was performed according to the French legislation regarding Ethics and Human Research and was approved by the local Ethics Committee (Huriet-Serusclet law, DGS 2003/0395). Written informed consent was obtained from all patients. All patients met the 1992 NIH Consensus Conference guidelines for gastrointestinal surgery for obesity. These patients underwent bariatric surgery at the Department of Digestive Surgery and Liver Transplantation of the University of Nice (France). All patients had a preoperative work-up (repeated at 6 and 12 months after surgery) and underwent a wedge-liver biopsy at the time of surgery. A second liver biopsy and a concomitant diagnostic work-up were offered to patients who underwent a LRYGB, and who initially presented with criteria for NASH (on a liver biopsy) and completed a minimum follow-up period of 40 months after surgery. Between January 2002 and December 2009, of the 84 patients with a NAS ≥ 5 on the wedge-liver biopsy at the time of surgery, 33 had a follow-up of <36 months, 13 were lost to follow-up and 29 refused to reiterate the biopsy. The comparison of clinical and biochemical parameters of the nine NASH patients with a second liver biopsy (Table 1) compared with those corresponding to the 75 NASH patients without a second liver biopsy (Table 2) showed no significant differences regarding BMI ($P = 0.2473$), fasting glucose level ($P = 0.177$), fasting insulin level ($P = 0.311$), HOMA-IR ($P = 0.5976$), prevalence of type 2 diabetes (44 vs. 42.6% respectively), ALT

TABLE 1 | Patients' clinical and biochemical parameters at baseline and after a ≥ 40 -month follow-up period (patients with paired liver biopsies).

	T0	T ≥ 40	p
Number	9	9	ns
Time after surgery (months) (median, Q1; Q3)		55 (44; 75)	
BMI (kg/m ²) (median, Q1; Q3)	42.0 (38.7; 45.1)	27.1 (24.3; 31.8)	0.042
Δ BMI (kg/m ²) (median, Q1; Q3)		-13.7 (-16.4; -9.5)	
Fasting glucose (mmol/l) (median, Q1; Q3)	7.3 (5.3; 9.0)	4.7 (3.8; 5.5)	0.031
Fasting insulin (mU/l) (median, Q1; Q3)	24.7 (18.0; 33.0)	11.8 (6.5; 19.2)	0.032
HOMA-IR (median, Q1; Q3)	7.4 (3.5; 10.8)	1.9 (1.3; 3.5)	0.008
Diabetes (%)	4 (44)	0 (0)	ns
Metabolic syndrome (%)	7 (77)	2 (22)	ns
CRP (mg/dl) (median, Q1; Q3)	7.7 (5.7; 9.6)	0.6 (0.4; 2.4)	0.004

T0, baseline; T ≥ 40 , after a ≥ 40 -month follow-up period. BMI, Body-mass index; Δ BMI, Excess BMI loss; HOMA-IR, Homeostasis Model Assessment of Insulin Resistance; CRP, C-reactive protein; ns, not significant; p, the Mann-Whitney test or Fisher's exact test.

level ($P = 0.4038$) and CRP level ($P = 0.1828$). Overall, nine women met all the criteria and accepted the second biopsy. In addition, data from blood samples obtained from five morbidly obese patients, included in the same prospective ongoing study and who had no sign of NAFLD on liver histology (aged 37 ± 10 years; BMI 44 ± 3 kg/m²), from seven patients with biopsy-proven severe hepatic steatosis (aged 34 ± 8 years; BMI 46 ± 8 kg/m²), and from seven patients with biopsy-proven NASH (aged 40 ± 8 years; BMI 41 ± 3 kg/m²) were used in this study.

Population Characteristics

All patients were negative for hepatitis B and C viral markers, auto-antibodies indicative of autoimmune hepatitis, and had self-reported negligible alcohol consumption (<20 g/day in women and <30 g/day in men). Alcohol abuse was also excluded by interviewing the patients' relatives. Patients with a history of inflammatory disease (including rheumatoid arthritis, systemic lupus erythematosus, and inflammatory bowel disease), current infections, recent history of cancer (<5 years), and severe pulmonary or cardiac disease were not enrolled in the study. The patients' characteristics are described in Table 1. Before surgery and during the follow-up (6, 12 months and the last follow-up visit before the second liver biopsy), fasting blood samples were obtained and analyzed for alanine aminotransferase (ALT), glucose and insulin, triglycerides, high-density lipoprotein (HDL)-cholesterol, C-reactive protein, and caspase-generated keratin (K18 fragment). Metabolic syndrome was defined according to the modified International Diabetes Federation (IDF) criteria of three or more of the following: (i) central obesity defined by an increased waist circumference (≥ 80 cm), (ii) triglycerides ≥ 1.7 mmol/L or treatment for hyper-triglyceridemia; (iii) HDL-cholesterol <1.29 mmol/L; (iv)

TABLE 2 | Patients' clinical and biochemical parameters at baseline and after a 12-month follow-up period (patients without a second liver biopsy).

	T0	T0	T12	p
Number	75	30	30	
Gender (F/M)	57/18	23/7		
BMI (kg/m ²) (median, Q1; Q3)	43.7 (40.2; 47.2)	45.5 (41.0; 48.6)	28.8 (25.5; 32.3)	<0.001
Δ BMI (kg/m ²) (median, Q1; Q3)			−15.1 (−19.9; −13.4)	
Fasting glucose (mmol/l) (median, Q1; Q3)	5.5 (5.1; 7.4)	5.8 (5.1; 9.7)	4.7 (4.1; 5.2)	<0.001
Fasting insulin (mU/l) (median, Q1; Q3)	28.0 (18.0; 44.0)	27.0 (17.2; 39.5)	6.8 (4.9; 12.0)	<0.001
HOMA-IR (median, Q1; Q3)	7.8 (4.8; 12.4)	7.6 (5.8; 11.3)	1.3 (1.0; 2.1)	<0.001
Diabetes (%)	32 (42.6)	18(60)	4 (13.3)	<0.001
Metabolic syndrome (%)	36 (48)	21 (70)	9 (30)	0.002
CRP (mg/dl) (median, Q1; Q3)	9.0 (6.0; 14.5)	9.0 (6.8; 14.5)	2.9 (1.1; 4.1)	<0.001
ALT (IU/L) (median, Q1; Q3)	50.5 (36.0; 72.5)	53.5 (35.7; 69.5)	24.0 (18.0; 32.0)	<0.001
NAS (grade) (median, Q1; Q3)	5.0 (5.0; 5.0)	5.0 (5.0; 5.0)		

T0, baseline; T12, 12-month follow-up. BMI, Body-mass index; Δ BMI, Excess BMI loss; HOMA-IR, Homeostasis Model Assessment of Insulin Resistance; CRP, C-reactive protein; ns, not significant; p, the Mann-Whitney test or Fisher's exact test.

systolic blood pressure ≥ 130 mmHg or diastolic blood pressure ≥ 85 mmHg or treatment for hypertension, and (v) fasting plasma glucose ≥ 5.6 mmol/L or previously diagnosed type-2 diabetes mellitus (Alberti et al., 2006). Type-2 diabetes was defined by two measurements of elevated fasting plasma glucose ≥ 7 mmol/L. Insulin resistance was evaluated using the homeostatic model assessment (HOMA-IR) index (Wallace et al., 2004). Nine patients (only women) with biopsy-proven NASH had liver biopsies repeated at a median follow-up of 55 [44; 75] months after surgery. The first liver biopsy was a wedge biopsy obtained at the beginning of the LRYGB, with no ischemic preconditioning. The second was a needle-biopsy of the liver, obtained using the percutaneous approach. The quality of the biopsies of the nine included patients was sufficient for interpretation and the length of each liver biopsy was over 15 mm. It is however important to underline the fact that potential limitations of comparing wedge to needle biopsies exist. Biopsies were stained with hematoxylin-eosin-saffron and sirius red. Liver biopsies were reviewed by two liver pathologists who were blinded to the clinical and biological characteristics of the patients. Histopathological analyses were performed according to the scoring system of Kleiner et al. (2005). Four histopathological features were semi-quantitatively evaluated: grade of steatosis (0, $<5\%$; 1, 5–33.3%; 2, 33.3–66.6%; 3, $>66.6\%$), lobular inflammation (0, no inflammatory foci; 1, <2 inflammatory foci per 200x field; 2, 2–4 inflammatory foci per 200x field; 3, >4 inflammatory foci per 200x field), hepatocellular ballooning (0, none; 1, few balloon cells; 2, many cells/prominent ballooning), and liver bridging fibrosis (classified into seven stages according to the NASH Clinical Research Network Scoring System Definition F0, no fibrosis; F1a, mild zone 3 sinusoidal fibrosis; F1b, moderated zone 3 sinusoidal fibrosis; F1c, peri-portal sinusoidal fibrosis; F2, zone 3 sinusoidal fibrosis and peri-portal sinusoidal fibrosis; F3, bridging fibrosis; and F4, cirrhosis). The NAFLD activity score (NAS) is defined as the unweighted sum of scores for steatosis (0–3), lobular inflammation (0–3), and ballooning (0–2), thus ranging from 0 to 8 (Kleiner et al., 2005).

Circulating Levels of Transaminases and K18 Fragment

Plasma alanine aminotransferase (ALT) levels were determined using an *in vitro* test with pyridoxal phosphate activation on a Roche/Hitachi cobas c system (ALTPM, cobas, Meylan, France). Keratin 18 (K18) is cleaved by the caspases during apoptosis, generating soluble protein fragments. The M30 Apoptosense[®] ELISA assay specifically measures apoptosis (the caspase-generated K18 fragment, K18-Asp396). All samples were analyzed in duplicate following the manufacturer's instructions. The within assay (WA% CV) variation was $<10\%$ and between assay (BA% CV) variation was $<10\%$ for samples >100 U/L. The minimum detectable concentration was 25 U/L. Keratins are released into the circulation as protein complexes. These complexes are remarkably stable during sample collection and long-term storage. Furthermore, plasma/serum samples can be exposed to repetitive freeze-thaw cycles without loss of activity (Olofsson et al., 2007).

IHC Analysis

Immunostaining for cleaved caspase-3 (Asp175) was performed using rabbit polyclonal antibodies against amino-terminal residues adjacent to (Asp175) in human caspase 3. Sections measuring 2 μm were cut from each paraffin block and were put to dry at 37°C during 12 h. After deparaffinization and rehydration, all sections were pretreated at pH 6 with Flex TRS Low (PTLink DAKO, Glostrup, Denmark) during 20 min. Endogenous peroxidase was blocked in 1% hydrogen peroxide for 5 min (DAKO, Glostrup, Denmark) at room temperature. After rinsing with phosphate buffered saline, the sections were incubated with cleaved caspase-3 (Asp175) antibody (#9661, Cell Signaling) for 20 min at room temperature. Then sections were incubated with an appropriate secondary antibody from the Envision flex/HRP kit (Dako, Glostrup, Denmark) for 20 min, at room temperature. Next, slides were incubated in PBS, for 20 min, at room temperature, and then peroxidase activity was detected by diaminobenzidinetetrahydrochloride for 8 min

and used for visualization and haematoxylin (Dako, Glostrup, Denmark) during 6 min for nuclear counterstaining.

Statistical Analyses

The statistical significances between the two study groups were determined using the non-parametric Mann-Whitney test and Fischer's test. A $P < 0.05$ was considered statistically significant. Quantitative variables are presented as their medians (interquartile ranges).

RESULTS

The aim of this study was to investigate the potentially long-lasting beneficial effects of LRYGB on obesity-related liver complications. To this end, 84 morbidly patients with biopsy-proven NASH diagnosed at time of bariatric surgery (LRYGB) were studied. Of these, nine women with a median age of 51 [35; 59] years at the time of LRYGB had a second liver biopsy after ≥ 40 months of follow-up (Table 1).

LRYGB Improves the Metabolic Syndrome, Type-2 Diabetes, and Systemic Inflammation

We first evaluated the effects of LRYGB on weight loss, the metabolic syndrome, type-2 diabetes and systemic inflammation in our NASH patients with paired-liver biopsies. All patients lost more than 50% of excess BMI and had a median loss of -13.7 [-16.4 ; -9.5] kg/m^2 BMI points (Table 1). Insulin resistance, as evaluated by the HOMA-IR, fasting insulin and glycaemia were strongly improved after LRYGB, as shown in Table 1. Four patients with type-2 diabetes before surgery were in remission at the time of the follow-up. The metabolic syndrome was diagnosed in seven patients at the time of the initial surgery and persisted in only two patients by the end of the follow-up. Chronic low-grade inflammation, as evaluated by C-reactive protein, was also improved after LRYGB in all patients (Table 1). The beneficial effect of LRYGB on the metabolic syndrome and systemic inflammation could already occur 1 year after bariatric surgery as previously reported (Mathurin et al., 2006; Anty et al., 2008; Bertola et al., 2009). In line with this, the analysis of the clinical and biochemical parameters at baseline and at 12 months after LRYGB of 30 out of our 75 patients without second liver biopsy also showed a significant improvement of fasting insulin, glycaemia, HOMA-IR, metabolic syndrome, diabetes, and CRP (Table 2).

LRYGB Improves Hepatic Steatosis, Inflammation, and NAFLD Activity Score (NAS) in All Patients, and Improves Hepatic Fibrosis in a Large Majority

We then evaluated the effects of LRYGB on obesity-related liver complications. Liver steatosis was evaluated as severe (S3, $>66.6\%$ of hepatocytes) in all patients at the time of surgery. On the second biopsy, steatosis was improved in all patients: i.e., full correction in five patients (55.5%) and grade 1 (44.4%) in four patients (Figures 1A, 2A). The correction of hepatic

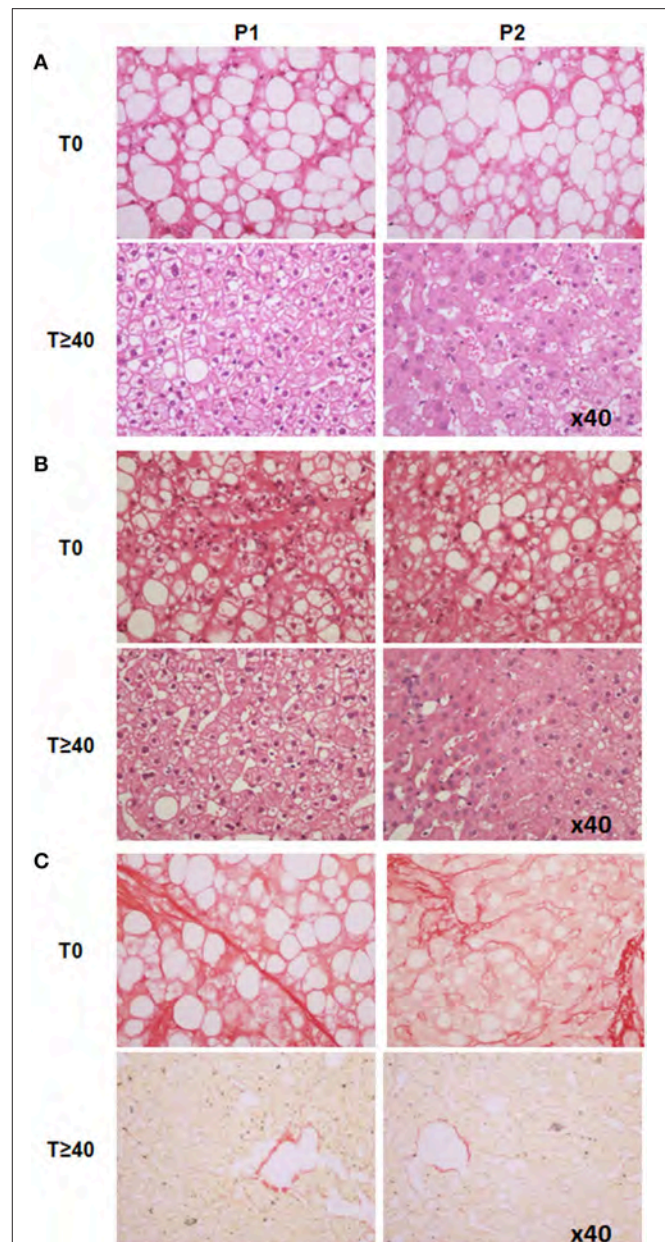
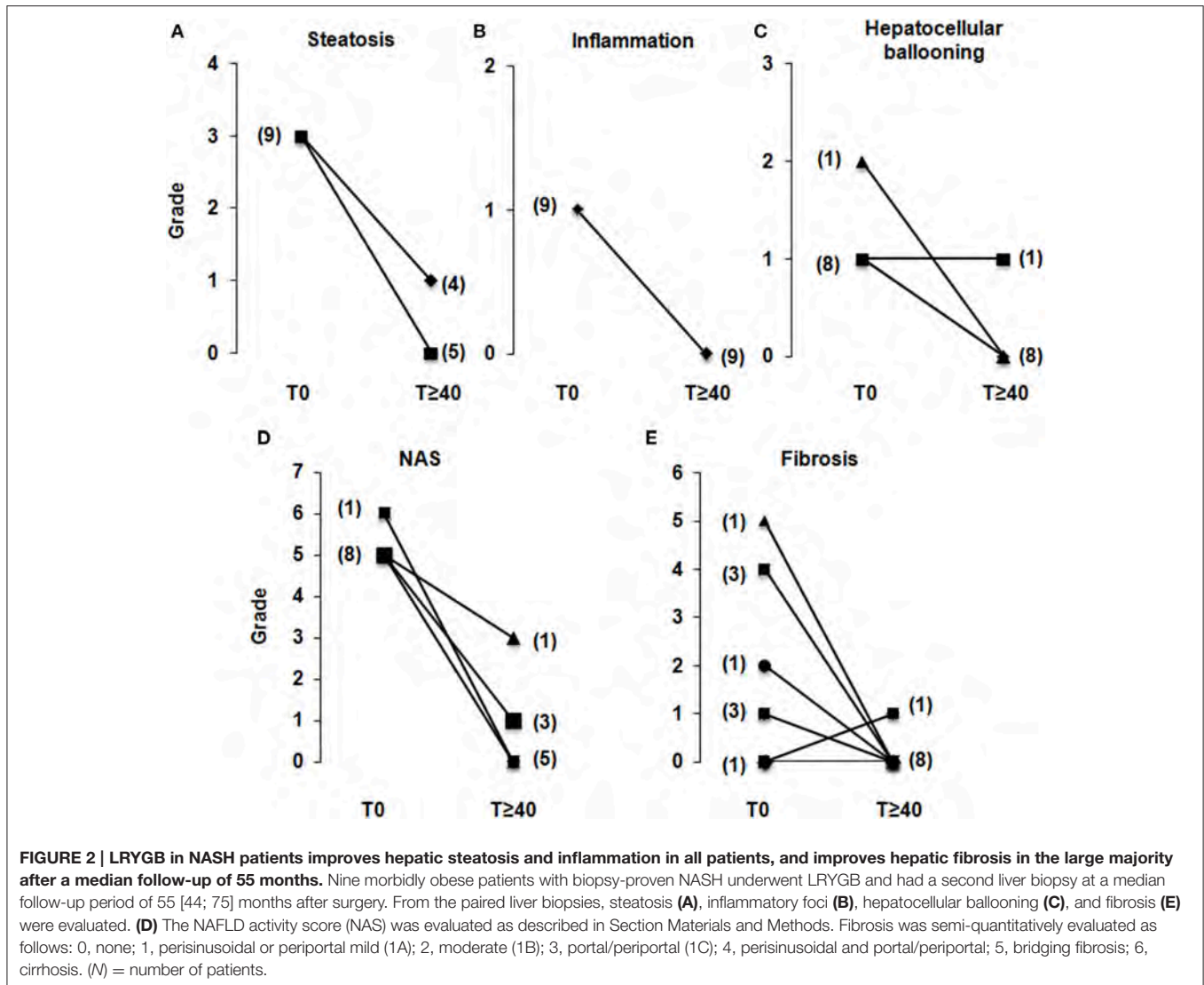


FIGURE 1 | Liver histology analysis of two representative patients (P1 and P2) at baseline and ≥ 40 -months after LRYGB. (A) Liver steatosis was improved (HES staining, x40). **(B)** Ballooned hepatocytes and hepatic inflammation, both present at baseline, were no longer present on the second liver biopsy (HES staining, x40). **(C)** P1 had bridging fibrosis ($F = 3$), P2 had zone three sinusoidal fibrosis and peri-portal sinusoidal fibrosis ($F = 2$). The second liver biopsy showed a significant improvement in fibrosis ($F = 0$) in both patients (Sirius red staining, x40). T0, baseline; T ≥ 40 , after a ≥ 40 -month follow-up period.

steatosis was associated with a more important loss of weight as evaluated by percentage of initial body weight (39 ± 6 vs. $24 \pm 3\%$, $P = 0.02$). Hepatic inflammation, present in all patients at the time of the surgery, was no longer present on the second biopsy in any patient (Figures 1B, 2B). Ballooned hepatocytes, another hallmark of NASH and a marker of liver-cell degeneration, were



found in all liver biopsies at the time of surgery, but were no longer present in the second liver biopsy in eight patients (88.8%; **Figures 1B, 2C**). Only one patient still had ballooned hepatocytes on the liver biopsy in spite of significant weight loss, improved metabolic syndrome, insulin resistance (HOMA-IR: from 5.4 to 2.3), hepatic steatosis (from S3 to S1) and hepatic inflammation (**Figure 2C**). As a consequence, the NAS, which was elevated in all patients at the time of surgery (eight patients with NAS = 5, and one with NAS = 6), dropped considerably in all patients by 2–6 full points (**Figure 2D**). The stage of fibrosis was more heterogeneous at the time of surgery, with only one patient showing advanced fibrosis ($F = 3$), three patients with moderate fibrosis ($F = 2$), four patients with mild fibrosis (1 with $F = 1B$, 3 with $F = 1A$) and one patient with no fibrosis ($F = 0$). The second liver biopsy showed a significant improvement in fibrosis ($F = 0$) in seven patients and a slight progression of liver fibrosis in one patient (from F0 to F1A; **Figures 1C, 2E**). One patient without fibrosis at the time of the surgery showed no signs of fibrosis on

the second biopsy. LRYGB was associated with corrected hepatic steatosis and inflammation in all patients, and improvement of fibrosis in 88.8% of patients.

LRYGB Improves Hepatic Injury and Hepatocyte Apoptosis in All Patients

NASH is also characterized by the substantial death of hepatocytes (Feldstein and Gores, 2005; Tran and Gual, 2013). Hepatocyte apoptosis plays an important role in the progression and the severity of obesity-related liver complications. We thus investigated the long-term effect of LRYGB on hepatocyte injury. ALT serum levels reached normal-range values in all patients by the last follow-up (ALT: 38 [29; 74] to 24 [20; 26] UI/L; **Figure 3A**). The serum levels of caspase-generated keratin 18 fragment (K18 fragment) were used to evaluate hepatocyte apoptosis. An average decrease of 35% in serum K18 fragment levels were found in 88.8% of patients after a median follow-up

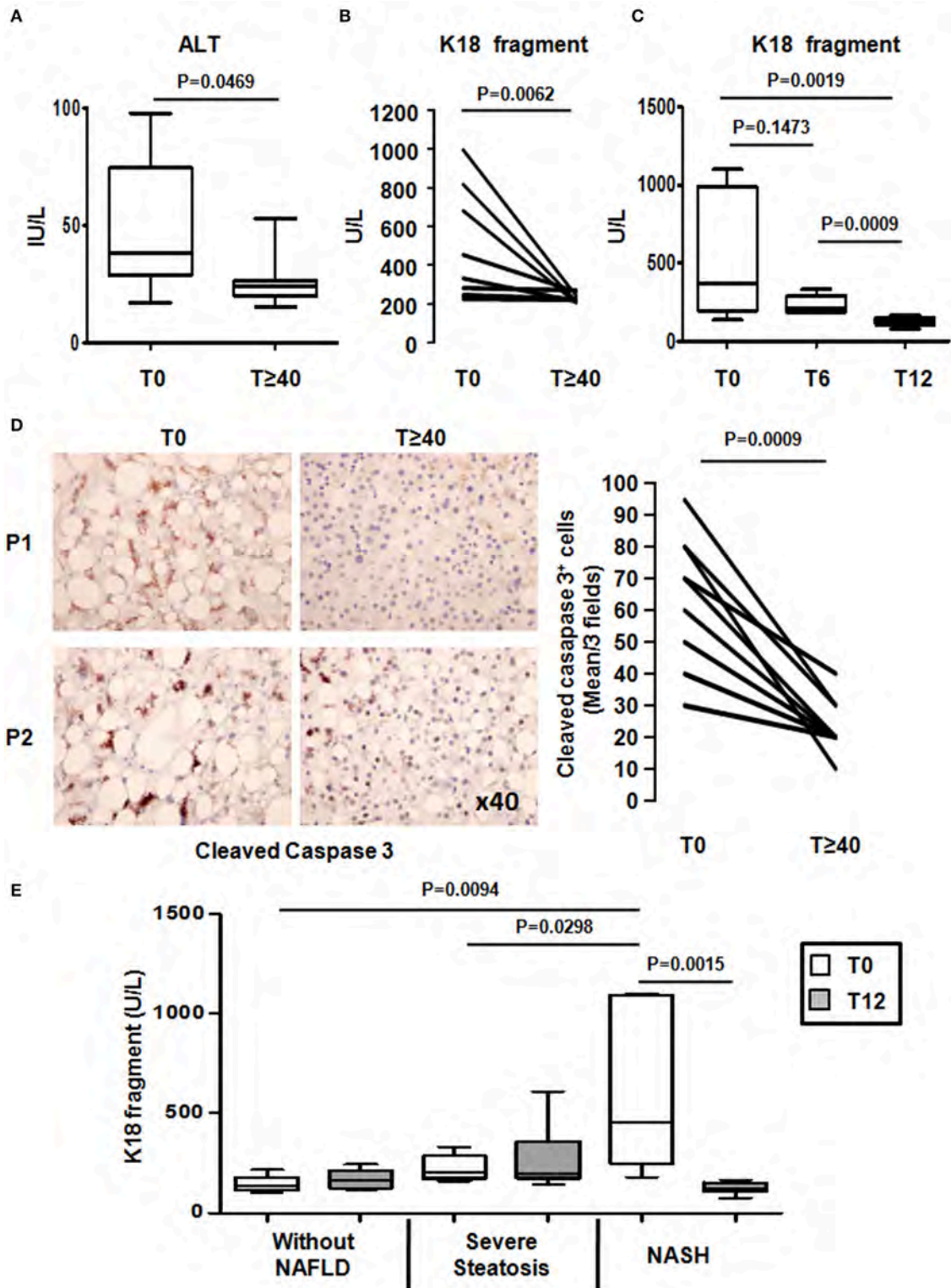


FIGURE 3 | LRYGB improves liver injury and hepatocyte apoptosis in NASH patients after a median follow-up of 55 months. Serum levels of **(A)** alanine aminotransferase (ALT) and **(B)** a marker of hepatocyte apoptosis [caspase-generated keratin 18 fragment (K18 fragment)] and **(D)** hepatic levels of cleaved caspase 3 were evaluated at baseline and at the median follow-up of 55 [44; 75] months after LRYGB in NASH patients. The levels of K18 fragment were also evaluated **(C)** at 6 months and at 1 year after a LRYGB and, **(E)** at baseline (T0) and 1 year (T12) after LRYGB in three additional groups of patients without NAFLD ($n = 5$), severe steatosis ($n = 7$), or NASH ($n = 7$). Results are expressed as the median [25th, 75th percentiles] **(A,C,E)**.

of 55 [44; 75] months after LRYGB (**Figure 3B**). One patient who already had low serum K18 fragment levels at the time of the LRYGB showed no significant changes (**Figure 3B**). Interestingly in the initially NASH patients, the K18 fragment levels reached those usually found in patients without hepatic complications just 1 year after LRYGB (Anty et al., 2010; Lavallard et al., 2011; **Figure 3C**). We then determined the hepatic caspase 3 activity, as evaluated by the cleaved caspase 3 (Asp175) levels in the paired liver biopsies with a median follow-up of 55 [44; 75] months after LRYGB. As shown in **Figure 3D**, the percentage of cleaved caspase 3 positive hepatocytes strongly decreased (−40% average decrease) in all patients at the time of follow-up. We also evaluated the K18 fragment levels in three additional groups of morbidly obese patients without any signs of NAFLD ($n = 5$), severe steatosis ($n = 7$), or severe steatosis associated with NASH ($n = 7$): assessed from a liver biopsy at baseline and at 1 year after LRYGB. While the K18 fragment levels showed no significant difference in patients with hepatic steatosis, they were increased in patients with NASH compared with patients without NASH at the time of surgery (**Figure 3E**). At 1 year after LRYGB, the levels of the K18 fragment had strongly decreased in all NASH patients (**Figure 3E**). Altogether, these data indicate that LRYGB had a beneficial effect on hepatocyte apoptosis by 1 year post-surgery, and that this was maintained for the median follow-up period of 55 [44; 75] months.

DISCUSSION

While there is strong evidence for the beneficial effects of the LRYGB on excess weight and resolution or reduction of type 2-diabetes (with remission in 63.5% of cases; Ribaric et al., 2014), its long term impact on liver histology in NASH patients needs to be better characterized. Most studies with paired liver biopsies reported a mean interval between LRYGB and a second liver biopsy of 19 ± 4 (range: 12–25) months (Silverman et al., 1995; Clark et al., 2005; Mattar et al., 2005; Mottin et al., 2005; Barker et al., 2006; Csendes et al., 2006; Klein et al., 2006; Furuya et al., 2007; Liu et al., 2007; Lassailly et al., 2013).

In this study, a second biopsy was performed on previously morbidly obese patients with liver biopsy-proven severe steatosis and NASH after a median interval of 55 [44; 75] months after LRYGB. As reported herein and previously, 1 year after surgery (Anty et al., 2008; Bertola et al., 2009; Ribaric et al., 2014; **Table 2**), insulin resistance, the metabolic syndrome and systemic inflammation had all improved. These positive effects are thus maintained after a median follow-up period of 55 [44; 75] months. A beneficial impact of LRYGB on hepatic steatosis was also observed in all of our patients, from total resolution (in 55.6% of cases) to striking improvement (S3 to S1: 44.4%). As previously reported, LRYGB already improved hepatic steatosis, evaluated by paired liver biopsies, at a median follow up of 18 [12; 23] months after LRYGB (Silverman et al., 1995; Clark et al., 2005; Mattar et al., 2005; Mottin et al., 2005; Barker et al., 2006; Klein et al., 2006; Furuya et al., 2007; Liu et al., 2007). Furthermore, the improvement of hepatic steatosis

is not specific to a LRYGB procedure. A recent meta-analysis compiled results from different bariatric procedures, including LRYGB, gastric banding, sleeve gastrectomy, duodenal switch, and biliopancreatic diversion and reported an improvement of hepatic steatosis in 90% of cases (Chavez-Tapia et al., 2010). Therefore, our study demonstrates that the beneficial impact of LRYGB on insulin resistance, systemic inflammation, and hepatic steatosis obtained 1 year after surgery is maintained for at least 40 months (median 55 [44; 75]).

Regarding the hepatic inflammation and fibrosis, some studies with paired liver biopsies reported an improvement in the histopathological criteria for NASH in the short term (mean follow-up of 21.35 ± 4.5 months; Clark et al., 2005; Barker et al., 2006; de Almeida et al., 2006) and fibrosis (Clark et al., 2005; Mattar et al., 2005; Barker et al., 2006; Furuya et al., 2007) after LRYGB surgery. In our study, a median follow-up period of 55 months after LRYGB exhibited beneficial effects on inflammatory foci, ballooning and fibrosis. Our NASH patients showed 100% improvement in inflammatory foci and 88.8% improvement in ballooned hepatocytes after LRYGB surgery. As a consequence, the NAS decreased in 100% of cases. Despite the heterogeneous nature of the degree of hepatic fibrosis in our patients at the time of LRYGB surgery, hepatic fibrosis improved in 88.8% of cases. One patient showed a slight increase in fibrosis (from F0 to F1A). No explanation could be found concerning the patient with no resolution of hepatocyte ballooning. Indeed, this patient lost significant weight and had decreased metabolic syndrome features, decreased insulin resistance (HOMA-IR: from 5.4 to 2.3) and improved ALT levels. Other liver complications were also reduced, including hepatic steatosis (from S3 to S1), inflammation and fibrosis (from F2 to F0). A recent report has shown that the disappearance of NASH in nearly 85% of cases and decreased pathological features of NAFLD already occur 1 year after the bariatric surgery in a cohort of 109 morbidly obese patients with biopsy-proven NASH (Lassailly et al., 2015). The beneficial effect of bariatric surgery (mainly LRYGB procedure) on NASH could thus rapidly occur in the first year and be maintained up to 40 months after the surgery.

We next found that hepatocyte apoptosis, as evaluated by the serum K18 fragment had already improved 1 year after LRYGB and remained low until the last follow-up (at 55 [44; 75] months). This was also confirmed by a strong decrease in hepatic caspase 3 activity, as evaluated by the levels of hepatocyte cleaved caspase 3 for at least 40 months after LRYGB surgery. In our patients, this serum hepatocyte apoptotic marker increased approximately four-fold in patients with NASH, which is in accordance with previous reports on overweight, obese and severely obese patients (Wieckowska et al., 2006; Anty et al., 2008; Younossi et al., 2008; Feldstein et al., 2009; Tamimi et al., 2011; Joka et al., 2012; Shen et al., 2012), and correlates with NAS ($r = 0.549$, $P < 0.001$, $n = 41$). However, it has been recently reported that K18 fragment level could be inadequate as a screening test for staging NASH according to its limited sensitivity (Cusi et al., 2014). In concert, these data suggest that this non-invasive marker combined with other clinical/laboratory parameters may be helpful to monitor the evolution of NASH after bariatric surgery. Wai-Sun Wong et al. recently reported that the levels of the serum K18 fragment

reflected disease activity in a prospective longitudinal study on overweight/obese patients undergoing paired liver biopsies with a follow-up time of 3 years (Wong et al., 2010).

The improvement in hepatocyte death and reduction of inflammation after LRYGB surgery could prevent the progression of hepatic complications. Indeed, apoptotic hepatocytes are engulfed by Kupffer cells, which results in activation and inflammation. The activation of stellate cells by apoptotic bodies or by TGF β from activated Kupffer cells then leads to liver fibrosis (Malhi and Gores, 2008). Furthermore, a pan-caspase inhibitor or an overexpression of the anti-apoptotic Bcl2 protein was shown to reduce fibrosis in an animal model of NAFLD and fibrosis, respectively (Mitchell et al., 2009; Wittek et al., 2009).

Although, the main weakness of the present study lies in the small size of the sample and the gender bias (only females were included), the exhaustive preoperative and postoperative work-up and the paired liver biopsies allowed for a complete characterization of our patients with NASH. We were thus able to demonstrate that the LRYGB surgery results in the concomitant remission of systemic inflammation, insulin resistance and NASH features (steatosis, inflammation, and hepatocellular ballooning) in all patients at a median follow-up of 55 months. We also found a rapid decrease in hepatocyte apoptosis, as evaluated by serum levels of K18 fragment. These results should be confirmed in additional studies with a larger sample size and a longer follow-up (>6 years) to better understand the molecular mechanisms that are involved in the remission of obesity-related liver complications after LRYGB surgery, as well as after other bariatric procedures to determine if they could share these beneficial effects. Because pharmacological therapy has only marginal and perhaps clinically irrelevant effects on NASH and fibrosis (Ratziu,

2013), and in light of our results, the implications for the protective effects of LRYGB surgery against the progression of obesity-related liver complications may become particularly relevant.

AUTHOR CONTRIBUTIONS

AS, RA, AI, and PG: study concept and design; AS, RA, and SP: acquisition of data; AS, SP, SB, DR, AI, and PG: analysis and interpretation of data; AS, AI, and PG: drafting and critical revision of the article for important intellectual content; AS, CL, BB, AT, JG, AS, AI, and PG: precious help with editing the manuscript at different stages; RA, PG: statistical analysis; PG obtained funding; PG and AI: study supervision.

FUNDING

This work was supported by grants from Inserm (France), the University of Nice, the Programme Hospitalier de Recherche Clinique (Centre Hospitalier Universitaire de Nice), and charities (Association Française pour l'Etude du Foie (AFEF)/LFB to PG, AFEF/Aptalis to BB, Société Francophone du Diabète (SFD) to PG, SFD/Roche Pharma to PG, SFD/MSD to BB). This work was also funded by the French Government (National Research Agency, ANR) through the "Investments for the Future" LABEX SIGNALIFE, program reference #ANR-11-LABX-0028-01 and #ANR-15-CE14-0016-01.

ACKNOWLEDGMENTS

The authors thank Dr. Marie-Christine Saint Paul for expert histology.

REFERENCES

- Alberti, K. G., Zimmet, P., and Shaw, J. (2006). Metabolic syndrome—a new world-wide definition. A consensus statement from the International Diabetes Federation. *Diabet. Med.* 23, 469–480. doi: 10.1111/j.1464-5491.2006.01858.x
- Anty, R., Dahman, M., Iannelli, A., Gual, P., Staccini-Myx, A., Ben Amor, I., et al. (2008). Bariatric surgery can correct iron depletion in morbidly obese women: a link with chronic inflammation. *Obes. Surg.* 18, 709–714. doi: 10.1007/s11695-007-9276-y
- Anty, R., Iannelli, A., Patouraux, S., Bonnafous, S., Lavallard, V. J., Senni-Buratti, M., et al. (2010). A new composite model including metabolic syndrome, alanine aminotransferase and cytokeratin-18 for the diagnosis of non-alcoholic steatohepatitis in morbidly obese patients. *Aliment. Pharmacol. Ther.* 32, 1315–1322. doi: 10.1111/j.1365-2036.2010.04480.x
- Barker, K. B., Palekar, N. A., Bowers, S. P., Goldberg, J. E., Pulcini, J. P., and Harrison, S. A. (2006). Non-alcoholic steatohepatitis: effect of Roux-en-Y gastric bypass surgery. *Am. J. Gastroenterol.* 101, 368–373. doi: 10.1111/j.1572-0241.2006.00419.x
- Bertola, A., Deveaux, V., Bonnafous, S., Rousseau, D., Anty, R., Wakkach, A., et al. (2009). Elevated expression of osteopontin may be related to adipose tissue macrophage accumulation and liver steatosis in morbid obesity. *Diabetes* 58, 1251–1253. doi: 10.2337/db08-0400
- Chavez-Tapia, N. C., Tellez-Avila, F. I., Barrientos-Gutierrez, T., Mendez-Sanchez, N., Lizardi-Cervera, J., and Uribe, M. (2010). Bariatric surgery for non-alcoholic steatohepatitis in obese patients. *Cochrane Database Syst. Rev.* CD007340. doi: 10.1002/14651858.cd007340.pub2
- Clark, J. M., Alkhuraishi, A. R., Solga, S. F., Alli, P., Diehl, A. M., and Magnuson, T. H. (2005). Roux-en-Y gastric bypass improves liver histology in patients with non-alcoholic fatty liver disease. *Obes. Res.* 13, 1180–1186. doi: 10.1038/oby.2005.140
- Csendes, A., Smok, G., and Burgos, A. M. (2006). Histological findings in the liver before and after gastric bypass. *Obes. Surg.* 16, 607–611. doi: 10.1381/096089206776944904
- Cusi, K., Chang, Z., Harrison, S., Lomonaco, R., Bril, F., Orsak, B., et al. (2014). Limited value of plasma cytokeratin-18 as a biomarker for NASH and fibrosis in patients with non-alcoholic fatty liver disease. *J. Hepatol.* 60, 167–174. doi: 10.1016/j.jhep.2013.07.042
- de Almeida, S. R., Rocha, P. R., Sanches, M. D., Leite, V. H., da Silva, R. A., Diniz, M. T., et al. (2006). Roux-en-Y gastric bypass improves the nonalcoholic steatohepatitis (NASH) of morbid obesity. *Obes. Surg.* 16, 270–278. doi: 10.1381/096089206776116462
- Feldstein, A. E., and Gores, G. J. (2005). Apoptosis in alcoholic and nonalcoholic steatohepatitis. *Front. Biosci.* 10, 3093–3099. doi: 10.2741/1765
- Feldstein, A. E., Wieckowska, A., Lopez, A. R., Liu, Y. C., Zein, N. N., and McCullough, A. J. (2009). Cytokeratin-18 fragment levels as noninvasive biomarkers for nonalcoholic steatohepatitis: a multicenter validation study. *Hepatology* 50, 1072–1078. doi: 10.1002/hep.23050
- Furuya, C. K. Jr., de Oliveira, C. P., de Mello, E. S., Faintuch, J., Raskowski, A., Matsuda, M., et al. (2007). Effects of bariatric surgery on nonalcoholic fatty liver disease: preliminary findings after 2 years. *J. Gastroenterol. Hepatol.* 22, 510–514. doi: 10.1111/j.1440-1746.2007.04833.x

- Joka, D., Wahl, K., Moeller, S., Schlue, J., Vaske, B., Bahr, M. J., et al. (2012). Prospective biopsy-controlled evaluation of cell death biomarkers for prediction of liver fibrosis and nonalcoholic steatohepatitis. *Hepatology* 55, 455–464. doi: 10.1002/hep.24734
- Klein, S., Mittendorfer, B., Eagon, J. C., Patterson, B., Grant, L., Feirt, N., et al. (2006). Gastric bypass surgery improves metabolic and hepatic abnormalities associated with nonalcoholic fatty liver disease. *Gastroenterology* 130, 1564–1572. doi: 10.1053/j.gastro.2006.01.042
- Kleiner, D. E., Brunt, E. M., Van Natta, M., Behling, C., Contos, M. J., Cummings, O. W., et al. (2005). Design and validation of a histological scoring system for nonalcoholic fatty liver disease. *Hepatology* 41, 1313–1321. doi: 10.1002/hep.20701
- Lassailly, G., Caiazzo, R., Buob, D., Pigeyre, M., Verkindt, H., Labreuche, J., et al. (2015). Bariatric surgery reduces features of Nonalcoholic steatohepatitis in morbidly obese patients. *Gastroenterology* 149, 379–388. doi: 10.1053/j.gastro.2015.04.014
- Lassailly, G., Caiazzo, R., Pattou, F., and Mathurin, P. (2013). Bariatric surgery for curing NASH in the morbidly obese? *J. Hepatol.* 58, 1249–1251. doi: 10.1016/j.jhep.2012.12.026
- Lavallard, V. J., Bonnafous, S., Patouraux, S., Saint-Paul, M. C., Rousseau, D., Anty, R., et al. (2011). Serum markers of hepatocyte death and apoptosis are non invasive biomarkers of severe fibrosis in patients with alcoholic liver disease. *PLoS ONE* 6:e17599. doi: 10.1371/journal.pone.0017599
- Liu, X., Lazenby, A. J., Clements, R. H., Jhala, N., and Abrams, G. A. (2007). Resolution of nonalcoholic steatohepatitis after gastric bypass surgery. *Obes. Surg.* 17, 486–492. doi: 10.1007/s11695-007-9086-2
- Malhi, H., and Gores, G. J. (2008). Cellular and molecular mechanisms of liver injury. *Gastroenterology* 134, 1641–1654. doi: 10.1053/j.gastro.2008.03.002
- Mathurin, P., Gonzalez, F., Kerdraon, O., Leteurtre, E., Arnalsteen, L., Hollebecque, A., et al. (2006). The evolution of severe steatosis after bariatric surgery is related to insulin resistance. *Gastroenterology* 130, 1617–1624. doi: 10.1053/j.gastro.2006.02.024
- Mathurin, P., Hollebecque, A., Arnalsteen, L., Buob, D., Leteurtre, E., Caiazzo, R., et al. (2009). Prospective study of the long-term effects of bariatric surgery on liver injury in patients without advanced disease. *Gastroenterology* 137, 532–540. doi: 10.1053/j.gastro.2009.04.052
- Mattar, S. G., Velcu, L. M., Rabinovitz, M., Demetris, A. J., Krasinskas, A. M., Barinas-Mitchell, E., et al. (2005). Surgically-induced weight loss significantly improves nonalcoholic fatty liver disease and the metabolic syndrome. *Ann. Surg.* 242, 610–617. discussion: 618–620. doi: 10.1097/01.sla.0000179652.07502.3f
- Mitchell, C., Robin, M. A., Mayeuf, A., Mahrouf-Yorgov, M., Mansouri, A., Hamard, M., et al. (2009). Protection against hepatocyte mitochondrial dysfunction delays fibrosis progression in mice. *Am. J. Pathol.* 175, 1929–1937. doi: 10.2353/ajpath.2009.090332
- Mitka, M. (2012). Bariatric surgery continues to show benefits for patients with diabetes. *JAMA* 307, 1901–1902. doi: 10.1001/jama.2012.3727
- Mottin, C. C., Moretto, M., Padoin, A. V., Kupski, C., Swarowsky, A. M., Glock, L., et al. (2005). Histological behavior of hepatic steatosis in morbidly obese patients after weight loss induced by bariatric surgery. *Obes. Surg.* 15, 788–793. doi: 10.1381/0960892054222830
- Must, A., Spadano, J., Coakley, E. H., Field, A. E., Colditz, G., and Dietz, W. H. (1999). The disease burden associated with overweight and obesity. *JAMA* 282, 1523–1529. doi: 10.1001/jama.282.16.1523
- Olofsson, M. H., Ueno, T., Pan, Y., Xu, R., Cai, F., van der Kuip, H., et al. (2007). Cytokeratin-18 is a useful serum biomarker for early determination of response of breast carcinomas to chemotherapy. *Clin. Cancer Res.* 13, 3198–3206. doi: 10.1158/1078-0432.CCR-07-0009
- Ratzl, V. (2013). Pharmacological agents for NASH. *Nat. Rev. Gastroenterol. Hepatol.* 10, 676–685. doi: 10.1038/nrgastro.2013.193
- Ribaric, G., Buchwald, J. N., and McGlennon, T. W. (2014). Diabetes and weight in comparative studies of bariatric surgery vs conventional medical therapy: a systematic review and meta-analysis. *Obes. Surg.* 24, 437–455. doi: 10.1007/s11695-013-1160-3
- Schauer, P. R., Bhatt, D. L., Kirwan, J. P., Wolski, K., Brethauer, S. A., Navaneethan, S. D., et al. (2014). Bariatric surgery versus intensive medical therapy for diabetes—3-year outcomes. *N. Engl. J. Med.* 370, 2002–2013. doi: 10.1056/NEJMoa1401329
- Setiawan, V. W., Stram, D. O., Porcel, J., Lu, S. C., Le Marchand, L., and Nouredin, M. (2016). Prevalence of chronic liver disease and cirrhosis by underlying cause in understudied ethnic groups: the multiethnic cohort. *Hepatology*. doi: 10.1002/hep.28677. [Epub ahead of print].
- Shen, J., Chan, H. L., Wong, G. L., Choi, P. C., Chan, A. W., Chan, H. Y., et al. (2012). Non-invasive diagnosis of non-alcoholic steatohepatitis by combined serum biomarkers. *J. Hepatol.* 56, 1363–1370. doi: 10.1016/j.jhep.2011.12.025
- Silverman, E. M., Sapala, J. A., and Appelman, H. D. (1995). Regression of hepatic steatosis in morbidly obese persons after gastric bypass. *Am. J. Clin. Pathol.* 104, 23–31. doi: 10.1093/ajcp/104.1.23
- Stevens, G. A., Singh, G. M., Lu, Y., Danaei, G., Lin, J. K., Finucane, M. M., et al. (2012). National, regional, and global trends in adult overweight and obesity prevalences. *Popul. Health Metr.* 10:22. doi: 10.1186/1478-7954-10-22
- Tamimi, T. I., Elgouhari, H. M., Alkhoury, N., Yerian, L. M., Berk, M. P., Lopez, R., et al. (2011). An apoptosis panel for nonalcoholic steatohepatitis diagnosis. *J. Hepatol.* 54, 1224–1229. doi: 10.1016/j.jhep.2010.08.023
- Tran, A., and Gual, P. (2013). Non-alcoholic steatohepatitis in morbidly obese patients. *Clin. Res. Hepatol. Gastroenterol.* 37, 17–29. doi: 10.1016/j.clinre.2012.07.005
- Wallace, T. M., Levy, J. C., and Matthews, D. R. (2004). Use and abuse of HOMA modeling. *Diabetes Care* 27, 1487–1495. doi: 10.2337/diacare.27.6.1487
- Wieckowska, A., Zein, N. N., Yerian, L. M., Lopez, A. R., McCullough, A. J., and Feldstein, A. E. (2006). *In vivo* assessment of liver cell apoptosis as a novel biomarker of disease severity in nonalcoholic fatty liver disease. *Hepatology* 44, 27–33. doi: 10.1002/hep.21223
- Witek, R. P., Stone, W. C., Karaca, F. G., Syn, W. K., Pereira, T. A., Agboola, K. M., et al. (2009). Pan-caspase inhibitor VX-166 reduces fibrosis in an animal model of nonalcoholic steatohepatitis. *Hepatology* 50, 1421–1430. doi: 10.1002/hep.23167
- Wong, R. J., Aguilar, M., Cheung, R., Perumpail, R. B., Harrison, S. A., Younossi, Z. M., et al. (2015). Nonalcoholic steatohepatitis is the second leading etiology of liver disease among adults awaiting liver transplantation in the United States. *Gastroenterology* 148, 547–555. doi: 10.1053/j.gastro.2014.11.039
- Wong, V. W., Wong, G. L., Choi, P. C., Chan, A. W., Li, M. K., Chan, H. Y., et al. (2010). Disease progression of non-alcoholic fatty liver disease: a prospective study with paired liver biopsies at 3 years. *Gut* 59, 969–974. doi: 10.1136/gut.2009.205088
- Yeh, M. M., and Brunt, E. M. (2014). Pathological features of fatty liver disease. *Gastroenterology* 147, 754–764. doi: 10.1053/j.gastro.2014.07.056
- Younossi, Z. M., Jarrar, M., Nugent, C., Randhawa, M., Afendy, M., Stepanova, M., et al. (2008). A novel diagnostic biomarker panel for obesity-related nonalcoholic steatohepatitis (NASH). *Obes. Surg.* 18, 1430–1437. doi: 10.1007/s11695-008-9506-y
- Younossi, Z. M., Koenig, A. B., Abdelatif, D., Fazel, Y., Henry, L., and Wymer, M. (2016). Global epidemiology of nonalcoholic fatty liver disease—Meta-analytic assessment of prevalence, incidence, and outcomes. *Hepatology* 64, 73–84. doi: 10.1002/hep.28431
- Younossi, Z. M., Stepanova, M., Afendy, M., Fang, Y., Younossi, Y., Mir, H., et al. (2011). Changes in the prevalence of the most common causes of chronic liver diseases in the United States from 1988 to 2008. *Clin. Gastroenterol. Hepatol.* 9, 524.e521–530.e521. doi: 10.1016/j.cgh.2011.03.020

Conflict of Interest Statement: The authors declare that the research was conducted in the absence of any commercial or financial relationships that could be construed as a potential conflict of interest.

Copyright © 2016 Schneck, Anty, Patouraux, Bonnafous, Rousseau, Lebeaupin, Bailly-Maitre, Sans, Tran, Gugenheim, Iannelli and Gual. This is an open-access article distributed under the terms of the Creative Commons Attribution License (CC BY). The use, distribution or reproduction in other forums is permitted, provided the original author(s) or licensor are credited and that the original publication in this journal is cited, in accordance with accepted academic practice. No use, distribution or reproduction is permitted which does not comply with these terms.

CD44 is a key player in non-alcoholic steatohepatitis

Stéphanie Patouraux^{1,2,3,†}, Déborah Rousseau^{1,2,†}, Stéphanie Bonnafous^{1,2,4}, Cynthia Lebeau^{1,2}, Carmelo Luci^{1,2}, Clémence M. Canivet^{1,2,4}, Anne-Sophie Schneck^{1,2,4}, Adeline Bertola^{1,2}, Marie-Christine Saint-Paul^{1,2,3}, Antonio Iannelli^{1,2,4}, Jean Gugenheim^{1,2,4}, Rodolphe Anty^{1,2,4}, Albert Tran^{1,2,4}, Béatrice Bailly-Maitre^{1,2}, Philippe Gual^{1,2,*}

¹INSERM, U1065, C3M, Team 8 “Hepatic Complications in Obesity”, Nice, France; ²Université Côte d’Azur, Nice, France; ³CHU of Nice, Biological Center, Pasteur Hôpital, Nice, France; ⁴CHU of Nice, Digestive Center, Nice, France

Background & Aims: Cluster of differentiation (CD)44 regulates adipose tissue inflammation in obesity and hepatic leukocyte recruitment in a lithogenic context. However, its role in hepatic inflammation in a mouse model of steatohepatitis and its relevance in humans have not yet been investigated. We aimed to evaluate the contribution of CD44 to non-alcoholic steatohepatitis (NASH) development and liver injury in mouse models and in patients at various stages of non-alcoholic fatty liver disease (NAFLD) progression.

Methods: The role of CD44 was evaluated in *CD44*^{-/-} mice and after injections of an α CD44 antibody in wild-type mice challenged with a methionine- and choline-deficient diet (MCDD). In obese patients, hepatic CD44 (n = 30 and 5 NASH patients with a second liver biopsy after bariatric surgery) and serum sCD44 (n = 64) were evaluated.

Results: Liver inflammation (including inflammatory foci number, macrophage and neutrophil infiltration and CCL2/CCR2 levels), liver injury and fibrosis strongly decreased in *CD44*^{-/-} mice compared to wild-type mice on MCDD. CD44 deficiency enhanced the M2 polarization and strongly decreased the activation of macrophages by lipopolysaccharide (LPS), hepatocyte damage-associated molecular patterns (DAMPs) and saturated fatty acids. Neutralization of CD44 in mice with steatohepatitis strongly decreased the macrophage infiltration and chemokine ligand (CCL)2 expression with a partial correction of liver inflammation and injury. In obese patients, hepatic CD44 was strongly upregulated in NASH patients ($p = 0.0008$) and correlated with NAFLD activity score (NAS) ($p = 0.001$), ballooning ($p = 0.003$), alanine transaminase ($p = 0.005$) and hepatic CCL2 ($p < 0.001$) and macrophage marker CD68 ($p < 0.001$) expression. Correction of NASH was associated with a strong decrease in liver CD44⁺ cells. Finally, the soluble form of CD44 increased with severe steatosis ($p = 0.0005$) and NASH ($p = 0.007$).

Conclusion: Human and experimental data suggest that CD44 is a marker and key player of hepatic inflammation and its targeting partially corrects NASH.

Lay summary: Human and experimental data suggest that CD44, a cellular protein mainly expressed in immune cells, is a marker and key player of non-alcoholic steatohepatitis (NASH). Indeed, CD44 enhances the non-alcoholic fatty liver (NAFL) (hepatic steatosis) to NASH progression by regulating hepatic macrophage polarization (pro-inflammatory phenotype) and infiltration (macrophage motility and the MCP1/CCL2/CCR2 system). Targeting CD44 partially corrects NASH, making it a potential therapeutic strategy.

© 2017 European Association for the Study of the Liver. Published by Elsevier B.V. All rights reserved.

Introduction

Global prevalence of non-alcoholic fatty liver diseases (NAFLD) ranges from 22% to 28%.¹ The spectrum of these hepatic abnormalities extends from isolated steatosis to steatohepatitis (non-alcoholic steatohepatitis, NASH) and steatofibrosis leading to cirrhosis and hepatocellular carcinoma. NAFLD is one of the main causes of cirrhosis and increases the risk of liver-related death and hepatocellular carcinoma. Despite this major public health concern, treatment of NAFLD is still elusive (apart from lifestyle changes) as there is lack of efficacious pharmacological treatment. Whereas the molecular mechanisms responsible for the progression from a “safe” state to NASH are still unclear, hepatic inflammation is a key factor involved in the progression of NAFLD. Recent findings suggest that cluster of differentiation (CD)44 could play an important role in the development and progression of NAFLD, by regulating adipose tissue and liver inflammation.^{2–5}

CD44 is expressed on many cell types that contribute to inflammation, such as leukocytes, neutrophils and macrophages. It has been recently reported in an animal model of obesity that CD44 plays an important role in adipose tissue inflammation by promoting macrophage recruitment, which in turn enhances insulin resistance and hepatic steatosis.^{2,3} Neutralization of CD44 by specific antibodies reduces fasting blood glucose levels,

Keywords: CD44; Liver; NAFLD; Steatosis; NASH; MCP1; Macrophages.

Received 27 May 2016; received in revised form 1 February 2017; accepted 2 March 2017

* Corresponding author. Address: INSERM U1065, Bâtiment Universitaire ARCHIMED, Equipe 8 “Complications hépatiques de l’obésité”, 151 route Saint Antoine de Ginestière, BP 2 3194, 06204 Nice Cedex 03, France. Tel.: +33 4 89 06 42 23; fax: +33 4 89 06 42 21.

E-mail address: philippe.gual@inserm.fr (P. Gual).

[†] These authors contributed equally as joint first authors.



Research Article

weight gain, liver steatosis and insulin resistance in a dietary mouse model of obesity.⁴ CD44 also promotes hepatic inflammatory cell recruitment during fatty liver formation in a lithogenic diet-fed mouse model.⁵ In line with these data, human adipose tissue CD44 is associated with localized inflammation and systemic insulin resistance;⁶ weight loss in obese patients is associated with a strong decrease in the gene expression of CD44 and the macrophage marker CD68 in subcutaneous adipose tissue.⁷ Since osteopontin (OPN), E-selectin and hyaluronic acid (HA) are the main ligands of CD44 and are involved in liver disease,^{8–12} we can presume that the activation of the CD44 pathway could be involved in NAFLD progression. As previously reported in human NAFLD, hepatic osteopontin and E-selectin are strongly upregulated with fibrosis and NASH, respectively.^{8,9} Upon injury, local HA production increases and is fragmented, generating low-molecular weight HA (LMW-HA) that functions as a pro-inflammatory danger-associated molecular pattern and cleared via CD44-mediated endocytosis.¹¹ The interaction of CD44 and HA is the dominant mechanism for neutrophil sequestration in inflamed liver sinusoids.¹³ HA is also a biomarker for severe fibrosis and cirrhosis in various liver diseases including NAFLD and alcoholic liver disease (ALD).^{14–16} The possible contribution of the CD44 pathway to the evolution from simple steatosis to NASH and fibrosis has not been fully investigated so far. We therefore evaluated the contribution of CD44 in NASH development and liver injury in experimental mouse models and in a cohort of patients at various stages of NAFLD progression.

Patients and methods

Human studies

Morbidly obese patients

A total of 93 patients (30 patients for the gene expression, 64 patients for the sCD44 and 5 patients for the follow-up) were recruited through the Department of Digestive Surgery and Liver Transplantation (Nice hospital) where they under-

went bariatric surgery for their morbid obesity. Bariatric surgery was indicated for these patients in accordance with French guidelines. Exclusion criteria were: presence of a hepatitis B or hepatitis C infection, excessive alcohol consumption (>20 g/d) or another cause of chronic liver disease as previously described.^{17–19} The characteristics of the study groups for the gene expression are described in Table 1. Before surgery, fasting blood samples were obtained and used to measure alanine and aspartate transaminases (ALT and AST, respectively), glucose, insulin and HbA1c. Insulin resistance was calculated using the homeostatic model assessment (HOMA-IR) index.²⁰ Liver biopsies were obtained during surgery and no ischemic preconditioning had been performed. A second liver biopsy and a concomitant diagnostic work-up were offered to five patients who underwent a laparoscopic Roux-en-Y gastric bypass (LRYGB), who initially displayed biopsy-proven NASH and completed a minimum follow-up period of 30 months after surgery. Hepatic histopathological analysis was performed according to the scoring system of Kleiner *et al.*²¹ Four histopathological features were semi-quantitatively evaluated: grade of steatosis (0, <5%; 1, 5%–30%; 2, >30%–60%; 3, >60%), lobular inflammation (0, no inflammatory foci; 1, <2 inflammatory foci per 200x field; 2, 2–4 inflammatory foci per 200x field; 3, >4 inflammatory foci per 200x field), hepatocellular ballooning (0, none; 1, few balloon cells; 2, many cells/prominent ballooning), and stage of fibrosis (from 0, none to 4, cirrhosis).

Control participants

Liver tissue was obtained from five lean participants (5 women; age, 44 ± 9 years; BMI, 21 ± 1.9 kg/m²) undergoing partial hepatectomy for benign tumours (neighbour tissues from four adenoma and one focal nodular hyperplasia). Three participants underwent a left lobectomy or a bisegmentectomy without ischemic preconditioning and two patients underwent a right hepatectomy with a potential ischemic preconditioning (missing data). Liver samples did not display any hepatic steatosis, inflammation or fibrosis. All participants gave their informed written consent to participate in this study in accordance with French legislation regarding Ethics and Human Research (Huriet-Serusclet law). The "Comité Consultatif de Protection des Personnes dans la Recherche Biomédicale de Nice" approved the study (07/04:2003, N° 03.017).

Animals and study design

19-week-old male wild-type (WT) and CD44-deficient (*CD44*^{-/-}) (B6.Cg-Cd44^{tm1Hbg}/J from Jackson Laboratory, Bar Harbor, ME, USA) C57BL/6 mice were acclimated to our animal facilities under a 12/12 h light/dark cycle at a temperature of 21 ± 2 °C and were fed *ad libitum* either a methionine- and choline-deficient diet (MCDD # 960439, Ctr diet # 960440) and Ssniff (MCDD # E15653-94; Ctr diet # E15654-04).

Table 1. Characteristics of the obese patients.

	Without NAFLD	Steatosis	NASH
n	8	13	9
Age (years)	34.7 ± 4.4	36.8 ± 2.7	41.0 ± 3.3
BMI (kg/m ²)	43.4 ± 0.5	42.9 ± 1.12	43.3 ± 1.9
ALT (IU/L)	17.4 ± 2.9	29.2 ± 2.4 [*]	104.8 ± 28.0 ^{*,#}
AST (IU/L)	20.7 ± 2.9	22.1 ± 1.0	60.2 ± 15.8 ^{*,#}
Fasting insulin (mIU/L)	9.7 ± 2.4	15.2 ± 3.8	41.8 ± 10.2 ^{*,#}
Fasting glucose (mmol/L)	4.8 ± 0.1	5.3 ± 0.2 [*]	8.3 ± 1.7 [*]
HOMA-IR	2.0 ± 0.5	3.7 ± 1.0	14.4 ± 3.9 ^{*,#}
HbA1c (%)	5.3 ± 0.1	5.6 ± 0.1	7.0 ± 0.7 ^{*,#}
NAFLD activity score (n)	0 (8)	2 (5) 3 (8)	5 (9)
Grade of steatosis (n)	0 (8)	2 (6) 3 (7)	3 (9)
Lobular inflammation (n)	0 (8)	0 (13)	1 (9)
Hepatocellular ballooning (n)	0 (8)	0 (13)	1 (9)
Hepatic gene expression (vs. lean)			
<i>TNFα</i>	1.80 ± 0.52	2.28 ± 0.35	7.63 ± 1.35 ^{*,#}
<i>IL1β</i>	1.23 ± 0.21	1.52 ± 0.28	7.80 ± 2.36 ^{*,#}
<i>MCPI</i>	1.26 ± 0.33	2.64 ± 0.64 [*]	6.48 ± 1.46 ^{*,#}

Without NAFLD: patients with normal liver histology; Steatosis: patients with steatosis; NASH: patients with severe steatosis and NASH. Data are expressed as mean ± SEM and compared using the non-parametric Mann Whitney test.

^{*} *p* < 0.05 compared with "Without NAFLD".

[#] *p* < 0.05 compared with Steatosis.

Anti-CD44 treatment

WT C57BL/6 male mice (19 weeks of age) were fed MCDD for 4 weeks. During the last 6 days of MCDD, mice received daily intra-peritoneal injections of either purified rat anti-mouse CD44 mAb (n = 5; IM7, BD Pharmingen, catalog #553131; BD Biosciences) or purified rat IgG2b, κ isotype control (n = 6; A95-1, BD Pharmingen, catalog #553986; BD Biosciences) (100 μ g/mouse the first day then 50 μ g/mouse). At the end of the treatment, the blood was collected and mice were immediately sacrificed, after which the liver was removed. One part of the liver was immediately frozen in liquid nitrogen and stored at -80°C until analysis. The second part was fixed in buffered formalin, paraffin-embedded, sectioned, and stained with hematoxylin-eosin-saffron or Masson's trichrome. The last part was used for flow cytometric analysis. The guidelines of laboratory animal care were followed, and the local ethical committee approved the animal experiments (NCE/2013-108, APAFIS#5100-2015121110477413 v6).

Flow cytometric analysis

The cells were surface-stained with antibodies against mouse CD45 (clone 30-F11), CD44 (clone IM7), F4/80 (clone BM8), CD11b (clone M1/70), CD11c (clone HL3), Gr1 (clone RB6-8C5), CD206 (clone C068C2) or CD301 (clone ER-MP23) purchased from BD Biosciences, eBioscience, Bio Rad ABD Serotec. Samples were acquired using a fluorescence activated cell sorting (FACS) Canto II flow cytometer, and the data were analyzed using the FACSDiva software version 8.0.1 (BD Biosciences).

Real-time quantitative PCR analysis

Total liver RNA was extracted using the RNeasy Mini Kit (74104, Qiagen, Hilden, Germany) and treated with Turbo DNA-free (AM 1907, Thermo Fisher Scientific Inc.) following the manufacturer's protocol. The quantity and quality of the RNA were determined using the Agilent 2100 Bioanalyzer with RNA 6000 Nano Kit (5067-1511, Agilent Technologies, Santa Clara, CA, USA). Total RNA (1 μ g) was reverse transcribed with a High-Capacity cDNA Reverse Transcription Kit (Thermo Fisher Scientific Inc.). Real-time quantitative PCR was performed in duplicate for each sample using the StepOne Plus Real-Time PCR System (Thermo Fisher Scientific Inc.) as previously described.^{15,22} TaqMan gene expression assays were purchased from Thermo Fisher Scientific Inc. and listed in [Supplementary data](#). Gene expression was normalized to the housekeeping gene β 2M (β 2 microglobulin, mouse) or RPLP0 (Ribosomal Phosphoprotein Large P0, mouse and human) and calculated based on the comparative cycle threshold Ct method ($2^{-\Delta\Delta Ct}$).

Immunohistochemistry

Sections measuring 2 μ m were cut from each paraffin block and were put to dry at 37°C for 12 h. After deparaffinization and rehydration, all sections were pre-treated at pH 6 with Flex Target Retrieval Solution (TRS) Low (PTLink DAKO, Glostrup, Denmark) for 20 min. Endogenous peroxidase was blocked in 1% hydrogen peroxide for 5 min (DAKO, Glostrup, Denmark) at room temperature. After rinsing with phosphate buffered saline, the sections were incubated with a ready to use anti-CD44 (8E1, #5640, Cell signaling) antibody for 20 min at room temperature. Then sections were incubated with an appropriate secondary antibody from the Envision flex/HRP kit (Dako, Glostrup, Denmark) for 20 min, at room temperature. Next, slides were incubated in phosphate buffered saline (PBS), for 20 min, at room temperature, and then peroxidase activity was detected by diaminobenzidine tetrahydrochloride for 8 min and used for visualization. Sides were then counterstained with haematoxylin (Dako, Glostrup, Denmark) for 6 min.

Statistical analysis

Statistical significance of differential gene expression between two study groups was determined using the nonparametric Mann-Whitney *U* test with the $2^{-\Delta\Delta Ct}$ of each group. Other data from mice and cell preparations were statistically analyzed using the Mann-Whitney *U* test or the Student's *t* test. Data from cell lines were statistically analyzed using the Student's *t* test. Correlations were analyzed using the Pearson's correlation test. $p < 0.05$ was considered as significant.

For further details regarding the materials used, please refer to the [Supplementary material](#) and the [CTAT table](#)

Results**Upregulation of hepatic expression of CD44 with steatohepatitis**

We first evaluated the hepatic level of CD44 in wild-type (WT) mice with MCDD-induced steatohepatitis. The hepatic level of the CD44 was strongly increased after 2 weeks of MCDD at the protein (Fig. 1A) and mRNA (Fig. 1B) levels. Steatohepatitis was thus associated with the hepatic upregulation of CD44 expression.

CD44 deficiency partially prevented liver injury, hepatic steatosis and steatohepatitis induced by MCDD challenge

The role of CD44 in liver injury and steatohepatitis induced by MCDD was then investigated using mice deficient for CD44. As expected, MCDD challenge was associated with elevated aspartate (AST) and ALT activity in WT mice (Fig. 1C). The $CD44^{-/-}$ mice showed less liver damage as shown by the lower AST and ALT levels. Furthermore, histological analyses displayed less hepatic steatosis and showed less accumulation of inflammatory foci in the livers of MCDD-fed $CD44^{-/-}$ mice compared with livers of MCDD-fed WT mice (Fig. 1D, E). These results indicated that the CD44 deficiency resulted in partial prevention of the liver injury, steatosis and steatohepatitis induced by MCDD challenge.

CD44 deficiency strongly prevented the recruitment of monocytes and neutrophils into the liver and liver inflammation induced by MCDD challenge

Since CD44 can regulate the homing of immune cells,^{3,5,10,13,23} we investigated the composition of immune cells in the liver by flow cytometric analysis. While MCDD challenge did not promote the enrichment of T cells ($CD4^{+}$ and $CD8^{+}$ cells) in liver (data not shown), MCDD challenge mediated a strong hepatic enrichment in macrophages ($F4/80^{+}$ cells), pro-inflammatory M1 macrophages ($F4/80^{+} CD11c^{+}$) and monocytes/neutrophils ($Gr1^{+}$) (Fig. 1F). Interestingly, CD44 deficiency robustly prevented the enrichment of monocyte/macrophages and M1 macrophages into the liver (Fig. 1F). This later was associated with less hepatic inflammation as evaluated by M1 markers including tumor necrosis factor ($TNF\alpha$), interleukin ($IL1\beta$), inducible nitric oxide synthase ($iNOS$), and monocyte chemoattractant protein ($MCP1$) (Fig. 1G). CD44 deficiency still prevented the more severe accumulation of inflammatory foci (MCDD-fed $CD44^{-/-}$ mice: 14 ± 4 foci number/10 fields, $n = 7$, vs. MCDD-fed WT mice: 34 ± 3 foci number/10 fields, $n = 6$, $p = 0.010$, data not shown) and non-parenchymal hepatic cells (MCDD-fed $CD44^{-/-}$ mice: 10 ± 1 million/liver, $n = 7$, vs. MCDD-fed WT mice: 17 ± 1 million/liver, $n = 6$, $p = 0.045$, data not shown) after four weeks of MCDD challenge. CD44 deficiency strongly prevented the recruitment of infiltrating monocytes ($F4/80^{+} CD11b^{high}$ cells) vs. resident Kupfer macrophages, ($F4/80^{+} CD11b^{+}$ cells) (Fig. 2A, B) and infiltrating neutrophils ($CD11b^{+} Gr1^{high}$ cells) (Fig. 2A, B) into the liver. Importantly, CD44 deficiency was not associated with the depletion of monocytes from the circulation (Fig. 2C), which would have explained the decreased infiltrating monocytes into the liver. In contrast, hepatic infiltrating neutrophils correlated with blood neutrophil levels (Fig. 2C). Since CD44 deficiency strongly altered the chemotaxis of peritoneal macrophages in response to $MCP1/CCL2^{23}$ and $MCP1/CCL2$ plays an important role in the

Research Article

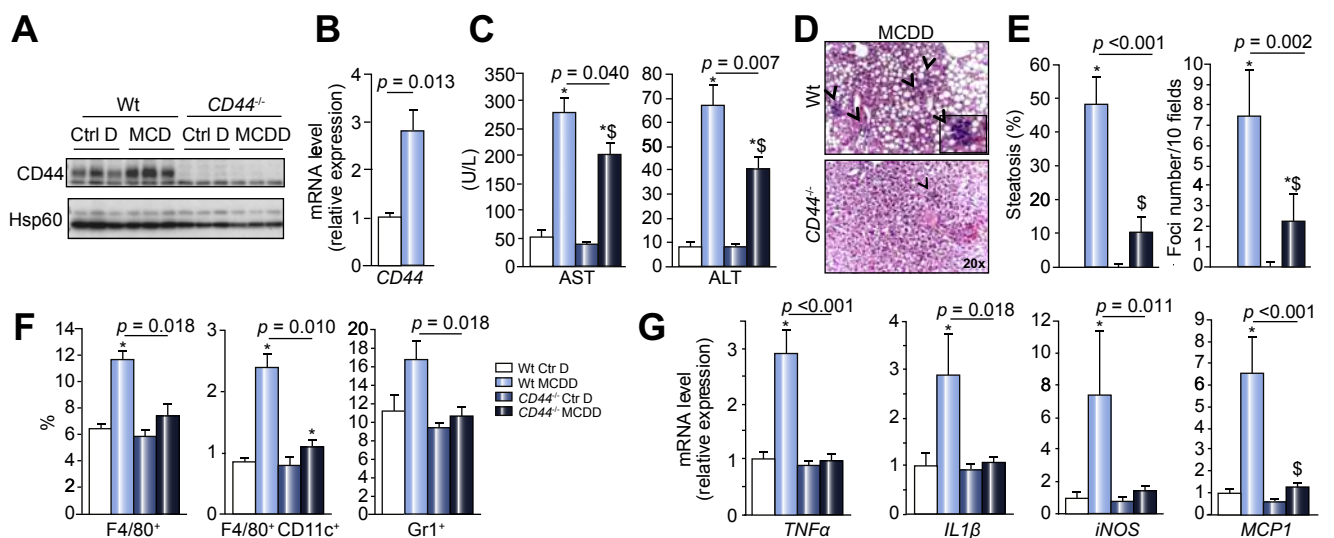


Fig. 1. CD44 deficiency partially prevented liver injury, hepatic steatosis and steatohepatitis induced by MCDD challenge. Wild-type (WT; $n = 31$) and $CD44^{-/-}$ ($n = 30$) mice fed a control diet (Ctr D) or MCDD for 2 weeks. Hepatic CD44 expression was evaluated in WT Ctr D and MCDD mice at the protein (A) (3 mice/group) and at the mRNA levels (B) (4–8 mice/group). (C) The plasma levels of ALT and AST were evaluated (WT: 14–17 mice/group; CD44: 12–18 mice/group). (D) H&E staining of liver tissue sections samples from WT and $CD44^{-/-}$ after MCDD as indicated. Representative pictures are shown. (E) Quantification of hepatic steatosis and inflammatory foci. (F) Hepatic non-parenchymal cells were stained for CD45, F4/80, CD11c and Gr1 and analyzed by flow cytometry (4–7 mice/group). (G) Hepatic mRNA expression levels of *TNF α* , *IL1 β* , *iNOS* and *MCP1* were analyzed by real-time quantitative PCR (4–15 mice/group). Data are presented as relative mRNA levels normalized to $\beta 2M$ mRNA levels. Data are expressed as means \pm SEM and statistically analyzed using the Mann-Whitney *U* test. * $p < 0.05$, compared with WT Ctr D mice; $^{\$}p < 0.05$, compared with $CD44^{-/-}$ Ctr D.

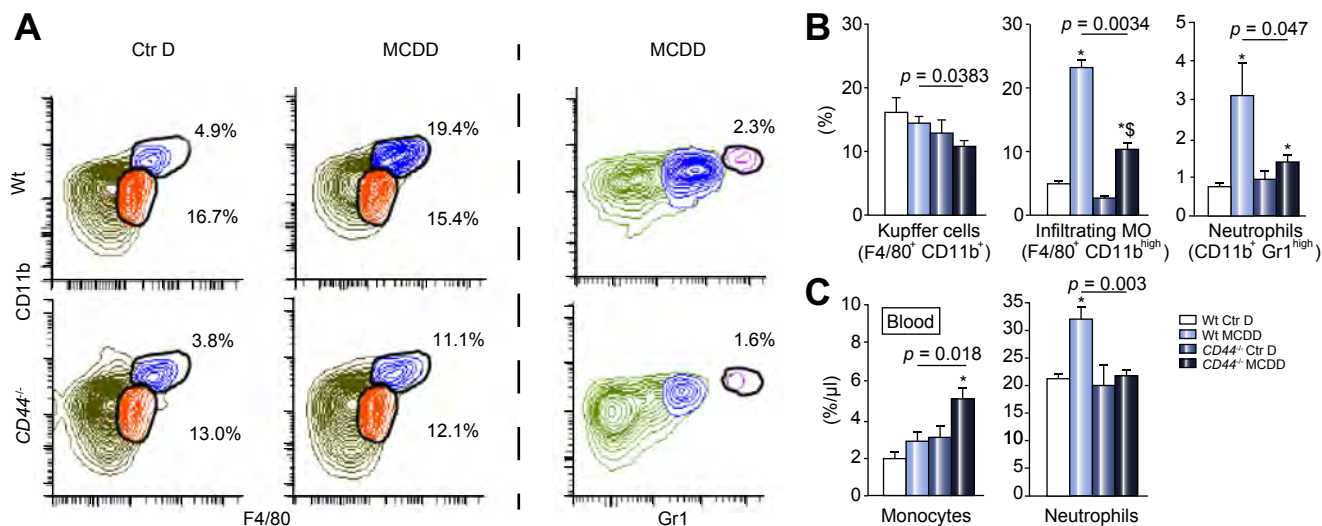


Fig. 2. CD44 deficiency partially prevented hepatic monocyte and neutrophil infiltration induced by MCDD challenge. Wild-type (WT; $n = 10$) and $CD44^{-/-}$ ($n = 11$) mice fed a control diet (Ctr D) or MCDD for 4 weeks. (A) and (B) Hepatic non-parenchymal cells were stained for CD45, F4/80, CD11c and Gr1 and analyzed by flow cytometry (4–7 mice/group). Percentage of Kupffer cells (F4/80 $^{+}$ CD11b $^{+}$), infiltrating macrophages (F4/80 $^{+}$ CD11b high) and neutrophils (CD11b $^{+}$ Gr1 high) are expressed as means \pm SEM and statistically analyzed using the Mann-Whitney *U* test. (C) Blood monocyte and neutrophil percentages (evaluated by automated differential cell counting) are expressed as means \pm SEM and statistically analyzed using the Mann-Whitney *U* test. * $p < 0.05$, compared with WT Ctr D mice, $^{\$}p < 0.05$, compared with $CD44^{-/-}$ Ctr D.

recruitment of macrophages into the liver,²⁴ the unresponsiveness of CD44-deficient macrophages to MCP1 and the lower levels of hepatic MCP1 expression in MCDD-fed $CD44^{-/-}$ mice (Fig. 1G) might be involved in the decreased number of hepatic infiltrating monocytes.

CD44 silencing or deficiency strongly enhanced the M2 macrophage polarization

In addition to the regulation of the MCP1-mediated macrophage chemotaxis, CD44 could also control the properties and the

activities of the macrophages. We then investigated its potential role in the macrophage polarization. Whereas CD44 deficiency did not alter the macrophage colony-stimulating factor (M-CSF)-mediated macrophage differentiation of bone marrow monocytes (Fig. 3A), it strongly enhanced the proportion of M2 bone marrow derived macrophages (BMDM) (CD206⁺-F4/80⁺ CD11b⁺ BMDM) in the basal condition and in response to IL4 (Fig. 3B). In RAW 264.7 macrophages, CD44 silencing with siRNA also led to a substantial increase in M2 macrophages (CD301⁺ cells), in the expression of CD301 and arginase 1 (*Arg1*; at the mRNA level) and in the IL10 secretion in response to IL4 (Fig. S1).

CD44 silencing or deficiency strongly limited pro-inflammatory phenotypes of macrophages

On the contrary, CD44 deficiency in BMDM or CD44 silencing in RAW 264.7 macrophages strongly decreased the expression of pro-inflammatory cytokines such as *IL6* and *TNF α* in response to lipopolysaccharides (LPS) (Figs. 3C, 4A, respectively). In addition to LPS, CD44 silencing in LPS-primed RAW 264.7 macrophages also strongly decreased the expression of pro-inflammatory cytokines such as *IL6*, *TNF α* and *IL1 β* in response to damage-associated molecular patterns (DAMPs) from damaged fatty primary hepatocytes (Fig. 4A). Supernatant of primary fatty hepatocytes isolated from MCDD-fed mice (2 weeks) and exposed to heat shock (increased lactate dehydrogenase (LDH) release, data not shown) also increased the CD44 expression in LPS-primed RAW 264.7 macrophages (Fig. 4A). Finally, CD44 silencing in RAW 264.7 macrophages also decreased the expression of *IL6* and *TNF α* in response to saturated fatty acid palmitate (PA) (Fig. 4B). palmitic acid (PA) stimulation further decreased the mRNA levels of M2 marker *CD206*, which was strongly overcome by the CD44 silencing (Fig. 4B). These results indicate that the deficiency of CD44 modified the properties of macrophages with higher susceptibility to M2 polarization and accordingly, lower pro-inflammatory phenotypes upon activation.

Neutralization of CD44 corrected the hepatic inflammation, macrophage recruitment and liver injury induced by MCDD challenge

We then investigated if the neutralization of CD44 by a specific antibody could correct the liver complications induced by MCDD. After 3 weeks of MCDD, mice received a daily intraperitoneal injection of either purified rat anti-CD44 mAb or isotype control for six additional days of MCDD. The treatment with anti-mouse CD44 mAb strongly depleted the hepatic CD44 positive cells (Fig. 5A), strongly decreased the liver injury as evaluated by the AST/ALT activity (Fig. 5B) and hepatic inflammation as evaluated by the presence of inflammatory foci (Fig. 5C, D). The correction of hepatic inflammation was also associated with less hepatic enrichment in macrophages (F4/80⁺ cells), pro-inflammatory M1 macrophages (F4/80⁺ CD11c⁺), monocytes/neutrophils (Gr1⁺) (Fig. 5E) and a strong decrease in liver and serum MCP1 levels (Fig. 5F). In these experimental conditions, the correction of steatohepatitis by CD44 neutralization was not associated with an improvement of hepatic steatosis (Fig. 5C, D).

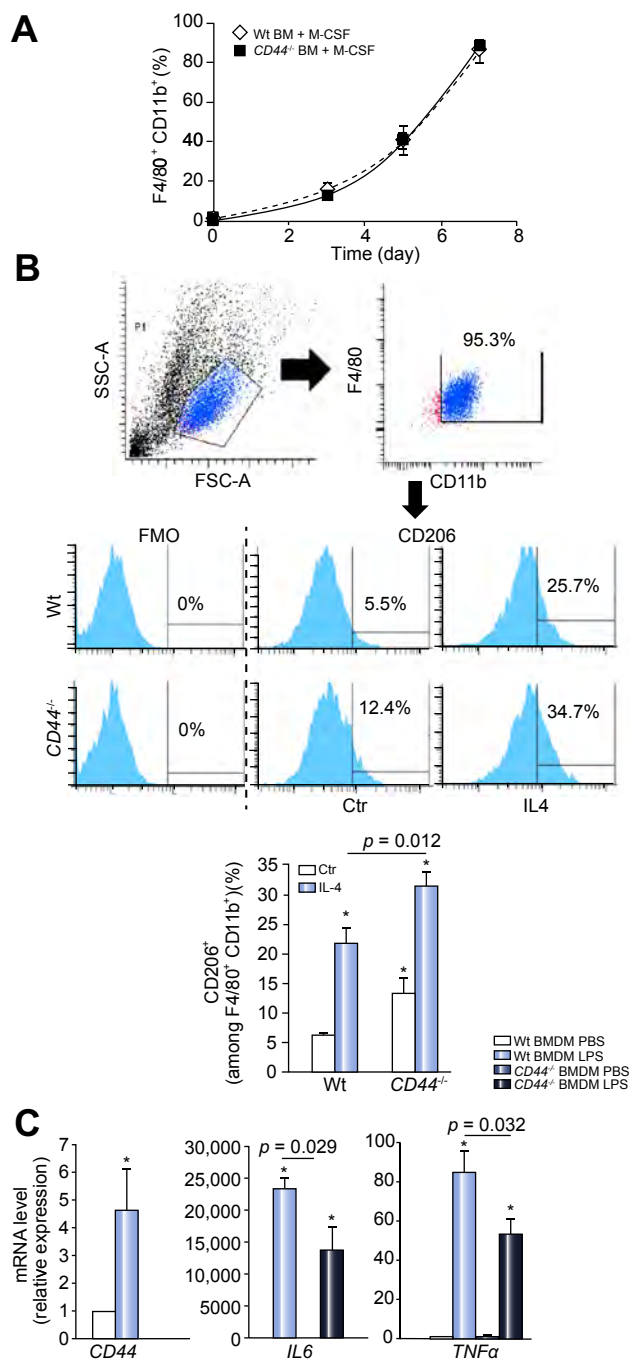


Fig. 3. CD44 deficiency in bone marrow derived macrophages enhanced IL4-mediated M2 polarization and decreased LPS-induced *IL6* and *TNF α* expression. (A) Bone marrow derived macrophage differentiation of WT and CD44^{-/-} monocytes after M-CSF stimulation has been analyzed at indicated time by flow cytometry and expressed as % of F4/80⁺ CD11b⁺ cells (n = 5). (B) WT and CD44^{-/-} bone marrow derived macrophages (BMDM) were incubated without or with IL4 (20 ng/ml) for 18–24 h, stained for CD45, F4/80, CD11b and CD206 and then analyzed by flow cytometry. The percentages of CD206⁺ cells among the F4/80⁺ CD11b⁺ cells are expressed as means \pm SEM and statistically analyzed using the Student's *t* test (n = 4). (C) WT and CD44^{-/-} BMDMs were incubated with PBS or LPS (100 ng/ml) for 6 h. The gene expressions of *CD44*, *IL6* and *TNF α* were then evaluated (n = 3). The mRNA levels were normalized to *RPLP0* mRNA levels and expressed as fold stimulation (mean \pm SEM) vs. WT BMDM + PBS. Data were statistically analyzed using the Student's *t* test. **p* < 0.05, compared with WT BMDM Ctr.

Research Article

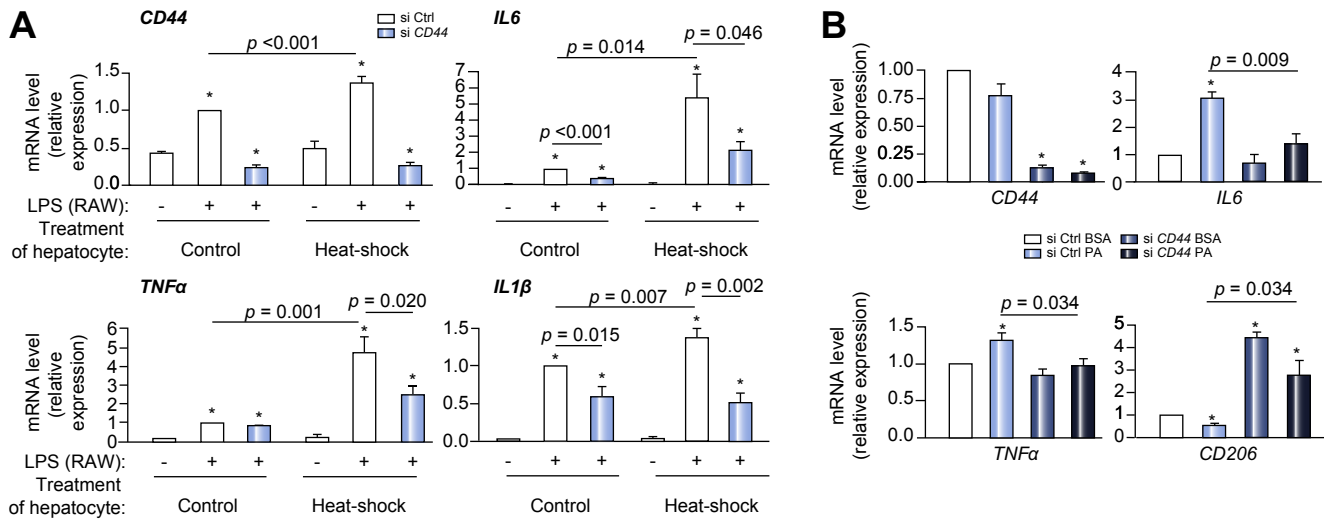


Fig. 4. CD44 silencing strongly decreased the expression of pro-inflammatory cytokines in activated macrophages. RAW 264.7 macrophages after control (siCtrl) or CD44 silencing (siCD44) were stimulated or not with (A) supernatants of control (37 °C for 6 h) and heat shock (45 °C for 6 h) primary fatty hepatocytes (from WT mice fed 2 weeks of MCDD) with or without LPS (100 ng/ml) for 6 h (n = 4) or (B) palmitic acid (PA) (500 μM) for 24 h in 'cell medium' supplemented with 1% bovine serum albumin (n = 3). The gene expressions of CD44, TNFα, IL6, IL1β and CD206 were then evaluated. The mRNA levels were normalized to RPLP0 mRNA levels and expressed as fold stimulation (mean ± SEM) vs. siCtrl/conditioned medium of fatty hepatocyte/LPS (A) or siCtrl BSA (B). Data were statistically analyzed using the Student's t test. *p < 0.05, compared with siCtrl/conditioned medium of fatty hepatocyte (A) or siCtrl BSA (B).

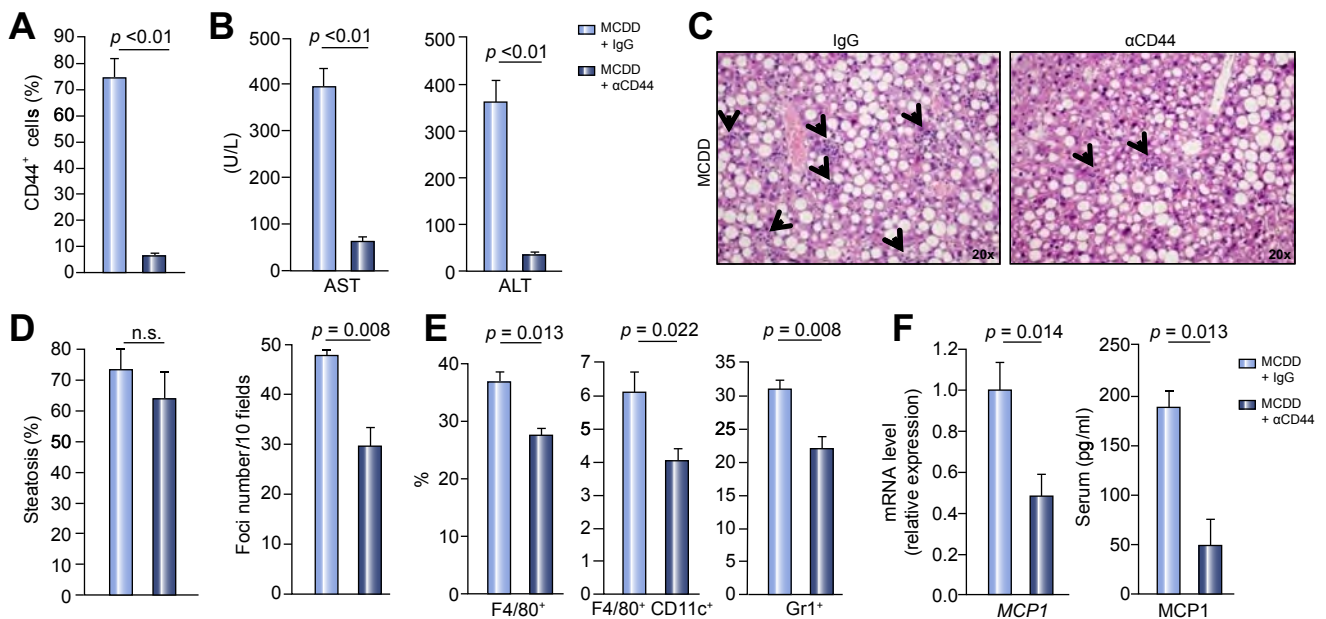


Fig. 5. Neutralization of CD44 corrected the hepatic inflammation, the macrophages recruitment and liver injury induced by MCDD challenge. After 3 weeks of MCDD, the mice received a daily intra-peritoneal injection of either purified rat anti-mouse CD44 mAb (αCD44) or purified rat IgG2b, κ isotype control (αIgG) for six additional days on MCDD diet (5–6 mice/group). (A and E) Hepatic non-parenchymal cells were stained for CD44, F4/80, CD11c and Gr1 and analyzed by flow cytometry. (B) ALT and AST plasma levels were evaluated. (C) H&E staining of liver samples from αCD44- and αIgG-treated mice as indicated. Representative pictures are shown. (D) Quantification of hepatic steatosis and inflammation (number of inflammatory foci). (F) Hepatic mRNA expression and plasma levels of MCP1 were analyzed by real-time quantitative PCR and ELISA, respectively. Data are expressed as means ± SEM and statistically analyzed using the Mann-Whitney U test.

CD44 deficiency strongly decreased the hepatic fibrosis induced by MCDD

Hepatic injury and inflammation are key actors in the fibrogenic process. Since the development of hepatic fibrosis required a

long-lasting MCDD challenge, WT and CD44^{-/-} mice were then challenged with MCDD for 7 weeks. In addition to reduced hepatic steatosis and inflammation (Fig. 6A), CD44 deficiency was also associated with less fibrosis as evaluated by collagen staining (Masson's trichrome stain, Fig. 6B) and lower gene expression of

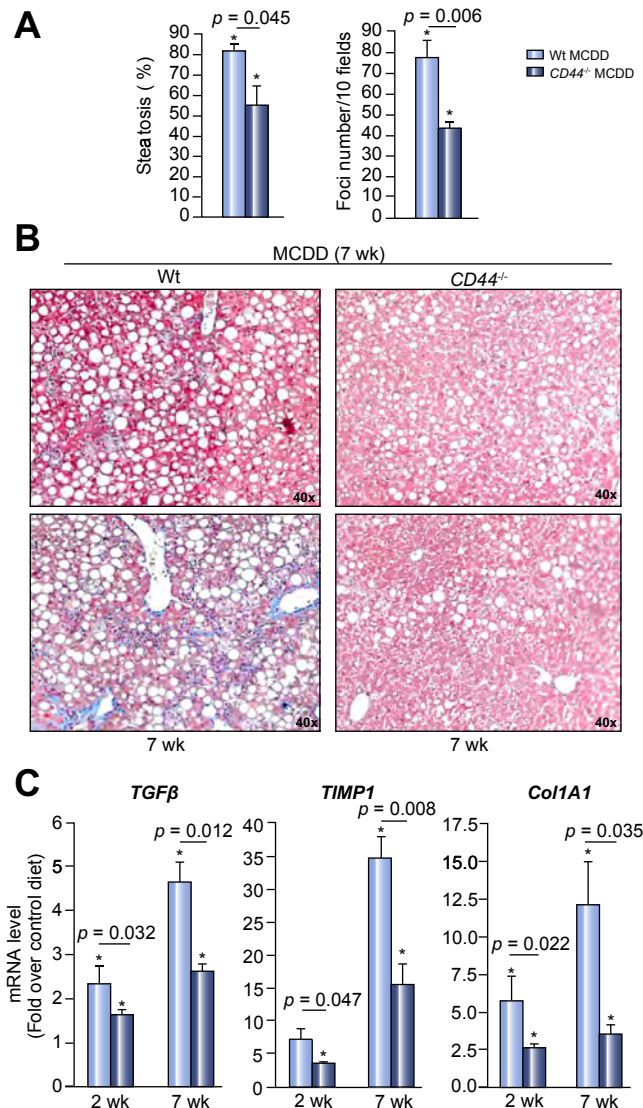


Fig. 6. CD44 deficiency strongly decreased the hepatic fibrosis induced by MCDD. WT and CD44^{-/-} mice were challenged with a Ctr D or MCDD for 7 weeks (5–6 mice/group). (A) Quantification of hepatic steatosis and inflammation (inflammatory foci) after H&E staining of liver samples. (B)(C) Hepatic fibrosis was evaluated by (B) collagen staining (Masson's trichrome) (representative pictures are shown) and (C) gene expression of markers of fibrosis including *TGFβ*, *TIMP1* and *Col1A1*. Data are presented as relative mRNA levels normalized to $\beta 2M$ mRNA levels. Data are expressed as means \pm SEM and statistically analyzed using the Mann-Whitney *U* test: **p* < 0.05, compared with WT Ctr D mice.

fibrosis markers like transforming growth factor (*TGFβ*), *TIMP1* and *Col1A1* (Fig. 6C). The partial prevention of hepatic fibrosis induced by CD44 deficiency was again associated with reduced liver injury, M1 macrophage enrichment as well as in MCP1 and CCR2 expression upon the long-term MCDD challenge (Fig. S2). Interestingly, the CD44 deficiency already prevented the upregulation of *TGFβ*, *TIMP1* and *Col1A1* in the early stages (in response to 2 weeks of MCDD) even before liver collagen accumulation (Fig. 6C). By regulating hepatic inflammation and liver injury, CD44 thus plays an important role in the progression of NAFLD to more severe complication (NASH-related fibrosis).

Hepatic CD44 correlated with NASH, hepatic MCP1 expression and liver macrophage enrichment in obese patients

We then investigated the relevance of our findings in the context of human NAFLD. We examined the relationship of hepatic CD44 expression to the progression of normal liver to hepatic steatosis and then NASH in liver biopsies obtained from morbidly obese patients undergoing bariatric surgery (Table 1). Patients were classified into three groups: without NAFLD, with hepatic steatosis (steatosis) and with NASH (NASH). Hepatic expression of CD44 was specifically upregulated in NASH patients at the mRNA (Fig. 7A) and protein levels (Fig. 7B) and preferentially correlated with the presence of NASH, hepatocyte ballooning and ALT activ-

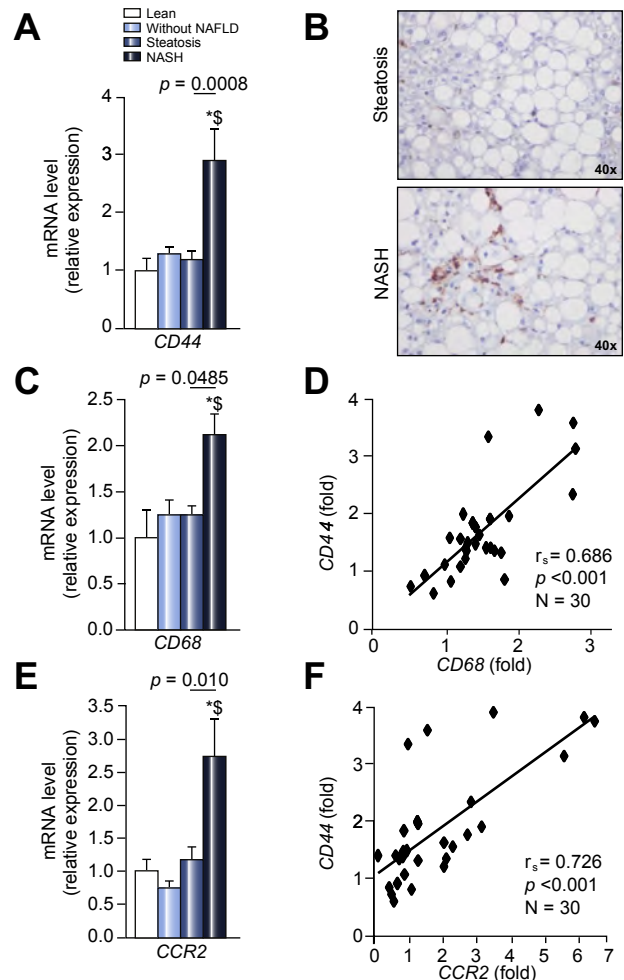


Fig. 7. Hepatic CD44 correlated with NASH, hepatic MCP1 expression and liver macrophage infiltration in obese patients. Liver CD44 (A), CD68 (C) and CCR2 (E) mRNA expression levels were analyzed by real-time quantitative PCR in lean patients (*n* = 4), in morbidly obese patients without NAFLD (*n* = 8), with hepatic steatosis (*n* = 13) and with NASH (*n* = 9). The gene expression was normalized to the mRNA levels of *RPLP0*. Results are expressed relative to the expression level in controls (means \pm SEM) and statistically analyzed using the Mann-Whitney *U* test. **p* < 0.05, compared with lean; \S *p* < 0.05, compared with obese patients without NAFLD. (B) α CD44 staining of liver tissue sections from morbidly obese patients with severe hepatic steatosis (*n* = 5) and with NASH (*n* = 5). Representative pictures are shown. Correlations between CD44 and CD68 (D) or CCR2 (F) mRNA expression levels (fold vs. lean) were analyzed using the Pearson's correlation test.

Research Article

Table 2. Correlation between hepatic CD44 expression and liver features in obese patients.

	Steatosis			NASH			Ballooning			NAS			ALT		
	r_s	p value	N	r_s	p value	N	r_s	p value	N	r_s	p value	N	r_s	p value	N
Liver CD44	0.480	0.007	30	0.668	< 0.001	30	0.531	0.003	30	0.562	0.001	30	0.496	0.005	30

Spearman's rank correlation test.

ity levels (Table 2). In line with our animal results, NASH was associated with the recruitment of additional macrophages (vs. resident Kupffer cells) as evaluated by the expression of CD68 (Fig. 7C) which strongly correlated with hepatic expression of CD44 (Fig. 7D). Hepatic expression of MCP1 (Table 1) and CCR2 (Fig. 7E) strongly increased with NASH. The upregulation of CD44 also correlated with markers of inflammation including TNF α , IL1 β , MCP1 (Fig. S3) and CCR2 (Fig. 7F). MCP1, which could play a key role in liver macrophage recruitment via CCR2, correlated with the hepatic expression of CD68 ($r_s = 0.481$, $p = 0.007$, $n = 30$) (data not shown) and CCR2 ($r_s = 0.808$, $p < 0.001$, $n = 30$) (Fig. S3).

Correction of NASH was associated with less hepatic CD44 positive cells in patients

We then investigated the potentially beneficial effect of bariatric surgery (LRYGB) on NASH, CD44 expression and macrophages enrichment in morbidly obese patients. Four women and one man, with a median age of 38 [26; 62] years at the time of LRYGB and with biopsy-proven NASH, had a second liver biopsy after ≥ 30 months of follow-up. The median interval between the LRYGB and the second liver biopsy was 45 [37; 81] months. LRYGB was associated with significant weight loss (Fig. 8A) (median BMI loss: -12.8 [-18.6 ; -8.7] kg/m 2), improvement of hepatic steatosis in all patients (total resolution for two patients) (Fig. 8B), and resolution of hepatic inflammation and hepatocyte ballooning in 100% of the cases (Fig. 8B). The intensity of the hepatic CD44 labeling, in addition to the number of CD44 positive cells, strongly decreased after surgery (Fig. 8C). This was associated with a decrease in hepatic macrophages (data not shown). The correction of NASH by bariatric surgery was thus associated with an improvement of CD44-positive cells (mainly monocytes/macrophages) in patients.

Serum levels of soluble CD44 increased with the severity of steatosis and NAFLD

Since soluble CD44 (sCD44) is generated by the proteolytic cleavage of the ectodomain of CD44 from cell surfaces and serum

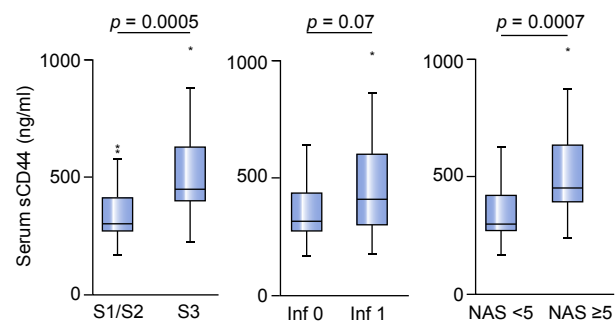


Fig. 9. The serum level of soluble CD44 increased with the severity of steatosis and NAFLD. (A) The serum sCD44 level was evaluated by ELISA in 64 obese patients with different grades of hepatic steatosis without or with NASH. Results are expressed with respect to (i) hepatic steatosis (severe [S3; $n = 21$] vs. mild or moderate hepatic steatosis [S1/S2; $n = 43$], to NASH vs. non-NASH (25 vs. 39) and to the NAFLD activity score (NAS) (NAS ≥ 5 [$n = 17$] vs. NAS < 5 [$n = 47$]). Results were expressed as the median (25th, 75th percentile) and statistically analyzed using the Mann-Whitney U test.

sCD44 levels could be associated with insulin resistance and hyperglycemia in patients,² we evaluated the relationship between sCD44 and liver complications in human. sCD44 levels were evaluated in 64 obese patients with different grades of hepatic steatosis without or with NASH. As shown in Fig. 9A, the serum level of sCD44 was higher in patients with severe steatosis (S3) (21 S3 vs. 43 with mild or moderate hepatic steatosis (S1/S2)) and tended to be higher in patients diagnosed NASH vs. non-NASH (25 NASH vs. 39 non-NASH). We then classified the patients with respect to their NAFLD activity score (NAS) generated by Brunt *et al.*²⁵ The serum sCD44 level was significantly higher in patients with NAS ≥ 5 vs. patients with NAS < 5 (17 vs. 47 with NAS < 5). In line with these results, the hepatic expression of ADAM10, a membrane-associated matrix metalloproteinases (MMPs) involved in the cleavage of the ectodomain of CD44, was upregulated in obese patients with severe steatosis compared to obese patients with moderate steatosis (Fig. S3C). Hepatic CD44 and its soluble form could thus be related to the development of hepatic inflammation in obese patients.

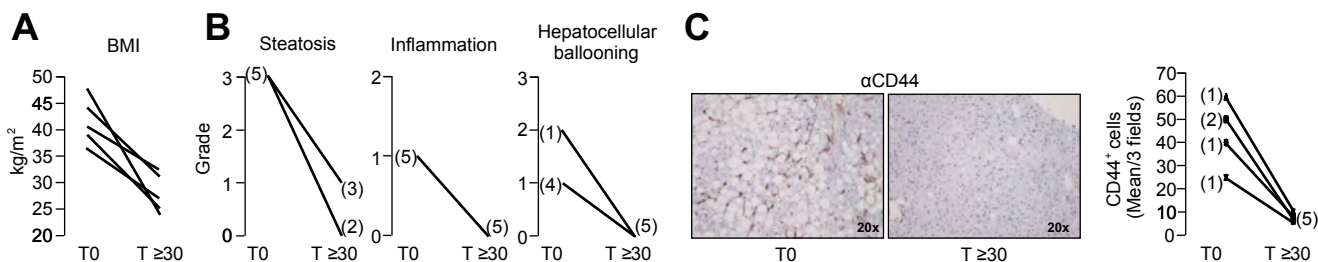


Fig. 8. Correction of NASH was associated with decreased hepatic CD44 $^+$ cells in patients. Four women and a man, with a median age of 38 [26; 62] years at the time of laparoscopic Roux-en-Y gastric bypass (LRYGB) and with biopsy-proven NASH, had a second liver biopsy after ≥ 30 months of follow-up (45 [37; 81] months). BMI (A), hepatic steatosis, inflammation (NASH) and hepatocellular ballooning (B) were evaluated before and after LRYGB. (C) α CD44 staining of liver samples from morbidly obese patients with NASH ($n = 5$) before and after LRYGB. Representative pictures and quantification of CD44-positive cells are shown.

Discussion

We first described in this study that steatohepatitis was associated with the upregulation of hepatic CD44 in mice and obese patients. While this upregulation of CD44 has also been reported in steatotic livers in mouse models of NAFLD,^{3,5} hepatic CD44 is more specifically increased in NASH patients. We then reported that CD44 deficiency strongly prevented liver steatosis, inflammation, injury and fibrosis in mice challenged with MCDD. This could be independent of adipose tissue inflammation and systemic insulin resistance since both events are not induced by MCDD.^{26,27} Furthermore, the prevention of hepatic complications by CD44 deficiency was associated with a strong decrease in hepatic infiltration of monocyte/macrophages and inflammation as evaluated by the number of inflammatory foci and expression of TNF α , IL1 β and iNOS, respectively. The prevention of macrophage infiltration into the liver by CD44 deficiency was not related to the decrease in circulating levels of monocytes. Whereas it has been reported that CD44 can direct lymphocytes to inflammatory sites,²⁸ the deficiency of CD44 did not impact the number of hepatic CD3⁺, CD4⁺ and CD8⁺ cells in our mice (data not shown). Since hepatic monocyte/macrophage infiltration strongly contributes to the development of steatohepatitis,^{29,30} CD44 deficiency could prevent the development of steatohepatitis by regulating the liver monocyte/macrophage infiltration.

This effect of CD44 deficiency on liver monocyte/macrophage recruitment could be explained by several mechanisms. It has been clearly established that the deficiency of CD44 in macrophages abrogated the chemotaxis induced by various chemoattractants including MCP1/CCL2 and osteopontin.²³ The decrease in hepatic expression of chemoattractants could also prevent the liver recruitment of monocytes/macrophages. We here reported that liver MCP1/CCL2 expression was already increased after 2 weeks of MCDD and the deficiency of CD44 strongly prevented this upregulation. In mice, CD44 deficiency also prevented the upregulation of hepatic CCR2 expression (CCL2 receptor) after 2 (data not shown) and 7 weeks (Fig. S2D) of MCDD. In contrast, hepatic (data not shown) and serum levels of osteopontin (Fig. S4) was later upregulated (after 4–7 weeks of MCDD) with a partial decrease in CD44^{-/-} mice (Fig. S4). This could indicate that osteopontin could be more related to hepatic fibrosis than steatohepatitis, as previously reported.^{15,31–35}

The prevention of hepatic inflammation by the CD44 deficiency was also associated with less hepatic neutrophil infiltration. While further investigations are required, we can suggest that CD44 could regulate the neutrophil infiltration via E-selectin based on recent reports.^{10,12} This ligand of CD44 was upregulated in NASH livers in mice (Fig. S2) and patients⁹ and its hepatic expression decreased in MCDD-fed CD44^{-/-} mice vs. MCDD-fed WT mice (Fig. S2).

We also showed that targeting CD44 with a specific antibody (daily injection for 6 days) corrected the steatohepatitis and liver injury in MCDD-fed mice. This was associated with a decrease in hepatic monocyte/macrophage enrichment and in hepatic and circulating levels of MCP1/CCL2. While the depletion of CD44-positive cells did not correct hepatic steatosis in our mouse models, it has been recently reported that targeting CD44 with the same approach (anti-CD44 antibody) for 4 weeks corrected liver steatosis in a high fat diet-fed mouse model. But the beneficial effects of this long-term treatment (4 weeks in this study vs. 6 days in our trial) results from a strong decrease in weight gain, visceral adipose tissue

macrophages and MCP1/CCL2 expression, fasting blood glucose levels, and improvement of insulin sensitivity compared to controls.⁴ This highlights that CD44 is also important in the recruitment of macrophages into adipose tissue leading to adipose tissue inflammation and insulin resistance as previously reported.² Adipose tissue insulin resistance increases lipolysis and the release of free fatty acids from adipocytes into the circulation, which in turn promote liver steatosis and NAFLD.³⁶ This upregulation of adipose tissue CD44 has also been reported in obese people.² Furthermore, we have previously reported that the correction of adipose tissue inflammation after bariatric surgery decreased the expression of CD44 and macrophage marker CD68 in human adipose tissue.⁷

While different results on the role of the CCL2/CCR2 system have been obtained in mice with different genetic backgrounds,^{37,38} the contribution of this system has recently been confirmed in mice challenged with a lithogenic diet through a marked reduction in leukocyte recruitment in the absence of CCL2 in mouse strains susceptible to fat accumulation.⁵ *In vivo*, macrophage tracking also indicated that in the absence of CCL2 or CCR2, accumulation of macrophages is reduced by 80% in the liver and around 40% in adipose tissue.²⁴ Furthermore, targeting CCR2 by deficiency or using a CCR2 inhibitor (CCR2-selective chemokine receptor antagonist RS102895) prevented the recruitment of macrophages into the liver, hepatic inflammation and fibrosis in choline-deficient amino acid-defined diet-fed mice.²⁹ The pharmacological inhibition of MCP1/CCL2 also prevented hepatic monocyte/macrophage infiltration, hepatic steatosis and inflammation in MCDD-fed mice.³⁰

In addition to the regulation of the monocyte/macrophage infiltration into the liver, we report here that the CD44 deficiency modified the properties of macrophages with higher susceptibility to anti-inflammatory (M2) polarization and lower pro-inflammatory phenotypes (M1) upon activation. The alteration of the M1/M2 balance is an important mechanism in the initiation of liver injury and NAFLD progression.^{39–41} The resulting exacerbated release of M1 resident Kupffer cell-derived mediators (such as TNF α) contributes to the pathogenesis of several liver lesions including hepatocyte steatosis and apoptosis, and inflammatory cell recruitment.^{39,42,43,44} Interestingly, the CD44 deficiency in macrophages prevented the expression of pro-inflammatory cytokines including TNF α and IL6 in response to DAMPs from damaged fatty hepatocytes, saturated fatty acid and pathogen-associated-molecular-pattern molecules such as LPS. In our MCDD-fed mice, hepatocyte steatosis and injury and LPS levels, as evaluated by the serum level of anti-LPS antibodies (Ctr D-fed WT mice: 380 \pm 58 ng/ml, n = 8, MCDD-fed mice: 629 \pm 51, n = 15, *p* = 0.006, upon 7 weeks of MCDD challenge, data not shown), strongly increased with steatohepatitis. CD44 deficiency in resident Kupffer cells could prevent their activation by increased levels of DAMPs, LPS and fatty acid. In turn, CD44^{-/-} Kupffer cells could secrete less pro-inflammatory cytokines (TNF α , IL6) and chemokines such as MCP1, leading to the prevention of hepatocyte glucido-lipid alteration and hepatic macrophage infiltration, respectively. Concerning hepatocyte alteration, MCDD-fed CD44^{-/-} mice displayed a lower hepatic expression of markers of cellular stresses (endoplasmic stress: *CHOP/BIP*, oxidative stress: *sestrin-2 [Sesn2]*) and lipogenesis (*Srebp1*) and hepatokine (*FGF21*) compared with MCDD-fed WT mice (Fig. S5). The prevention of freshly infiltrating hepatic macrophages could consecutively reduce the progression of chronic liver injury and fibrosis.

Research Article

We then reported a specific increase in hepatic CD44 expression with NASH in obese patients. Hepatic CD44 expression also correlated with hepatic expression of the macrophage markers *CD68*, *MCP1/CCL2*, *TNF α* and *IL1 β* . *CCR2* was also specifically upregulated with NASH and strongly correlated with *MCP1* ($r_s = 0.808$, $p < 0.001$, $n = 30$). *CD68* also correlated with the hepatic expression of *MCP1* ($r_s = 0.481$, $p = 0.007$, $n = 30$). Correction of NASH after bariatric surgery-induced weight loss was associated with a strong decrease in CD44-positive cells in the liver. While the recruitment of macrophages into the liver could be mediated by several chemokines,⁴⁵ *MCP1/CCL2* is upregulated in the serum and liver of patients with NASH.^{9,46} Upregulation of hepatic CD44 could thus be related to the recruitment of macrophages but also to the activation level of recruited and resident macrophages (Kupffer cells). Indeed, we here reported that the deficiency of CD44 strongly decreased the expression of *TNF α* and *IL6* in activated macrophages. In accordance with this, the circulating level of sCD44, which results from the proteolytic cleavage of CD44 by membrane-associated matrix metalloproteinases such as ADAM10, was significantly higher in obese patients with $NAS \geq 5$ vs. patients with $NAS < 5$. Since CD44 is also expressed in the adipose tissue, we cannot rule out that its circulating levels could also be related to adipose tissue inflammation and insulin resistance as recently reported.² Although serum sCD44 and liver *ADAM10* levels increased in our mouse model of steatohepatitis (Fig. S2) and sCD44 concentration increased in patients with severe acute or chronic liver disease from different etiologies (142 patients including 14 with acute hepatitis; 45 with noncirrhotic chronic liver disease, 34 with cirrhosis),⁴⁷ sCD44 as biomarker to accurately estimate NASH should be validated in a larger cohort of patients.

In conclusion, CD44 plays an important role in the development of NASH by regulating hepatic macrophage polarization (pro-inflammatory phenotype) and infiltration (macrophage motility and the *MCP1/CCL2/CCR2* system). In mice, targeting CD44 through deficiency or by depletion can prevent and correct steatohepatitis, respectively. In patients, hepatic CD44 and serum sCD44 increase with hepatic inflammation. By regulating the macrophage infiltration in the adipose tissue, CD44 could also enhance the development of adipose tissue inflammation and hepatic steatosis. Since CD44 is also expressed in other immune cells and in fibroblasts/stellate cells,^{48,49} studies focusing on the role of CD44 in specific cells should provide more insight into the pathogenesis of NASH/NAFLD.

Financial support

This work was supported by grants from INSERM (France), the University of Nice, the Programme Hospitalier de Recherche Clinique (Centre Hospitalier Universitaire of Nice), and charities (Association Française pour l'Etude du Foie (AFEF)/LFB to PG, AFEF/Aptalis to BBM, Société Francophone du Diabète (SFD) to PG, SFD/Roche Pharma to PG, SFD/MSD to BBM, European Foundation for the study of Diabetes/Lilly European Diabetes Research Programme to PG). This work was also funded by the French Government (National Research Agency, ANR) through the "Investments for the Future" LABEX SIGNALIFE: program reference #ANR-11-LABX-0028-01 and #ANR-15-CE14-0016-01.

Conflict of interest

The authors who have taken part in this study declared that they do not have anything to disclose regarding funding or conflict of interest with respect to this manuscript.

Authors' contributions

PG, SP and DR conceived the research and wrote the paper. SP, DR, SB, C Lebeaupin and C Luci planned and performed the experiments. CMC, RA, AI, MCSP and JG participated in human sample and data collection. AB, BBM, AT and all the other authors corrected and approved the final submitted draft.

Acknowledgments

The authors thank i) Dr V. Corcelle and the INSERM U1065 animal facility staff for their excellent care of mice; ii) Dr D. Alcor and the C3 M Imaging CORE Facility (Microscopy and Imaging platform Côte d'Azur, MICA; and iii) Dr F Larbret and the flow cytometry platform, Archet Hospital. We also thank Dr C. Postic (INSERM U1016 Institut Cochin, Paris, France) and Dr S. Lotersztajn (INSERM UMR 1149-Center for Research on Inflammation, Paris, France) for helpful discussions. We also thank Julie Cazareth (CNRS UMR7275, Flow Cytometry Facility, Institut de Pharmacologie Moléculaire et Cellulaire, Sophia-Antipolis, France) for performing multiplex bead array assays.

Supplementary data

Supplementary data associated with this article can be found, in the online version, at <http://dx.doi.org/10.1016/j.jhep.2017.03.00>.

References

Author names in bold designate shared co-first authorship

- [1] Younossi ZM, Koenig AB, Abdelatif D, Fazel Y, Henry L, Wymer M. Global epidemiology of nonalcoholic fatty liver disease-Meta-analytic assessment of prevalence, incidence, and outcomes. *Hepatology* 2016;64:73–84.
- [2] Kodama K, Horikoshi M, Toda K, Yamada S, Hara K, Irie J, et al. Expression-based genome-wide association study links the receptor CD44 in adipose tissue with type 2 diabetes. *Proc Natl Acad Sci U S A* 2012;109:7049–7054.
- [3] Kang HS, Liao G, DeGraff LM, Gerrish K, Bortner CD, Garantziotis S, et al. CD44 plays a critical role in regulating diet-induced adipose inflammation, hepatic steatosis, and insulin resistance. *PLoS One* 2013;8:e58417.
- [4] Kodama K, Toda K, Morinaga S, Yamada S, Butte AJ. Anti-CD44 antibody treatment lowers hyperglycemia and improves insulin resistance, adipose inflammation, and hepatic steatosis in diet-induced obese mice. *Diabetes* 2015;64:867–875.
- [5] Egan CE, Daugherty EK, Rogers AB, Abi Abdallah DS, Denkers EY, Maurer KJ. CCR2 and CD44 promote inflammatory cell recruitment during fatty liver formation in a lithogenic diet fed mouse model. *PLoS One* 2013;8:e65247.
- [6] Liu LF, Kodama K, Wei K, Tolentino LL, Choi O, Engleman EG, et al. The receptor CD44 is associated with systemic insulin resistance and proinflammatory macrophages in human adipose tissue. *Diabetologia* 2015;58:1579–1586.
- [7] Bertola A, Deveaux V, Bonnafous S, Rousseau D, Anty R, Wakkach A, et al. Elevated expression of osteopontin may be related to adipose tissue macrophage accumulation and liver steatosis in morbid obesity. *Diabetes* 2009;58:125–133.

- [8] Nagoshi S. Osteopontin: Versatile modulator of liver diseases. *Hepato Res* 2014;44:22–30.
- [9] Bertola A, Bonnafous S, Anty R, Patouraux S, Saint-Paul MC, Iannelli A, et al. Hepatic expression patterns of inflammatory and immune response genes associated with obesity and NASH in morbidly obese patients. *PLoS One* 2010;5:e13577.
- [10] Katayama Y, Hidalgo A, Chang J, Peired A, Frenette PS. CD44 is a physiological E-selectin ligand on neutrophils. *J Exp Med* 2005;201:1183–1189.
- [11] Ruppert SM, Hawn TR, Arrigoni A, Wight TN, Bollyky PL. Tissue integrity signals communicated by high-molecular weight hyaluronan and the resolution of inflammation. *Immunol Res* 2014;58:186–192.
- [12] Bertola A, Park O, Gao B. Chronic plus binge ethanol feeding synergistically induces neutrophil infiltration and liver injury in mice: a critical role for E-selectin. *Hepatology* 2013;58:1814–1823.
- [13] McDonald B, Kubes P. Interactions between CD44 and Hyaluronan in Leukocyte Trafficking. *Front Immunol* 2015;6:68.
- [14] Rostami S, Parsian H. Hyaluronic Acid: from biochemical characteristics to its clinical translation in assessment of liver fibrosis. *Hepat Mon* 2013;13:e13787.
- [15] Patouraux S, Bonnafous S, Voican CS, Anty R, Saint-Paul MC, Rosenthal-Allieri MA, et al. The osteopontin level in liver, adipose tissue and serum is correlated with fibrosis in patients with alcoholic liver disease. *PLoS One* 2012;7:e35612.
- [16] Lavallard VJ, Bonnafous S, Patouraux S, Saint-Paul MC, Rousseau D, Anty R, et al. Serum markers of hepatocyte death and apoptosis are non invasive biomarkers of severe fibrosis in patients with alcoholic liver disease. *PLoS One* 2011;6:e17599.
- [17] Bekri S, Gual P, Anty R, Luciani N, Dahman M, Ramesh B, et al. Increased adipose tissue expression of hepcidin in severe obesity is independent from diabetes and NASH. *Gastroenterology* 2006;131:788–796.
- [18] Anty R, Bekri S, Luciani N, Saint-Paul MC, Dahman M, Iannelli A, et al. The inflammatory C-reactive protein is increased in both liver and adipose tissue in severely obese patients independently from metabolic syndrome, Type 2 diabetes, and NASH. *Am J Gastroenterol* 2006;101:1824–1833.
- [19] Bertola A, Ciucci T, Rousseau D, Bourlier V, Duffaut C, Bonnafous S, et al. Identification of adipose tissue dendritic cells correlated with obesity-associated insulin-resistance and inducing th17 responses in mice and patients. *Diabetes* 2012;61:2238–2247.
- [20] Wallace TM, Levy JC, Matthews DR. Use and abuse of HOMA modeling. *Diabetes Care* 2004;27:1487–1495.
- [21] Kleiner DE, Brunt EM, Van Natta M, Behling C, Contos MJ, Cummings OW, et al. Design and validation of a histological scoring system for nonalcoholic fatty liver disease. *Hepatology* 2005;41:1313–1321.
- [22] Patouraux S, Rousseau D, Rubio A, Bonnafous S, Lavallard VJ, Lauron J, et al. Osteopontin deficiency aggravates hepatic injury induced by ischemia-reperfusion in mice. *Cell Death Dis* 2014;5:e1208.
- [23] Zhu B, Suzuki K, Goldberg HA, Rittling SR, Denhardt DT, McCulloch CA, et al. Osteopontin modulates CD44-dependent chemotaxis of peritoneal macrophages through G-protein-coupled receptors: evidence of a role for an intracellular form of osteopontin. *J Cell Physiol* 2004;198:155–167.
- [24] Oh DY, Morinaga H, Talukdar S, Bae EJ, Olefsky JM. Increased macrophage migration into adipose tissue in obese mice. *Diabetes* 2012;61:346–354.
- [25] Brunt EM, Kleiner DE, Wilson LA, Belt P, Neuschwander-Tetri BA. Nonalcoholic fatty liver disease (NAFLD) activity score and the histopathologic diagnosis in NAFLD: distinct clinicopathologic meanings. *Hepatology* 2011;53:810–820.
- [26] Jha P, Knopf A, Koefeler H, Mueller M, Lackner C, Hoefler G, et al. Role of adipose tissue in methionine-choline-deficient model of non-alcoholic steatohepatitis (NASH). *Biochim Biophys Acta* 2014;1842:959–970.
- [27] Leclercq IA, Lebrun VA, Starkel P, Horsmans YJ. Intrahepatic insulin resistance in a murine model of steatohepatitis: effect of PPARgamma agonist pioglitazone. *Lab Invest* 2007;87:56–65.
- [28] DeGrendele HC, Estess P, Siegelman MH. Requirement for CD44 in activated T cell extravasation into an inflammatory site. *Science* 1997;278:672–675.
- [29] Miura K, Yang L, van Rooijen N, Ohnishi H, Seki E. Hepatic recruitment of macrophages promotes nonalcoholic steatohepatitis through CCR2. *Am J Physiol Gastrointest Liver Physiol* 2012;302:G1310–G1321.
- [30] Baeck C, Wehr A, Karlmark KR, Heymann F, Vucur M, Gassler N, et al. Pharmacological inhibition of the chemokine CCL2 (MCP-1) diminishes liver macrophage infiltration and steatohepatitis in chronic hepatic injury. *Gut* 2012;61:416–426.
- [31] Syn WK, Choi SS, Liaskou E, Karaca GF, Agboola KM, Oo YH, et al. Osteopontin is induced by hedgehog pathway activation and promotes fibrosis progression in nonalcoholic steatohepatitis. *Hepatology* 2011;53:106–115.
- [32] Urtasun R, Lopategi A, George J, Leung TM, Lu Y, Wang X, et al. Osteopontin, an oxidant stress sensitive cytokine, up-regulates collagen-I via integrin alpha(V)beta(3) engagement and PI3K/pAkt/NFkappaB signaling. *Hepatology* 2012;55:594–608.
- [33] Coombes JD, Swiderska-Syn M, Dolle L, Reid D, Eksteen B, Claridge L, et al. Osteopontin neutralisation abrogates the liver progenitor cell response and fibrogenesis in mice. *Gut* 2015;64:1120–1131.
- [34] Coombes JD, Choi SS, Swiderska-Syn M, Manka P, Reid DT, Palma E, et al. Osteopontin is a proximal effector of leptin-mediated non-alcoholic steatohepatitis (NASH) fibrosis. *Biochim Biophys Acta* 2016;1862:135–144.
- [35] Arriazu E, Ge X, Leung TM, Magdaleno F, Lopategi A, Lu Y, et al. Signalling via the osteopontin and high mobility group box-1 axis drives the fibrogenic response to liver injury. *Gut* 2016. <http://dx.doi.org/10.1136/gutjnl-2015-310752>.
- [36] Tran A, Gual P. Non-alcoholic steatohepatitis in morbidly obese patients. *Clin Res Hepatol Gastroenterol* 2013;37:17–29.
- [37] Kassel KM, Guo GL, Tawfik O, Luyendyk JP. Monocyte chemoattractant protein-1 deficiency does not affect steatosis or inflammation in livers of mice fed a methionine-choline-deficient diet. *Lab Invest* 2010;90:1794–1804.
- [38] Galastri S, Zamara E, Milani S, Novo E, Provenzano A, Delogu W, et al. Lack of CC chemokine ligand 2 differentially affects inflammation and fibrosis according to the genetic background in a murine model of steatohepatitis. *Clin Sci (Lond)* 2012;123:459–471.
- [39] Tacke F, Zimmermann HW. Macrophage heterogeneity in liver injury and fibrosis. *J Hepatol* 2014;60:1090–1096.
- [40] Sakaguchi S, Takahashi S, Sasaki T, Kumagai T, Nagata K. Progression of alcoholic and non-alcoholic steatohepatitis: common metabolic aspects of innate immune system and oxidative stress. *Drug Metab Pharmacokinet* 2011;26:30–46.
- [41] Wan J, Benkdane M, Teixeira-Clerc F, Bonnafous S, Louvet A, Laffid F, et al. M2 Kupffer cells promote M1 Kupffer cell apoptosis: a protective mechanism against alcoholic and nonalcoholic fatty liver disease. *Hepatology* 2014;59:130–142.
- [42] Huang W, Metlakunta A, Dedousis N, Zhang P, Sipula I, Dube JJ, et al. Depletion of liver Kupffer cells prevents the development of diet-induced hepatic steatosis and insulin resistance. *Diabetes* 2010;59:347–357.
- [43] Li Z, Yang S, Lin H, Huang J, Watkins PA, Moser AB, et al. Probiotics and antibodies to TNF inhibit inflammatory activity and improve nonalcoholic fatty liver disease. *Hepatology* 2003;37:343–350.
- [44] Koca SS, Bahcecioglu IH, Poyrazoglu OK, Ozercan IH, Sahin K, Ustundag B. The treatment with antibody of TNF-alpha reduces the inflammation, necrosis and fibrosis in the non-alcoholic steatohepatitis induced by methionine- and choline-deficient diet. *Inflammation* 2008;31:91–98.
- [45] Marra F, Tacke F. Roles for chemokines in liver disease. *Gastroenterology* 2014;147:577–594 e571.
- [46] Haukeland JW, Damas JK, Konopski Z, Loberg EM, Haaland T, Goverud I, et al. Systemic inflammation in nonalcoholic fatty liver disease is characterized by elevated levels of CCL2. *J Hepatol* 2006;44:1167–1174.
- [47] Falletti E, Pirisi M, Fabris C, Bortolotti N, Soardo G, Gonano F, et al. Circulating standard CD44 isoform in patients with liver disease: relationship with other soluble adhesion molecules and evaluation of diagnostic usefulness. *Clin Biochem* 1997;30:69–73.
- [48] Meran S, Luo DD, Simpson R, Martin J, Wells A, Steadman R, et al. Hyaluronan facilitates transforming growth factor-beta1-dependent proliferation via CD44 and epidermal growth factor receptor interaction. *J Biol Chem* 2011;286:17618–17630.
- [49] Midgley AC, Rogers M, Hallett MB, Clayton A, Bowen T, Phillips AO, et al. Transforming growth factor-beta1 (TGF-beta1)-stimulated fibroblast to myofibroblast differentiation is mediated by hyaluronan (HA)-facilitated epidermal growth factor receptor (EGFR) and CD44 co-localization in lipid rafts. *J Biol Chem* 2013;288:14824–14838.